Investigations into the cellular interactome of the PB2 protein expressed by seasonal and highly pathogenic avian influenza viruses

D i s s e r t a t i o n

zur Erlangung des akademischen Grades

d o c t o r r e r u m n a t u r a l i u m

(Dr. rer. nat.)

im Fach Biologie

eingereicht an der

Lebenswissenschaftlichen Fakultät

der Humboldt-Universität zu Berlin

von

Ulrike Arnold

Präsidentin der Humboldt-Universität zu Berlin

Prof. Dr.-Ing. Dr. Sabine Kunst

Dekan der Lebenswissenschaftlichen Fakultät

Prof. Dr. Bernhard Grimm

Gutachter:
1. Prof. Andreas Herrmann
2. PD Thorsten Wolff
3. Dr. Benedikt Beckmann

Tag der mündlichen Prüfung: 10.07.2018

Abstract

Influenza virus replication relies on the functionality of its trimeric RNA dependent RNA polymerase complex under the conditions provided by the infected cell. PB2 is an essential component of this complex and is known to be a key factor for influenza virus host range. Given its importance, the interplay of PB2 with the cellular host proteome was investigated in several studies and various interaction partners such as protein phosphatase 6 (PP6) have been reported. However, these studies were mostly performed with laboratory/mouse-adapted strains or in the context of transiently transfected cells.

Here, a combined affinity-purification/mass spectrometric approach was performed to identify novel interaction partners of PB2 of seasonal and highly pathogenic viral strains in infected human alveolar epithelial cells (A549). The subsequent analysis of selected cellular interaction partners aimed to determine the influence of these proteins on the replication cycle of these non-laboratory adapted viral strains. Furthermore, differences in their relevance for the seasonal and the highly pathogenic influenza viruses were investigated in order to gain further insights into the basis of the diverse replication characteristics of these viruses in human cells.

By generation and use of recombinant influenza viruses carrying a Strep-tag at the C-terminus of their PB2 protein, affinity purification upstream of mass spectrometry (MS) enriched PB2 and its interaction partners while non-specific contaminants got reduced. To further increase specificity, and thereby confidence in the results, Stable isotopic labelling by amino acids in cell culture (SILAC) quantification method was employed and an internal control, namely A549 cells infected with un-tagged seasonal virus, was included. The mass spectrometric analysis resulted in a list of 487 protein groups that were significantly changed and more abundant in tagged samples in comparison to the internal control. The list included already described polymerase regulator like ANP32A as well as proteins like SLC12A2 that have not been shown to interact with PB2 so far. After addition of more stringent filter criteria, the list was further condensed resulting in 22 hit proteins. A selection of 13 proteins was further analyzed, and co-precipitation with PB2 was confirmed for 9 proteins. Moreover, polymerase activity assay in hit protein overexpressing cells revealed an inhibitory or stimulatory effect of 11 proteins on polymerase activity. Five of these proteins showed different effects on the polymerase activity of the seasonal or the highly pathogenic influenza virus strain.

Out of the proteins shown to have an influence on polymerase activity and to co-precipitate with PB2 in an overexpression setting, HSPA8 was selected for further investigation. HSPA8

belongs to the 70 kilo Dalton heat shock protein (HSP70) family. Besides its various roles in cellular homeostasis, HSPA8 was previously shown to interact with influenza virus M1 protein and was proposed to play a role in the nuclear export of viral ribonucleoprotein (vRNP). Co-precipitation of endogenous HSPA8 with PB2 was demonstrated by immunoprecipitation from lysates of A549 cells infected with seasonal or highly pathogenic influenza virus. In addition, confocal microscopy showed HSPA8 relocates into the nucleus of infected A549 cells. While the influence of HSPA8 on the highly pathogenic strain remained unclear due to inconclusive results, its importance for seasonal influenza virus life cycle was demonstrated. Overexpression of HSPA8 resulted in increased polymerase activity. On the other hand, HSP8 knock down resulted in reduction of viral replication and viral polymerase activity of up to ~ 70 % and ~ 40 %, respectively. Intriguingly, the knock down of HSPA8 led to a strong decrease of PB2 protein expression. However, this was only observed for seasonal PB2. These results indicate a role of HSPA8 as a PB2 chaperone, necessary for protein stability of seasonal but not highly pathogenic influenza virus.

Zusammenfassung

Die Replikation von Influenzaviren ist angewiesen auf die Funktionalität des trimeren RNA abhängigen RNA Polymerase Komplexes im Kontext der infizierten Zelle. PB2 ist ein essentieller Bestandteil dieses Komplexes und bekannt für seine Schlüsselrolle in der Bestimmung des Wirtsspektrums von Influenzaviren. Aufgrund der Bedeutung von PB2 wurde das Zusammenspiel des zellulären Wirtsproteoms mit dem viralen Protein bereits in mehreren Studien untersucht und verschiedene PB2-Interaktionspartner, wie zum Beispiel die Protein Phosphatase 6 (PP6), wurden identifiziert. Diese Studien wurden allerdings meist mit Labor/Maus-adaptierten Influenzastämmen oder im Kontext von transient transfizierten Zellen durchgeführt.

Diese Arbeit diente der Identifizierung neuer Interaktionspartner von PB2 eines saisonalen und eines hochpathogenen Influenzavirus Stammes im Kontext infizierter humaner alveolar Epithelzellen (A549) unter Einsatz massenspektrometrischer Analysen von affinitätschromatographisch gereinigten Proteinkomplexen. Die anschließende Untersuchung ausgewählter zellulärer Interaktoren hatte zum Ziel deren Einfluss auf den Replikationszyklus der nicht Labor-adaptierten Stämme zu bestimmen. Außerdem sollten mögliche Unterschiede in Ihrer Relevanz für das saisonale und das hochpathogene Influenzavirus identifiziert werden um Hinweise auf die Grundlage für das verschiedene Replikationsverhalten dieser Viren in humanen Zellen zu erlangen.

Die Erzeugung und Nutzung von Influenzaviren die einen Strep-tag am C-Terminus ihres PB2 Proteins tragen ermöglichte eine affinitätschromatographische Anreicherung von PB2 und seiner Interaktionspartner gegenüber unspezifischer Kontaminationen. Um die Spezifität weiter zu erhöhen wurde die sogenannte „Stable isotopic labelling by amino acids in cell culture (SILAC)“ Quantifizierungsmethode angewendet. Darüber hinaus wurde eine interne Kontrolle, A549 Zellen infiziert mit einem saisonalen Stamm ohne Strep-tag am PB2 Protein, in die Untersuchung mit einbezogen. Die massenspektrometrische Analyse zeigte eine signifikante Anreicherung von 487 Proteingruppen in Strep-tag Proben im Vergleich zur internen Kontrolle. Diese Kandidatenliste enthielt sowohl bereits bekannte Polymerase-regulatoren wie ANP32A, als auch Proteine, wie z.B. SLC12A, die noch nicht als Interaktionspartner von PB2 beschrieben wurden. Das Hinzufügen weiterer Filterkriterien, resultierte in einer 22 Proteine umfassenden Hitliste. Eine Auswahl an 13 Proteinen wurde tiefer gehend analysiert und eine Komplexbildung mit PB2 konnte für 9 Proteine bestätigt werden. Darüber hinaus offenbarte ein Polymerase-Aktivitäts-Assay in Hit-Protein über-exprimierenden Zellen einen stimulierenden bzw. hemmenden Effekt von 11 Proteinen. Fünf

dieser Proteine zeigten einen regulatorischen Einfluss auf die Polymerase-Aktivität des saisonalen und des hochpathogenen Stammes.

Aus den Proteinen, die nach Überexpression mit PB2 kopräzipitierten und einen Einfluss auf die Polymerase-Aktivität zeigten, wurde das Protein HSPA8 zur weiteren Untersuchung ausgewählt. HSPA8 gehört zur Familie der 70 kDa Hitzeschockproteine (HSP70) und erfüllt mehrere Aufgaben in der Aufrechterhaltung der Zellhomöostase. Darüber hinaus interagiert HSPA8 mit dem Influenzavirusprotein M1. Dieser Interaktion wurde eine Rolle im nuklearen Export von viralen Ribonukleoproteinen (vRNPs) zugeschrieben. Kopräzipitation von endogenem HSPA8 mit PB2 wurde mit Hilfe von Immunopräzipitation in A549 Zellen nach Infektion mit saisonalem oder hochpathogenem Influenzavirus gezeigt. Darüber hinaus zeigt eine Untersuchung mit Hilfe konfokaler Mikroskopie die Relokalisation von HSPA8 in den Kern infizierter A549 Zellen. Während ein Einfluss von HSPA8 auf den hochpathogenen Influenzastamm aufgrund uneindeutiger Ergebnisse nicht abschließend geklärt werden konnte, wurde seine Bedeutung für den Vermehrungszyklus des saisonalen Stammes aufgezeigt. Eine Überexpression von HSPA8 führte zu einer Steigerung der Polymerase-Aktivität. Die Erniedrigung des HSPA8 Spiegels mittels transfizierter siRNA resultierte wiederum in einer Verringerung der viralen Replikation um rund 70 % und einer Verringerung der Polymerase-Aktivität um rund 40 %. Interessanterweise führte die Erniedrigung des HSPA8 Spiegels auch zu stark verminderter PB2-Expression. Dies wurde jedoch nur im Falle des saisonalen Influenzastammes beobachtet. Dieser Befund deutet auf eine Rolle von HSPA8 als PB2-Chaperon, notwendig für Proteinstabilität von saisonalen aber nicht hochpathogenen Influenzaviren, hin.

Contents

Contents I

List of Figures III

List of Tables V

List of Abbreviations VII

1 Introduction 2
1.1 Influenza virus 2
1.1.1 Disease 2
1.1.2 Taxonomy 2
1.1.3 Morphology and structure 3
1.1.4 Replication 6
1.2 The trimeric polymerase complex 8
1.2.1 Viral polymerase structure 9
1.2.2 Transcription and replication 10
1.2.3 Regulation by host cell factors 11
1.2.4 The polymerase component PB2 12
1.3 Low pathogenicity and highly pathogenic influenza viruses 14
1.3.1 Low pathogenicity and highly pathogenic influenza viruses in birds 14
1.3.2 Avian influenza viruses in humans 15
1.3.3 Differences and similarities of seasonal H3N2 and HPAI H5N1 viruses in humans 17
1.4 Heat shock proteins 19
1.4.1 HSPA8 20
1.4.2 HSPA8 and influenza 22
1.5 Mass spectrometry 24
1.5.1 MS principles 24
1.5.2 Stable isotopic labelling by amino acids in cell culture (SILAC) 26
1.6 Aim of this study 28

2. Materials and Methods 30
2.1 Materials 30
2.1.1 Chemicals and Consumables 30
2.1.2 Kits 32
2.1.3 Enzymes 33
2.1.4 Cell lines 33
2.1.5 Bacterial strains 33
2.1.6 Virus strains 33
2.1.7 Plasmids 34
2.1.8 Antibodies 36
2.1.9 Primer 36
2.1.10 siRNA 37

2.1.11 Cell culture media ... 38
2.1.12 Media for bacteria ... 39
2.1.13 Buffer and solutions ... 39
2.1.14 Technical equipment ... 42
2.1.15 Software and web tools ... 43
2.2 Methods ... 44
2.2.1 Cell culture ... 44
2.2.2 Infectious work ... 45
2.2.3 Molecular biology methods ... 48
2.2.4 Biochemical Methods ... 55
2.2.5 Cell biology Methods ... 56
2.2.6 SILAC Mass spectrometry analysis ... 59

3. Results ... 64
3.1 Proteomic analysis of the PB2 interactome of influenza A/Panama/2007/99 (H3N2) and A/Thailand/(KAN-1)/04 (H5N1) viruses 65
3.1.1 Generation and functional characterization of PB2-Strep viruses for co-precipitation experiments ... 65
3.1.2 Experimental setup ... 68
3.1.3 MS data evaluation ... 70
3.1.4 Protein classification ... 73
3.1.5. Hit protein classification and network analysis ... 75
3.2 Data validation ... 79
3.2.1 Co-immunoprecipitation ... 79
3.2.2 Polymerase activity assay ... 81
3.3 Characterization of HSPA8 as a novel PB2 interaction partner ... 85
3.3.1 Co-precipitation of PB2 with Endogenous HSPA8 ... 86
3.3.2 HSPA8 relocates into the nucleus in infected cells ... 87
3.3.3 siRNA mediated depletion of HSPA8 expression influences A/Panama/2007/99 and A/Thailand/(KAN-1)/04 replication ... 90
3.3.4 Knock down of HSPA8 leads to a depletion of A/Panama/2007/99 PB2 ... 92

4. Discussion ... 94
4.1 Mass spectrometric analysis revealed the PB2 interactome of non-laboratory adapted seasonal and highly pathogenic avian influenza virus strains ... 94
4.2 HSPA8 is a novel regulator of the non-laboratory adapted seasonal influenza virus polymerase ... 105

Bibliography ... 114

Supplementary information ... 125

Appendix ... 137

List of Figures

Figure 1.1. Electron microscopy and schematic illustration of influenza A virus structures 4
Figure 1.2. Replication cycle of influenza A viruses 7
Figure 1.3. Structural details of the trimeric polymerase complex 9
Figure 1.4. Ribbon diagram and subunit domain structure of the polymerase protein PB2 13
Figure 1.5. Laboratory-confirmed cases of avian influenza virus in humans 16
Figure 1.6. Hemagglutinin, species specificity and pathogenicity 17
Figure 1.7. Model for the substrate binding and release cycle of HSPA8.. 21
Figure 1.8. Model of the HSPA8 related nuclear export of vRNPs 23
Figure 1.9. Principle of stable isotopic labeling by amino acids in cell culture (SILAC). 27
Figure 2.1. Generation of pHW2000-PB2-Strep plasmids 49
Figure 3.1. PB2 sequence information of constructed influenza A viruses 65
Figure 3.2. Growth characteristics of WT and Strep-PB2 viruses 66
Figure 3.3. Recombinant PB2-Strep proteins co-precipitate viral NP 67
Figure 3.4. Workflow of SILAC experiments 69
Figure 3.5. Precipitation control for SILAC experiments 70
Figure 3.6. Correlation of protein ratios between replicates 71
Figure 3.7. Significance and t-test difference of identified proteins 72
Figure 3.8. Comparison of MS data with different PB2/polymerase complex interactome screens 73
Figure 3.9. Functional classification of proteins in the filtered protein list 74
Figure 3.10. STRING network of PB2 interactome screen hit proteins 78
Figure 3.11. Validation of the co-precipitation of A/Thai/04 PB2 with selected hit proteins 80
Figure 3.12. Validation of the co-precipitation of A/Pan/99 PB2 with selected hit proteins 81
Figure 3.13. Schematic representation of the influenza polymerase activity assay 82
Figure 3.14. Functional investigation of MS data by polymerase activity assay 83
Figure 3.15. Co-precipitation of PB2 with endogenous HSPA8 86

Figure 3.16. HSPA8 relocates into the nucleus at late time points of A/Pan/99-WT infection 88

Figure 3.17. HSPA8 relocates into the nucleus at late time points of A/Thai/04-WT infection 89

Figure 3.18. Depletion of HSPA8 influences A/Pan/99-WT and A/Thai/04-WT replication 91

Figure 3.19. Knock down of HSPA8 leads to a depletion of A/Pan/99 PB2 93

Figure 4.1. Cellular functions of HSPA8 105

Figure 4.2. Proposed model for the role of HSPA8 in the influenza virus replication cycle 110

List of Tables

Table 1.1. vRNA segments and encoded proteins of influenza A/Pan/99 and A/Thai/04 5

Table 2.1. Composition of SDS polyacrylamide gels 55

Table 2.2. Amount of expression plasmids transfected per well of a 12-well plate used for polymerase activity assay 58

Table 2.3. Steps for desalting of peptides 62

3.1. Infection state of light, intermediate and heavy A549 cells in the 4 conducted SILAC experiments 68

Table 3.2. List of hit proteins 75

Table 3.3. Combined results of the co-immunoprecipitation and polymerase activity assay experiments 84

Table 4.1. Experimental setups of proteome screens used for comparison with our filtered protein list 99

List of Abbreviations

2DE	Two-dimensional gel electrophoresis
A/Pan/99	A/Panama/2007/1999
A/Thai/04	A/Thailand/1(KAN-1)/2004
A549cells	Human alveolar epithelial cells
aa	Amino acid
ACN	Acetonitrile
APH	Amphipathic helicase
AP-MS	Affinity-purification mass spectrometry
ATP	Adenosine triphosphate
Bcl-2-associated athanogene	BAG
C	Cytosine
CCT	Chaperonin containing TCP-1
CID	Collision induced dissociation
Co-IP	Co-Immunoprecipitation
CPE	Cytopathic effects
cRNA	Complementary RNA
csRNA	Capped small RNA
dd	Double distilled
DMEM	Dulbecco's modified Eagle medium
E	Glutamic acid
ESI	Electrospray ionization
FDR	False discovery rate
FT	Fourier transformation
FTICMS	Fourier transform-ion cyclotron
Fw	Forward
G	Guanosine
GO	Gene ontology
H/L	Heavy to light
HA	Hemagglutinin
HEK293T cells	Human embryonic kidney 293T
HeLa cells	Henrietta Lacks cells
HPAIV	Highly pathogenic avian influenza virus
Hsc70	Heat shock cognate 71 kDa protein
HSP	Heat shock protein
HSPA1A	Heat shock 70 kDa protein 1A
HSPA8	Heat shock cognate 71 kDa protein
HSV-1	Herpes simplex virus type 1
IAA	Iodoacetamide
IFNβ	Interferon β
IMPα	Importin-α
IMPβ1	Importin-β1
IVPI	Intravenous pathogenicity index
K	Lysine
KEGG	Kyoto Encyclopedia of Genes and Genomes
LC	Liquid chromatography
LCAR	Low-complexity acidic region

LPAIV	Low pathogenicity avian influenza virus
LRR	Leucine-rich repeat
LRT	Lower respiratory tract
LTQ	Linear ion trap quadrupole
M/L	Intermediate to light
m/z	Mass-to-charge ratio
M1	Matrix protein 1
M16I	Methionine to isoleucine substitution at position 16
M2	Matrix protein 2
MALDI	Matrix-assisted laser desorption/ionization
MAVS	Mitochondrial antiviral signaling protein
MBCS	Multibasic cleavage site
MCL	Markov Cluster algorithm
MCM	Minichromosome maintenance
MDCK cells	Madin-Darby Canine Kidney cells
MEM	Minimal essential medium
MINT	Molecular interaction database
ml	Minutes
MOI	Multiplicity of infection
mRNA	Messenger RNA
mRNP	Messenger ribonucleoprotein
MS	Mass spectrometry
MS/MS	Tandem mass spectrometry
MS1	First MS scan
MS2	Second MS scan
NA	Neuraminidase
Na	Sodium
NB	Non-bound
NCBI	National Center for Biotechnology Information
NCR	Non-coding region
NEF	Nucleotide exchange factors
NEP	Nuclear export protein
NLS	Nuclear localization sequences
NP	Nucleoprotein
NS1	Non-structural protein 1
nt	Nucleotides
NT	Non-target
NTP	Nucleoside triphosphate
OIE	World organization for animal health
ON	Overnight
p.i.	Post infection
p.t.	Post transfection
PA	Polymerase acidic protein
PA-X	Polymerase acidic protein X
PB1	Polymerase basic protein 1
PB1-F2	Polymerase basic protein
PB2	Polymerase basic protein 2
PB2-S1	Polymerase basic protein 2 S1
PBS	Phosphate buffered saline
PCR	Polymerase chain reaction

PlasmID	Plasmid information database
Pol I	RNA polymerase I
Pol II	DNA-dependent RNA polymerase II
PPI	Protein-protein interactions
PTMs	Post-translational modifications
R	Arginine
rev	Reverse
RNA	Ribonucleic-acid
sa	Sialic acids
SAα2,3	α-2,3-linked sialic acid
SAα2,6	α-2,6-linked sialic acid
SDS PAGE	Sodium dodecyl sulfate polyacrylamide gel electrophoresis
sec	Seconds
sHSP	Small heat shock protein
SILAC	Stable isotopic labelling by amino acids in cell culture
snoRNA	Small nucleolar RNA
snRNA	Small nuclear RNA
SOC	Super optimal broth with catabolite repression
ss	Single-stranded
STRING	Search Tool for the Retrieval of Interacting Genes/Proteins
TOF	Time-of-flight
U	Uridine
UPS	Ubiquitin-proteasome system
URT	Upper respiratory tract
vRNA	Viral RNA
vRNP	Viral ribonucleoprotein
WCL	Whole cell lysate
WHO	World health organization

1 Introduction

1.1 Influenza virus

1.1.1 Disease

Influenza, or colloquially “the flu”, is an acute respiratory disease caused by the influenza virus [1]. Strains circulating in humans replicate mainly in the upper respiratory tract including the nose and throat, and the lower respiratory tract, including the trachea, bronchial epithelium and lung [2]. Influenza viruses are transmitted from person to person via aerosolized droplets which are shed from infected persons by coughing or sneezing, or by contact with contaminated hands and surfaces.

After an incubation period of one to three days, infected individuals start to show the typical clinic signs of influenza disease [3]. These include sudden onset, fever, cough, headache, muscle and joint pain, sore throat, runny nose and severe malaise [1]. Most people recover within a week without medical treatment. However, influenza can also lead to severe illness and death, particularly among children under 5 years of age, elderly people over 65 and individuals with chronic medical conditions.

Influenza viruses circulate worldwide. In temperate climates the disease occurs in seasonal epidemics with peaks in infection rates during the winter months, whereas in tropical regions epidemics can occur throughout the year [1]. According to the World Health Organization (WHO), influenza viruses cause 3 to 5 million cases of severe illness and up to 250.000 to 500.000 deaths each year.

1.1.2 Taxonomy

Influenza viruses belong to the *Orthomyxoviridae* family which is comprised of 7 genera: Thogotovirus, Isavirus, Quaranjavirus, influenza virus A, B, and C, and the recently identified influenza virus D [4]. The influenza virus genera contain only 1 species each, influenza A, B, C or D virus, and are classified based on the antigenicity of the nucleoprotein (NP) and matrix protein 1 (M1) [5].

The 4 influenza virus species also differ in their ability to infect host species. In addition to its natural reservoir, water birds, influenza A viruses are also able to infect other bird species, such as poultry and a wide range of mammals: cats, dogs, whales, pigs, bats

and humans [6]. The host spectrum of influenza B, C and D viruses is much more restricted. Influenza D viruses have only been isolated from swine and cattle so far [4], whereas influenza B virus infection is restricted to seals and humans [7]. In addition to its ability to replicate in dogs and pigs, influenza C viruses can also infect humans, however causing usually only mild symptoms in humans [8].

The influenza A virus species can be further divided into subtypes according to the surface proteins hemagglutinin (HA) and neuraminidase (NA). To date, 11 different NA and 18 HA subtypes have been identified [9]. However, only the subtypes H1N1 and H3N2 are currently circulating in the human population [1]. In 1980, a common nomenclature for influenza viruses was established by the WHO [10]. The name includes the virus genus, the host of origin (if the strain was not isolated from a human case), the geographical region where the virus was isolated, the strain number or name and the year of isolation. In the case of influenza A viruses, the subtype based on HA and NA is also included. For example, influenza A/Panama/2007/1999 (H3N2) represents a human H3N2 virus that was isolated in 1999 in Panama. Due to the frequency of human infections and the risk that influenza A virus poses to human health, it will be the main focus of the study presented in this thesis.

1.1.3 Morphology and structure

Influenza viruses contain an envelope and a segmented, single-stranded (ss) ribonucleic-acid (RNA) genome of negative polarity. The envelope is a lipid bilayer derived from the host cell during budding of progeny virions from the cell membrane. The newly formed virions have a spherical or filamentous shape (figure 1.1.A) and vary from around 100 nm in diameter for spherical virions up to 20 µm in length for the filamentous form [11,12].

Influenza A virions contains 8 unique genome segments of viral RNA (vRNA) (figure 1.1.B). Each of these segments is associated with multiple nucleoprotein monomers and one monomer of each of the viral polymerase proteins: polymerase acidic protein (PA), polymerase basic protein 1 (PB1) and polymerase basic protein 2 (PB2) [13,14]. Together, each vRNA-NP-polymerase complex is referred to as one viral ribonucleoprotein (vRNP) (figure 1.1.C). The NP monomers in the internal region of the vRNP interact with each other, forming an antiparallel double helix that is closed by a loop [15]. The genomic RNA ends at the opposite side are not associated with NP. However, they are partially complementary and can form a double stranded panhandle structure that is bound to the trimeric polymerase complex [16,17]. The panhandle is formed by

interactions between the highly conserved 5`-end and 3`-end non-coding regions (NCRs) that contain promoter elements for the viral polymerase [18,19].

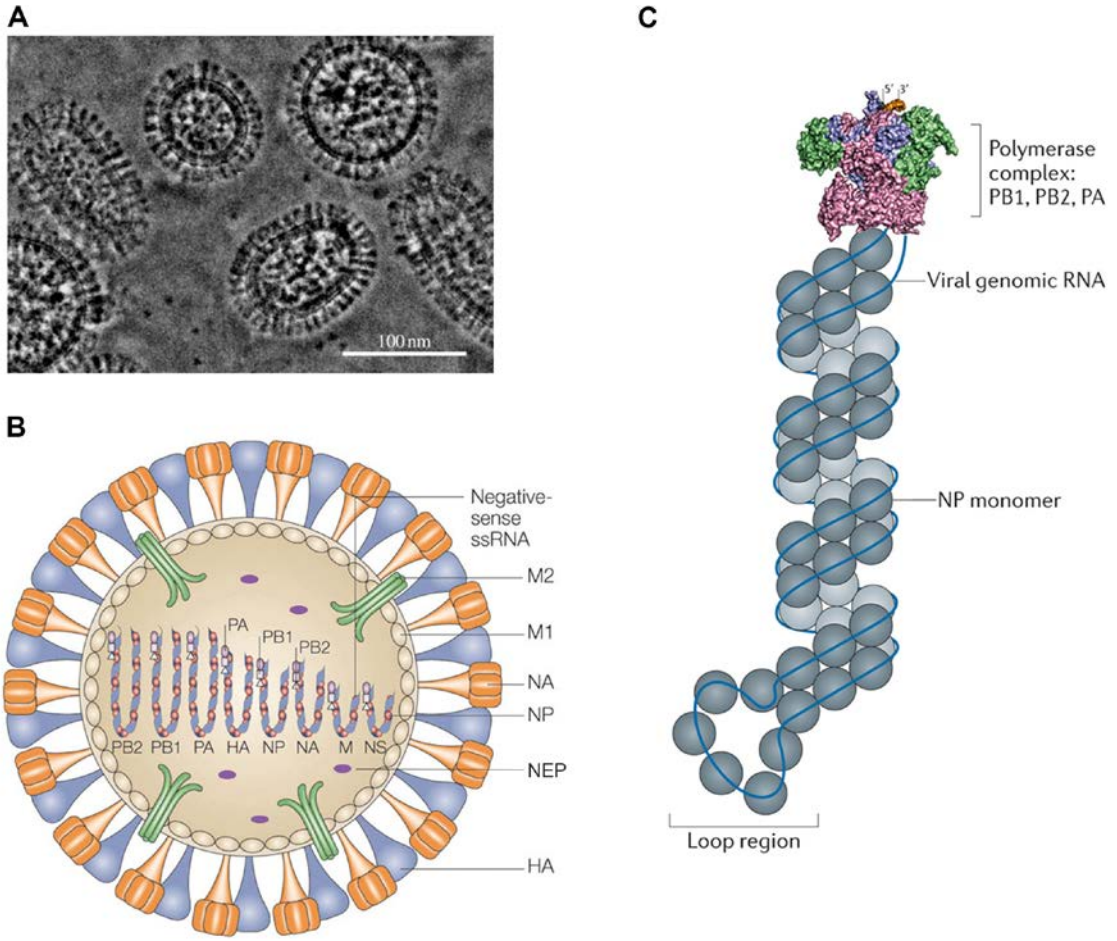

Figure 1.1. Electron microscopy and schematic illustration of influenza A virus structures. A ZPC-TEM micrograph for inactivated influenza A/NewCaledonia/20/99 (H1N1). Adapted from [20]. **B** Schematic model of influenza A virus particle. The 8 single stranded RNA (ssRNA) genomic segments encode the structural proteins PB2, PB1, PA, HA, NP, NA, M1, M2 and NEP, the putative structural protein NS1 and the non-structural protein PB1-F2 that is only present in infected cells but not in incoming virions. Adapted from [21]. **C** Schematic representation of an influenza vRNP. The viral ssRNA is associated with multiple copies of NP and a single trimeric polymerase complex composed of PA (green), PB1 (blue) and PB2 (purple). The polymerase complex is bound to the double stranded panhandle structure at the complementary genomic ends (5'- and 3'-end depicted in dark grey and yellow, respectively). Contacts between NP monomers form an antiparallel double helix that is joined by a closed loop region. Adapted from [22,23].

Each of the 8 genome segments of influenza A virus encode one major viral protein. In addition, segments 7 and 8 encode the matrix protein 2 (M2) and nuclear export protein (NEP) that are derived from splice variants of the matrix protein 1 (M1) and non-structural protein 1 (NS1) viral messenger (mRNA), respectively [24,25]. These 10 pro-

teins represent the minimal number of proteins expressed by influenza A viruses. Depending on the viral strain, up to 7 additional proteins can be expressed from segments 1, 2, 3 and 7 either by alternative splicing (e.g. polymerase basic protein 2 S1 (PB2-S1)), ribosomal frame shift (e.g. polymerase acidic protein X (PA-X)) or through the usage of an alternative start codon (e.g. polymerase basic protein F2 (PB1-F2)) [26-30].

Table 1.1. vRNA segments and encoded proteins of influenza A/Pan/99 and A/Thai/04. Adapted from [31].

Genome Segment	Protein name	Protein length (aa)		Protein function
		A/Pan/99	A/Thai/04	
1	PB2	759	759	Subunit of the viral polymerase; involved in the recognition of 5`-capped host pre-mRNAs
2	PB1	757	757	Catalytic subunit of the viral polymerase; responsible for RNA chain elongation
	PB1-F2	90	90	Virulence factor; induces mitochondria-associated apoptosis
3	PA	716	716	Subunit of the viral polymerase; RNA endonuclease activity for cap snatching
4	HA	566	568	Receptor binding; mediates membrane fusion for release of vRNPs
5	NP	498	498	Major component of vRNPs; controls the nuclear cytoplasmic vRNA transport
6	NA	469	449	Cleaves sialic acids for the release of progeny virions
7	M1	252	252	Main component of the viral membrane; multiple roles in virion assembly and infection
	M2	97	97	Membrane protein that forms a proton channel; important for genome unpacking during virus entry
8	NS1	230	225	Antagonist of antiviral host cell response; regulates viral and host gene expression
	NEP	121	121	Mediates vRNP export from the nucleus

The viral strains used in this study, A/Panama/2007/1999 (H3N2) and A/Thailand/1(KAN-1)/2004 (in this thesis denoted as A/Pan/99 and A/Thai/04), are known to express at least 11 proteins (table 1.1). The proteins forming the trimeric polymerase complex, PB2, PB1 and PA, are encoded by segments 1, 2 and 3, respectively. Together with NP, expressed from segment 5, and the vRNA, they form vRNPs and are thereby structural components of influenza virions. Segment 7 encodes the structural proteins M1, which forms a layer between vRNPs and the viral envelope, and M2, a pH-dependent proton channel embedded in the envelope [32,33]. The spike-like structures on the lipid envelope are formed by the viral surface glycoproteins HA and NA. Binding of sialic acids (sa), which act as receptors for influenza viruses, and fusion of the viral and cellular envelope during endocytosis are mediated by the homotrimeric protein HA [34]. It is synthesized as a precursor protein (HA_0) that is post-translationally cleaved into HA_1 and HA_2. This cleavage is necessary to activate the fusion potential of HA and is thereby crucial for virus infectivity [35]. Whereas the HA protein is responsible for viral entry, tetrameric NA mediates the release of progeny viruses from the cellular membrane by cleavage of sialic acids [36]. Another structural protein, NEP, is encoded by segment 8 and mediates the nuclear export of newly formed vRNPs in the late phase of infection [37,38]. The NS1 protein, which is expressed from the same segment, acts as an antagonist of the antiviral host response [39]. The non-structural protein PB1-F2 enhances virus-induced cell death by suppressing the mitochondrial inner-membrane potential [40].

1.1.4 Replication

Influenza viruses are, like all other viruses, obligate intracellular pathogens that rely on the metabolism of their host cell for replication. The viral replication cycle involves 3 major steps: (1) viral attachment to the host cell, entry and uncoating, (2) viral gene expression and replication and (3) virion assembly, budding and release (figure 1.2).

(1) Influenza viruses attach to their host cell by binding to sialic acids on the cell surface, mediated by the viral protein HA [41]. Upon receptor binding, the viral particle enters the cell by clathrin-dependent and -independent endocytosis [42]. The acidic environment of the endosome triggers a conformational change of the HA protein that results in the exposure of the fusion peptide, which ultimately leads to fusion of the viral and endosomal membranes [43]. The low pH also results in the opening of proton channels in the viral envelope formed by M2, and a subsequent acidification of the virion interior [44].

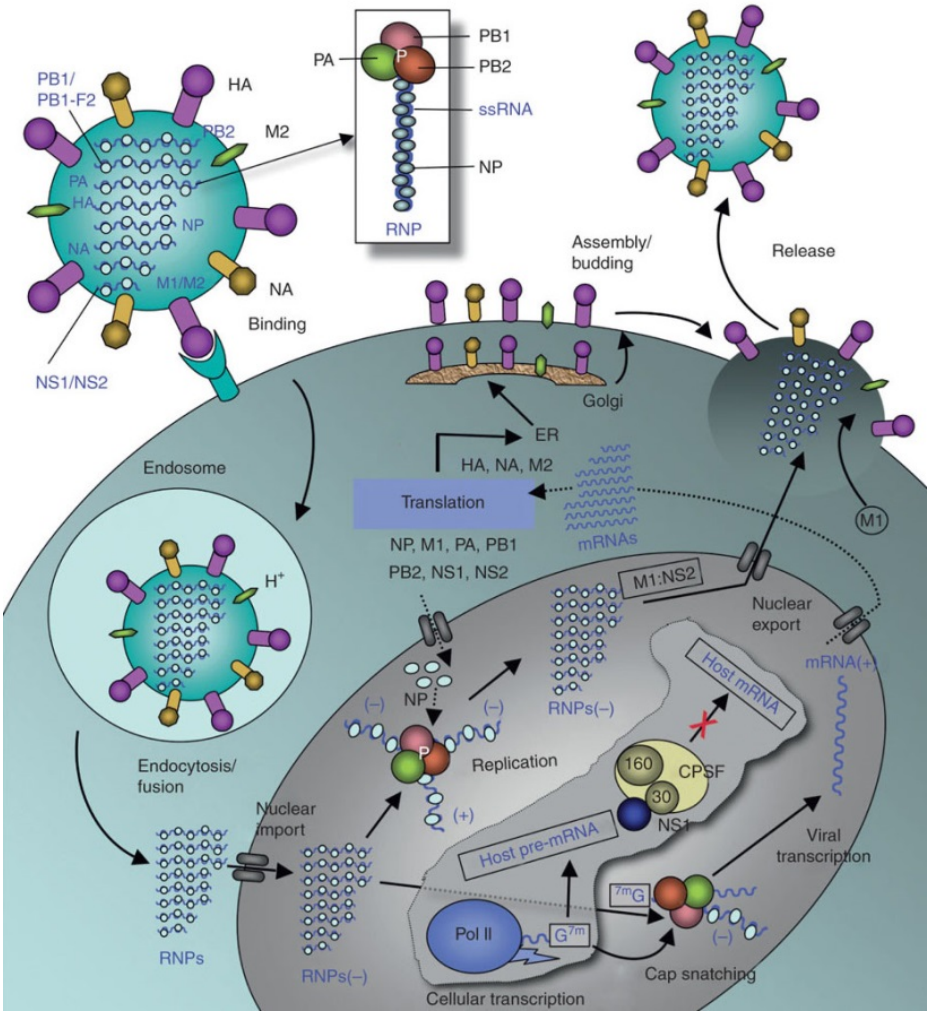

Figure 1.2. Replication cycle of influenza A viruses. Schematic representation of the Replication cycle of influenza A viruses, which is described in detail in the text. Adapted from Das et al. [45].

This allows the vRNPs to dissociate from the M1 proteins and to be released into the host cell cytoplasm [46], enabling their subsequent transportation into the nucleus. Nuclear import of vRNPs is mediated by the cellular importin-α – importin-β1 (IMPα-IMPβ1) pathway, in association with nuclear localization sequences (NLS) in the proteins of the vRNPs [47].

(2) Viral transcription as well as genome replication takes place in the nucleus of the infected cell. Both processes are catalyzed by the trimeric RNA-dependent RNA polymerase. After transcription, viral protein translation (which takes place in the cytoplasm and is catalyzed be the cellular translation machinery) and genome replication new vRNPs are formed. For further details about these processes see section 1.2.2.

Newly formed vRNPs are transported out of the nucleus in an exportin-1 (CRM1)-dependent manner. The CRM1 export machinery interacts with vRNPs in a 'daisy-chain' complex with viral NEP and M1, both transported into the nucleus after translation. CRM1 is bound to NEP that in turn is associated with M1, which interacts with vRNPs [48]. After nuclear export, newly-formed vRNPs are transported through the cytoplasm to the plasma membrane on microtubule networks, in association with RAB11-positive recycling endosomes [22]. At the plasma membrane the vRNPs unite with the post translationally modified (e.g. glycosylated, lipidation or phosphorylation) proteins HA, NA and M2, which are located at lipid raft domains [11,49].

(3) Assembly and budding of viral particles occurs at cholesterol-rich lipid raft domains in the plasma membrane of the infected cell where NA and HA accumulate, the so called budozones [50-52]. During assembly the M1 protein acts as a linker between the viral envelope and the viral genome, by binding to vRNPs as well as the cytoplasmic tails of NA and HA. Furthermore, M1 acts as a linker between HA and M2 [52]. The M2 protein, found at the edges of the budozones, mediates virus budding and scission by its amphipathic helicase (APH) region [52]. During M2-APH region mediated, cholesterol-dependent membrane curvature, M2 is found at the neck of the growing bud [52]. Constriction of the neck by M2 and cleavage of sialic acids by the NA protein ultimately leads to scission and release of progeny viral particles from the cell surface [36,52].

1.2 The trimeric polymerase complex

The viral RNA-dependent RNA polymerase is a trimeric complex that is composed of the viral proteins PA, PB1 and PB2. The complex is bound to the double stranded panhandle structure of each viral genomic RNA segment and, together with NP, forms the vRNP (for further details see section 1.1.3) [13,14]. Viral transcription as well as genome replication is catalyzed by the viral polymerase. Each component of the polymerase has distinct functions in these processes. PA and PB2 are involved in cap-snatching from cellular RNAs, which is essential for viral transcription. While PB2 binds the 5`-cap of nascent host capped RNAs via its cap-binding domain, the endonuclease PA cleaves the RNA downstream of the cap [53]. The capped RNA fragment is then used as a primer to initiate viral transcription. PB1, the catalytic subunit of the viral polymerase complex, is responsible for RNA chain elongation [54].

1.2.1 Viral polymerase structure

PB1 forms the center of the trimeric polymerase complex. It interacts with the N-terminal domain of PB2 via its C-terminal extension and is sandwiched between the C-terminal and N-terminal domains of PA (see figure 1.3.A and B) [23]. The core of the polymerase complex is composed of PB1, the N-terminal region of PB2 and the C-terminal domain of PA, while its flexible peripheral appendices are formed by the N-terminal endonuclease domain of PA, and the cap-binding, mid-link, 627 and NLS domains of PB2 [23] (for further details on PB2 structure see 1.2.4).

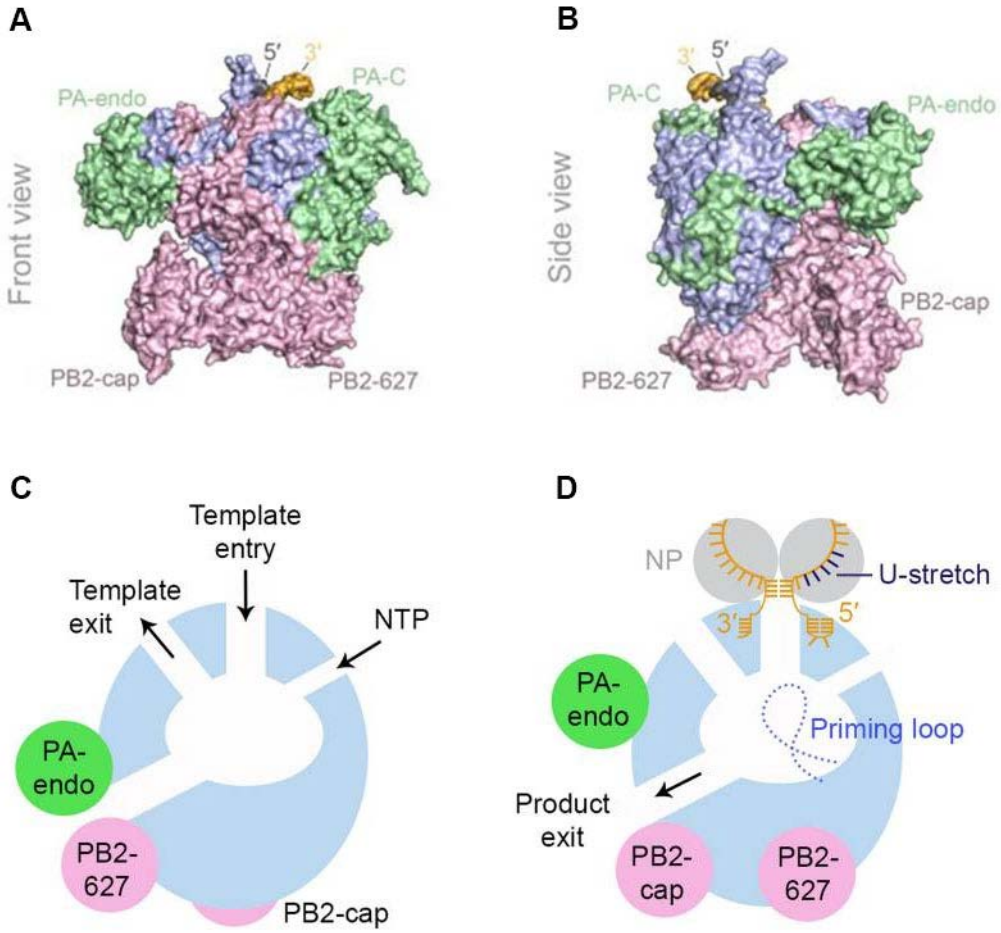

Figure 1.3. Structural details of the trimeric polymerase complex. A Front view and **B** side view of the polymerase structure surface model. PA, PB1 and PB2 subunits are depicted in green, blue and pink, respectively. The PA C-terminal (PA-C) and endonuclease (PA-endo) domains as well as the PB2 627-domain (PB2-627) and cap-binding (PB2-cap) domain are indicated. The 3′ terminus of vRNA is shown in yellow and the 5′ terminus in grey. **C** Model of the inactive, vRNA unbound, state and the **D** transcription pre-initiation state of the viral polymerase. The PB2 cap-binding domain and the PA endonuclease domain undergo rearrangements upon vRNA binding which results in a cap-snatching compatible conformation. 3'- and 5'-termini of the vRNA are depicted in yellow and NP is shown in light grey. Adapted from *te Velthuis et al.* [23].

The 5`- and 3`-termini of the genomic double stranded panhandle structure bind to distinct but spatially close sites in the polymerase complex. The 5`-end interacts with a pocket at the interface of PB1 and the C-terminal domain of PA, while the 3`-end binds on the surface of the polymerase at a site that is composed of amino acid (aa) residues from all 3 polymerase subunits [23]. Consistent with reports that cap-snatching is activated by vRNA binding to the polymerase, the determination of X-ray crystallographic structures of the polymerase complex revealed a conformational change in the complex upon binding to vRNA. The peripheral endonuclease domain of PA and the cap-binding domain of PB2 undergo major rearrangements, which result in a cap-snatching compatible orientation (figure 1.3.C and D) [23]. The polymerase active site is accessible via several channels; the template exit and entry channel, both located on the same side of the polymerase, the nucleoside triphosphate (NTP) entry channel and the product exit channel [23]. Another important feature is the priming loop located in the central cavity. This PB1 β-hairpin protrudes into the active site and has been shown to be important for primer independent replication initiation [55].

1.2.2 Transcription and replication

Viral transcription as well as genome replication takes place in the nucleus of the infected cell. The synthesis of viral mRNA, known as primary transcription, is independent of *de novo* viral protein synthesis but dependent on capped primers [56]. These are obtained from the 5`-end of cellular RNAs in a process called cap-snatching [57]. First, PB2 binds to the 5`-cap of cellular capped RNA; this is followed by cleavage of the RNA 10 to 13 nucleotides (nt) downstream of the cap by PA [53]. The preferred substrates for cap snatching are small nuclear RNAs (snRNA), small nucleolar RNAs (snoRNA) and capped small RNAs (csRNA) [23]. Subsequently, the 3`-end of the capped primer and the 3`-end of the vRNA template enter the polymerase active site via the product exit channel and the template entry channel, respectively [23]. After transcription initiation by the addition of a Guanosine (G) or a Cytosine (C) to the 3`-end of the primer, PB1 catalyzes the transcription of viral mRNAs and then adds a poly(A) tail by stuttering along the uridine-rich sequence at the 5`-end of the vRNA [58]. Stuttering is proposed to be due to steric hindrance of the polymerase caused by the 5`-end of the vRNA template [23]. The assembly of the newly synthesized viral mRNA into host-like messenger ribonucleoprotein (mRNP) structures is likely mediated by the binding of their 5`-cap to the nuclear cap-binding complex [23].

Processed viral mRNAs are transported to the cytoplasm and translated by the host cell translation machinery. Whether or not the trimeric polymerase complex is a stable

component of viral mRNAs also during their export to the cytoplasm is still a matter of debate [59-61]. Early transcription from incoming vRNPs leads to the expression of the early gene products PA, PB1, PB2 and NP, which are then subsequently transported into the nucleus [62]. While PB2 is imported by the importin α/β pathway on its own, PB1 and PA form a dimeric complex in the cytoplasm which is subsequently imported by RanBP5 [63]. The involvement of cellular chaperone proteins such as Hsp90 in the nuclear import of polymerase proteins has been proposed [64]. In the nucleus, the PB1-PA dimer and PB2 assemble to form the polymerase complex which then subsequently forms new vRNPs in combination with viral RNA and NP. These newly created vRNPs then serve as a template for transcription of the late genes HA, NA, NEP, M2 and M1 [62].

Replication of the viral genome, on the other hand, occurs in two steps and is primer independent. First a full-length genomic complementary RNA (cRNA) with positive polarity is synthesized. This is initiated by the formation of pppApG dinucleotides on residues Uridine (U) 1 and C2 at the vRNA 3`-end, which is dependent on structural support by the priming loop, and is catalyzed by the resident polymerase [23]. This newly synthesized cRNA serves in the second step as the template for the generation of newly formed full-length genomic vRNA. In this phase initiation begins on residues U4 and C5 and is independent of the priming loop. To allow for synthesis of a full-length cRNA copy, the pppApG dinucleotide is transferred to U1 and C2 residues [23]. The second stage of the replication cycle requires newly translated NP and polymerase proteins to form vRNPs with the newly synthesized genomic vRNA, thereby protecting the viral genome from degradation [65] and enabling it to be packaged in new virions.

1.2.3 Regulation by host cell factors

As an obligate intracellular parasite, influenza virus and its polymerase are dependent on the function of cellular proteins for replication. Several host cell factors have been described to interact with the polymerase complex and to regulate viral transcription and replication. Unlike other RNA viruses, influenza virus genome replication occurs in the nucleus and not in the cytoplasm of infected cells. More precisely, viral genomic transcription and replication is proposed to occur in DNase insensitive nuclear regions like the nuclear matrix, or close to the chromatin. The targeting of the viral polymerase to these nuclear regions is suggested to be mediated by its interactions with the nuclear matrix protein NXP2/MORC3, the chromatin remodelers CHD1 and CHD6 and the DNA-dependent RNA polymerase II (Pol II) function modulator CLE/C14orf166 [23].

The viral polymerase complex was also shown to interact with the serine-5 phosphorylated form of the C-terminal domain of the large subunit of Pol II, a form that is known to recruit cellular capping enzymes, hence facilitating its access to nascent capped host RNAs [66]. In addition, this interaction brings the viral RdRp close to the cellular factors involved in splicing and assembly of mRNPs, thus promoting viral mRNA processing. Since mRNAs for the viral proteins M1, NS1 and PB2 undergo splicing to allow for expression of M2, NEP and PB2-S1, it is not surprising that factors of the cellular splicing machinery, namely RED, SMU1, NS1-BP, SFPQ/PSF, hnRNPK and SF2/ASF, have been shown to be important for replication of influenza viruses [23].

The Pol II interacting cellular helicase minichromosome maintenance (MCM) complex, which is involved in Pol II elongation and DNA replication, was also demonstrated to participate in vRNA replication through interaction with PA. MCM seems to trigger the shift from initiation to elongation during viral RNA replication [67].

The second step of the replication cycle, vRNA synthesis from cRNA, was shown to be boosted through the interaction of the viral polymerase with the cellular factors of the protein family ANP32, ANP32A and ANP32B which are involved in cell death, mRNA export and transcription regulation by chromatin remodeling. PB2 627-domain related host restriction was assigned to species differences in ANP32A protein [68]. Also specific importin-α was shown to influence viral RNA replication in a host dependent manner by its interaction with PB2 (see section 1.2.4 for further information on ANP32A and importin-α) [69].

Stimulation of viral RNA replication by recruitment of NP to nascent vRNA during vRNP assembly or by promoting NP interactions with the viral RNA polymerase was shown to be mediated by the transcription factor HTAT-SF1, the spliceosome RNA helicase UAP56 (also known as DDX39B or BAT1) and the translation stimulator FMR1 [23].

1.2.4 The polymerase component PB2

The 759 aa long protein PB2 is part of the cap-snatching process and is an important factor in host range determination [70,71]. PB2 consists of several domains (figure 1.4). The N-terminal third mediates the interaction with the PB1 protein of the polymerase complex and includes the lid domain [23]. In addition, the N-terminal region also contains a mitochondrial localization signal. PB2 that accumulates in mitochondria interacts with the mitochondrial antiviral signaling protein (MAVS) and thereby inhibits MAV-mediated interferon β (IFNβ) expression [72]. However, the mitochondrial localization signal, and the resulting accumulation of PB2 in the mitochondria, has so far only been found in

seasonal influenza viruses and not in H5N1 viruses. The remaining 2/3 of the PB2 protein contain the mid domain, the cap-binding domain, the cap-627 linker, the 627-domain and the C-terminal nuclear-localization signal domain [23].

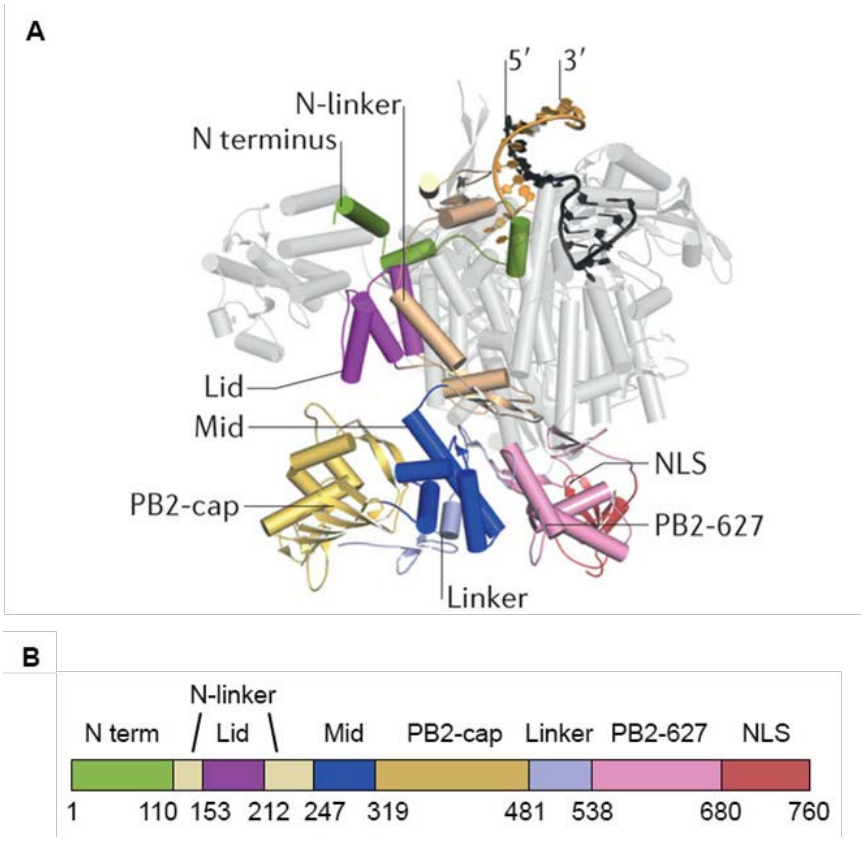

Figure 1.4. Ribbon diagram and subunit domain structure of the polymerase protein PB2. **A** The trimeric polymerase complex (PB1 and PA in light grey) is associated with the 3'- and 5'-termini (depicted in yellow and dark grey, respectively) of the viral RNA. **B** The PB2 subunit is composed of the N terminus, N-linker, lid domain, mid domain, PB2-cap domain, cap-627-linker, 627-domain and a nuclear localization signal (NLS). Adapted from [23,73].

The 627-domain is named after the amino acid position 627 which is linked to the host range of influenza viruses [71]. PB2 proteins from mammalian influenza isolates generally harbor a lysine (K) at position 627, whereas in avian isolates glutamic acid (E) is usually found at that position [71]. The role of the 627-domain in host adaptation was linked to differences between avian and mammalian ANP32A protein [68]. In comparison to mammalian ANP32A, the avian ANP32A protein possesses an additional 33 aa long sequence between its leucine-rich repeat (LRR) domain and its low-complexity acidic region (LCAR). When this 33 aa sequence was inserted into overexpressed mammalian ANP32A, the poor activity of avian RdRp in mammalian cells was rescued, while deletion of this sequence from overexpressed avian ANP32A abrogated avian

polymerase activity in mammalian cells [68]. It was observed, that infection of humans with avian H5N1 or H7N9 subtypes leads to the rapid selection of mammalian type K627 in PB2, which adapts the avian polymerase for the shorter mammalian ANP32A protein [68]. For further details on the 627-domain and host range determination see section 1.3.3.

Freshly translated PB2 is transported into the nucleus via the importin α/β pathway, [63] and a physical interaction between importin-α and PB2 has previously been demonstrated[69]. A study on this interaction revealed that mutation of the PB2 NLS results in the reduced, but not completely abrogated nuclear localization of this protein [69]. While the formation of the trimeric polymerase complex was not altered by the mutated PB2 protein, polymerase activity was abolished. Insertion of the ectopic SV40 TAg NLS into the mutant PB2 protein restored the diminished nuclear localization, but did not rescue polymerase activity [69]. Hence, it was concluded that the decrease in polymerase activity was not due to the reduced transport of PB2 into the nucleus. It was proposed that importin-α, in addition to its role in PB2 nuclear import, is also important for optimal viral RNA synthesis [69]. It was also observed that co-purification of human α-importins with the PB2 protein of avian H5N1 strains was reduced compared to the co-purification of human α-importins with PB2 of seasonal H3N2. This correlates with the reduced replication capacity of the avian influenza RdRp in human cells and suggests a role for PB2 interaction with importin-α in host range determination [69].

1.3 Low pathogenicity and highly pathogenic influenza viruses

1.3.1 Low pathogenicity and highly pathogenic influenza viruses in birds

Influenza strains that have evolved in birds are known as avian influenza viruses. On the basis of their pathogenicity in chickens, avian influenza viruses can be divided into low pathogenicity avian influenza virus (LPAIV) and highly pathogenic avian influenza virus (HPAIV) strains [74]. Whereas LPAIV strains normally only cause mild disease in poultry and wild birds, infection with HPAIV leads to a severe disease with a case fatality rate up to 100 % [75]. Only influenza viruses bearing H5 or H7 on their surface are known to be highly pathogenic in birds, and these HPAIV strains always arise by mutations of H5 or H7 in low pathogenicity strains. Amino acid changes in the proteolytic cleavage site of the HA protein have been associated with a shift in pathogenicity [74].

The world organization for animal health (OIE) defines an avian influenza virus isolate as highly pathogenic if it results in a case fatality rate of >75 %, or an intravenous pathogenicity index (IVPI) of >1.2 in experimentally infected chickens. Also low pathogenicity H5 and H7 strains that have a HA proteolytic cleavage site sequence similar to HPAIV are considered to be highly pathogenic [74]. However, H5 and H7 isolates of both low and high pathogenicity are notifiable. If HPAIV is detected, the whole livestock will be depopulated and other flocks in the surrounding area will also either be culled or quarantined to prevent the spread of disease. Besides the enormous economic loss caused by HPAIV outbreaks in birds, an outbreak of both low pathogenicity and highly pathogenic avian influenza virus also harbors the risk of introducing the infection into the human population.

1.3.2 Avian influenza viruses in humans

Certain avian influenza viruses have the potential to cross the species barrier into humans. For example, infection of humans with avian influenza viruses of the subtype H5N1, H7N9, H7N7 and H9N2 have been reported [76]. In patients infected with H7N9 or HPAI H5N1 viruses, the disease often has an aggressive clinical course.

After an incubation period of 2-17 or 1-10 days for H5N1 or H7N9, respectively, patients can develop high fever, cough and lower respiratory tract disease [77,78]. Some patients also show atypical symptoms including diarrhea, vomiting, abdominal pain and bleeding from the nose and gums [79]. Complications can include hypoxemia, bacterial and fungal secondary infections and multiple organ failure [76]. The case fatality rate of influenza virus disease in humans caused by avian H5N1 or H7N9 subtypes is much higher compared to infection with seasonal Influenza viruses.

The first cases of H5N1 infection in humans were reported in 1997 in Hong Kong during an H5N1 outbreak in poultry. Since then, a total number of 860 human H5N1 cases with 454 deaths (resulting in a case fatality rate of ~53 %) have been recorded by the WHO [80,81]. On the other hand, with 613 deaths since the first human case in China in 2013, H7N9 subtypes exhibit a case fatality rate of ~39% in humans [82]. So far, all 1,566 human cases of H7N9 infections have been reported from China. In comparison, the case fatality rates of the 1957 and 1968 influenza virus pandemics were around 0.1 %, and the devastating influenza virus pandemic in 1918-19 had an approximate case fatality rate of >2.5 % [83].

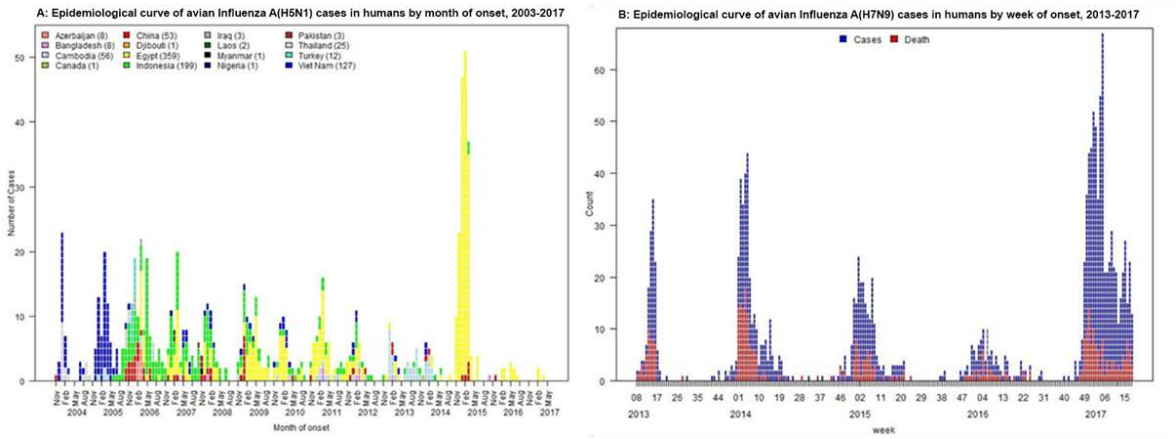

Figure 1.5. Laboratory-confirmed cases of avian influenza virus in humans. A Human cases of H5N1 infection since 2003 by month of onset. The different colors represent the country where the infection occurred. **B** Human cases of H7N9 infection since 2013 by week of onset. All cases were detected in China. Depicted are laboratory confirmed infections (blue) and lethal cases (red). Adapted from [84].

Avian influenza viruses are mainly transmitted from infected animals to humans. Patients had either direct contact (e.g while slaughtering) or indirect contact (e.g. whilst visiting a poultry market) with infected poultry. The limited cases of human-to-human transmission have been attributed to close contact between the index patient and subsequent cases [85,86]. For example, the mother and aunt of an 11-year old index patient from Thailand were both infected after providing bedside care for the sick girl whilst in the hospital [85]. Both mother and daughter succumbed to the disease. Tragic cases like this are however rare and sustained human-to-human transmission is yet to be reported. Health authorities nonetheless monitor patients infected with avian influenza viruses very closely. In 2012 a study published by *Herfst et al.* showed that only 9 aa substitutions in the genome of a highly pathogenic H5N1 virus isolated from a human case could be sufficient to facilitate airborne transmission from ferret to ferret, the best available small animal model for influenza research in mammals [87]. Even though none of the ferrets died after infection with the mutated airborne virus, this study illustrates the potential of avian influenza viruses to become transmissible via aerosols between mammals.

1.3.3 Differences and similarities of seasonal H3N2 and HPAI H5N1 viruses in humans

HA

All known influenza viruses, with the exception of influenza viruses found in bats, attach to their host cells by binding of HA (embedded in the virus envelope) to sialic acids present on the surface of susceptible cells. Sialic acids are composed of nine-carbon backbone sugar units which are attached to the end of longer sugar chains that line the surface of vertebrate cells [88]. Human adapted influenza viruses preferentially bind to sialic acids that are anchored to the sugar chain by an α-2,6-linkage (SAα2,6), which are abundant on the human respiratory epithelia [89,90]. In contrast, avian influenza viruses prefer α-2,3-linked sialic acids (SAα2,3) that can be found in the avian intestinal tract as well as in the lower respiratory tract of humans [91,92] (figure 1.6.A).

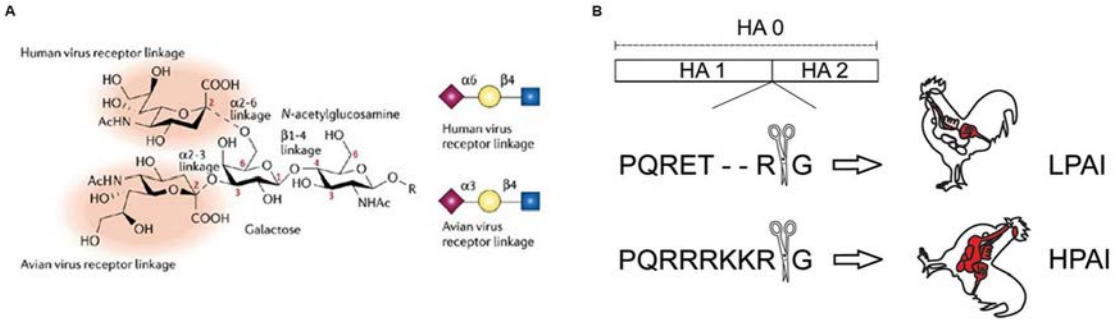

Figure 1.6. Hemagglutinin, species specificity and pathogenicity. A Structure of sialic acid and its linkage to the last galactose of sugar chains which are present mainly on proteins and lipids on vertebrate cell membranes. Human viruses preferentially bind to α-2,6-linked sialic acids (human virus receptor linkage) whereas avian viruses prefer α-2,3-linked sialic acids (avian virus receptor linkage). Adapted from [93]. **B** HA cleavage site of LPAI and HPAI viruses. The cleavage of the precursor protein HA_0 into HA_1 and HA_2 by cellular proteases is essential for viral infectivity. HA proteins of LPAIV contain a monobasic cleavage site that can only be cleaved by extracellular trypsin-like proteases present in the respiratory and intestinal tract of poultry. The introduction of additional basic amino acid residues into this cleavage site allows the HA protein to be cleaved by intracellular furin-like proteases that are ubiquitously expressed. The acquisition of a multibasic cleavage site enables the virus to spread systemically and become highly pathogenic in poultry. Adapted from *Schrauwen et al.* [94].

Whereas seasonal influenza viruses can infect the upper respiratory tract (URT) as well as the lower respiratory tract (LRT) in humans through binding of HA to SAα2,6 on for example epithelial cells of the pharynx or on type II pneumocytes of the lung, H5N1 viruses attach to SAα2,3 on type II pneumocytes, alveolar macrophages and non-ciliated bronchiolar cells in the human LRT [92,95]. Hence, the preference of avian HA for

SAα2,3, which usually acts as a species barrier between birds and humans, facilitate a LRT manifestation, e.g. pneumonia, in humans that become infected with avian H5N1[79]. While infection with seasonal influenza virus is usually limited to the respiratory tract, patients infected with H5N1 can also present with symptoms including diarrhea, vomiting and seizures, that hint at a systemic spread of the virus [1,79]. This suspicion is supported by isolation of the H5N1 virus from cerebrospinal fluid, rectal, throat and serum specimens from a 4-year old boy that died from the infection and the detection of viral RNA in rectal and blood samples of several other fatal human cases [96,97] .

In avian species, infection with a highly pathogenic influenza virus strain is always accompanied by a systemic spread of the virus, whereas infection with a low pathogenicity strain is restricted to the respiratory and intestinal tracts [98]. This shift in tissue tropism, and resulting shift from low pathogenicity to highly pathogenic, is known to be due to the acquisition of a multibasic cleavage site (MBCS) in the HA protein of LPAI viruses [99,100]. While the HA protein of LPAIV can only be cleaved by extracellular trypsin-like proteases present in the intestinal and respiratory tract in poultry, the acquisition of a MBCS enables the HA to be cleaved by ubiquitous intracellular furin-like proteases and the virus to be spread systemically (figure 1.6.B) [101,102]. However, the association between systemic spread, pathogenicity and the presence of a MBCS in HA is less clear in mammals. None of the pandemic or seasonal human influenza virus strains carry a MBCS in HA. The introduction of a multibasic cleavage site into the HA protein of a human seasonal H3N2 strain didn`t lead to a systemic virus spread or an increase in virus pathogenicity in ferrets [103]. In contrast, the presence of a MBCS is indispensable for the systemic spread of H5N1 in ferrets [104]. And even though all H5N1 isolates from human cases harbor a multibasic cleavage site, the severity of the disease in humans varies from mild to lethal [105]. Hence, the presence of a MBCS does not entirely correlate directly with an aggressive clinical disease course in humans.

PB2

The adaptation of the polymerase complex of avian influenza viruses to mammalian host factors is of great importance for interspecies transmission, since it allows for efficient replication in the new host. Several mutations in the proteins of the viral polymerase complex have been described to increase avian influenza polymerase activity in mammalian cells, for example L472V and L598P in the PB1 protein [106]. However, most of these adaptive mutations were found in the PB2 protein [107]. This includes the most prominent and intensively studied mutation E27K.

PB2 proteins from mammalian influenza virus isolates generally contain a lysine (K) at position 627, whereas in avian isolates glutamic acid is usually found at this position [71]. The importance of the aa at position 627 for host adaptation is supported by the finding that the polymerase activity of an avian influenza virus RdRp in human embryonic kidney 293T (HEK293T) cells, is dramatically increased after the exchange of glutamic acid with lysine at position 627 [108]. In addition, the substitution of the mammalian-type PB2 enables H5N1 avian influenza viruses to replicate in a broader range of mammalian cells and at lower temperatures [109]. PB2 K627 is also linked to an increased virulence of a human H5N1 isolate in mice [110]. The role of the 627-domain in host adaptation was linked to differences between the avian and mammalian ANP32A protein [68] (see section 1.2.4).

Even though all these data underline the importance of lysine at position 627 in PB2 for avian influenza viruses in mammalian hosts, differences in amino acids at this position alone are not solely responsible for the effective infection of humans with avian influenza viruses and the clinical outcome of the disease. Several avian influenza virus isolates from human cases lack the E627K substitution in their PB2 protein [79]. For example the HPAIV strain used in this study, A/Thailand/1(KAN-1)/2004, that was originally isolated from a 6-year old boy who succumbed to the infection, harbors the avian-type E627 PB2 [111,112]. To compensate for the lack of PB2-K627, A/Thai/04 acquired an adaptive mutation in the nuclear export protein, namely a methionine to isoleucine substitution at position 16 (M16I), to enhance its polymerase activity in mammalian cells [112]. The acquisition of the M16I substitution only in human isolates of HPAIV with avian-type E627 but not with mammalian-type K627, underlines the importance of the polymerase, and especially the PB2 protein, for adaption of HPAIV to humans.

1.4 Heat shock proteins

Members of the heat shock protein (HSP) family are ubiquitous proteins that can be found in every organism [113]. The gene families that encode heat shock proteins are highly conserved among species and were originally named after their expression in response to heat shock [114] (gene names are used throughout the thesis to describe the genes as well as the proteins for clarity reasons). However, they are not only induced by heat stress but also after exposure to other stressful conditions such as cold, nicotine, ischemia, UV light, anoxia, heavy metal ions, surgical stress and viral agents [114]. HSPs are important for the stabilization and three-dimensional refolding of (damaged) proteins during stress [115]. HSPs functions in protein folding, assembly, translocation

and degradation are however not only essential under stressful conditions but also during optimal cellular growth [115].

Heat shock proteins can be grouped into 6 major families based on their approximate molecular weight: HSP100, HSP90, HSP70, HSP60, HSP40 and small HSPs (sHSP) [116]. Each family is part of the protein "life cycle". For example, while HSP60 is important for the early stages of protein folding, HSP90 acts at the late stages of protein folding and targets substrates for proteolysis [117]. The HSP100 family disembles misfolded proteins containing aggregates and delivers substrates to proteases [117]. HSP70 family members have a coordinating function by directing protein substrates for folding, translocation, unfolding, disaggregation or degradation [117]. Hence, even though their name highlights their role during cellular stress, members of the heat shock protein families are also constitutively expressed and play a fundamental role in cellular homeostasis.

1.4.1 HSPA8

HSPA8, also known as heat shock cognate 71 kDa protein (Hsc70), belongs to the most abundant chaperone family, HSP70, and is a major cytosolic molecular chaperone [118]. However, HSPA8 is also located in various cellular locations such as the nucleus and close to the cellular membrane [118].

HSPA8 consists of three regions: an N-terminal 44 kDa adenosine triphosphate (ATPase) domain, also known as ATP binding domain, a central 18 kDa substrate binding domain and a C-terminal 10 kDa "variable" or "lid" domain [118]. Even though HSPA8 shares 85 % amino acid similarity with the stress inducible, well described heat shock 70 kDa protein 1A (HSPA1A), also sometimes referred to as HSP70, HSPA8 differs greatly in its C-terminal domain which is involved in mediating substrate specificity [118]. The binding of HSPA8 to small hydrophobic stretches of substrate proteins is regulated in an ADP/ATP dependent manner (see figure 1.7) [119]. First, the substrate is bound to HSPA8 in its ATP-bound "low affinity, fast-exchange rate" state. Then, the intrinsic ATPase activity of HSPA8 leads to the hydrolysis of ATP, in cooperation with co-chaperones. This initializes a conformational change in HSPA8 and the transition to its ADP-bound "high affinity, slow-exchange rate" state [119]. The protein substrate is released after ADP is exchanged for a new molecule of ATP. ADP release is the rate limiting step in the ATPase reaction and is stimulated by nucleotide exchange factors (NEFs) [118]. The BAG domain protein family has been described as one type of human NEF [120]. The families 6 members, BAG1-6, are characterized by the presence of the

so-called BAG-domain at their C-terminus which is responsible for their binding to the ATPase domain of HSPA8. BAG-domain containing proteins compete with the ADP-state stabilizing co-chaperone Hip for binding to the HSPA8 ATPase domain, and modulate chaperone activity [118].

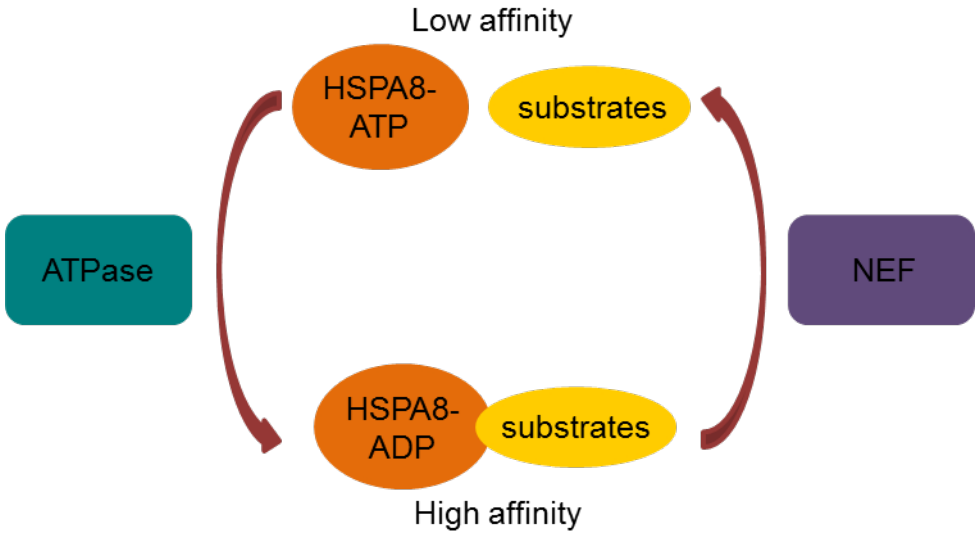

Figure 1.7. Model for the substrate binding and release cycle of HSPA8. Substrate binding and release is regulated in an ADP/ATP dependent manner. The substrate is bound with low affinity to the ATP-bound "high-exchange rate" state of HSPA8. In cooperation with co-chaperones, the ATPase domain of the heat shock protein hydrolyses ATP, whereupon the substrate is bound with high affinity to the ADP-bound "slow-exchange rate" state. Release of ADP is stimulated by NEFs and the ADP/ATP exchange results in substrate liberation. Adapted from Liu et al. [118].

HSPA8 was first described as a clathrin-uncoating ATPase during clathrin-mediated endocytosis [121]. Clathrin binds membrane cavities, which are stimulated by binding of ligands to transmembrane receptors, and leads to the formation of endosomes. HSPA8 mediates the release of clathrin by disrupting clathrin heavy chain interactions, which is important for fusion of the endosome with its target compartments [119]. Ever since its discovery, additional functions of the HSPA8 chaperone in a variety of cellular processes during optimal or stress conditions have been described. For example HSPA8 is involved in facilitating the maturation of newly synthesized proteins, it plays a role in nuclear export and import of substrate proteins and reactivates heat denatured proteins. HSPA8 is also part of the ubiquitin-proteasome degradation system [118]: It interacts with the E3 ubiquitin ligase CHIP, which leads to the coupling of ubiquitin chains to the chaperones substrate, resulting in its proteasomal degradation [119]. The NEF protein BAG2 acts as an inhibitor of this CHIP mediated degradation process [118]. HSPA8 has also been shown to play a role in the replication cycle of a variety of viruses. For ex-

ample, HSPA8 is important for the formation of the pre-replicative site of herpes simplex virus type 1 (HSV-1) [122], functions as a receptor for Japanese encephalitis virus [123] and interacts with the RNA-dependent RNA polymerase of turnip mosaic virus [124].

In contrast to other family members, HSPA8 is constitutively expressed and only moderately induced during cellular stress [118]. However, while HSPA8 shuttles between the cytoplasm and the nucleus, (with a preference for cytoplasmic localization under optimal growth conditions) HSPA8 concentrates in the nucleus during stress [118]. This nuclear localization of HSPA8 has also been observed in cells infected with influenza virus [125].

1.4.2 HSPA8 and influenza

The role of HSPA8 in influenza virus infection has been most extensively investigated in the context of vRNP nuclear export. *Watanabe et al.* showed that HSPA8 interacts with the influenza virus M1 protein [125]. This interaction is mediated by the N-terminal half of the HSPA8 substrate binding domain and the C-terminal half of M1 [126]. An involvement of the ATPase activity of the heat shock protein was shown to be unlikely [126]. Immunofluorescence staining of MDCK and HeLa cells infected with the influenza virus strain A/WSN/33 (H1N1) or A/PR8/33 (H1N1), respectively, revealed that HSPA8 was dominantly localized in the nucleus during infection [125]. However, the change in localization of HSPA8 was only observed at late time points of infection (9 hours post infection (p.i)), correlating with M1 expression and localization, and not at early time points (3 hours p.i). The importance of HSPA8 in the viral replication cycle was demonstrated by the reduced viral titers observed in HSPA8 siRNA treated cells [125].

The observation that M1 and NP failed to be exported from the nucleus in HSPA8 knock down cells led to the assumption that the heat shock protein is involved in the nuclear export of vRNPs [125]. The presence of HSPA8 in purified vRNP fractions and purified virions also argues for a virus supportive role of this factor [62]. It was proposed, that HSPA8 mediates the export of vRNPs through the CRM1-dependent pathway (see figure 1.8.) [62]. Further investigations revealed that HSPA8 not only does not interact with the nuclear export protein of influenza virus, it also competes with NEP for binding to M1 [126]. The observation that the binding between M1 and HSPA8 is stronger than the binding between M1 and NEP, further implies an important role for HSPA8 in the nuclear export of vRNPs [126]. A role for HSPA8 in the nuclear import of incoming vRNPs could not, however, be detected [62].

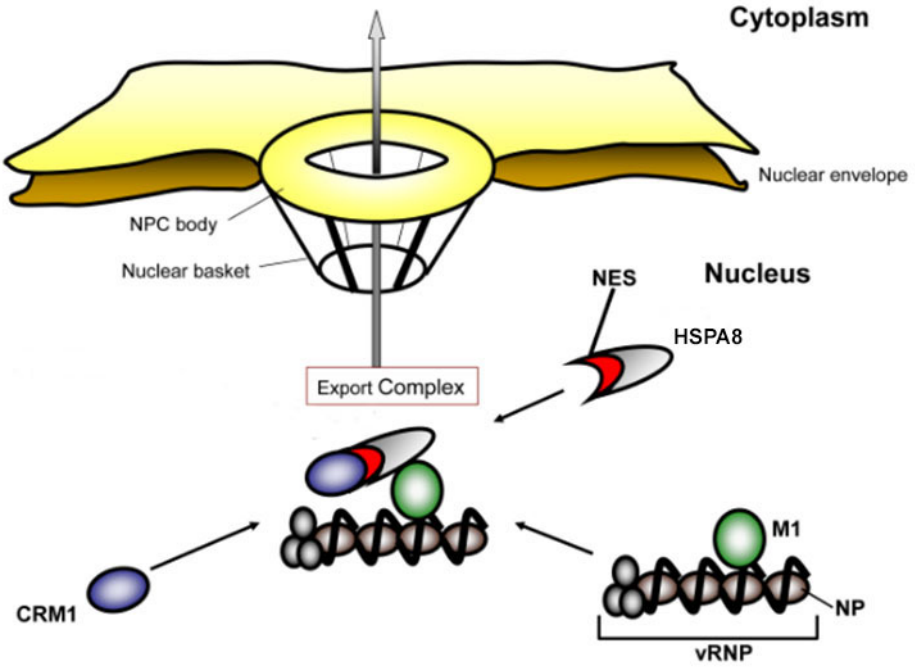

Figure 1.8. Model of the HSPA8 related nuclear export of vRNPs. vRNP bound M1 binds to HSPA8 which in turn interacts with CRM1 via its nuclear export signal. The CRM1-HSPA8-M1-vRNP complex is exported from the nucleus, CRM1 is released, and part of HSPA8 is potentially incorporated into newly formed virions. Adapted from *Watanabe et al*. [62].

Bortz et al. described a decrease in polymerase activity of the viral strains A/WSN/33 (H1N1) or A/VN/1203/04 (H5N1) after siRNA depletion of HSPA8 [127]. A549 cells were co-transfected with HSPA8 siRNA and polymerase activity assay reporter genes. After the knock down, cells were infected with A/VN/1203/04 or A/WSN/33 and polymerase activity was determined by the measurement of reporter gene expression.

In this experimental setup, HSPA8 knock down lead to a decrease in influenza virus polymerase activity. However, this effect was not seen in the classical influenza virus polymerase activity assay in 293T HSPA8 knock down cells. In this assay cells were not infected with influenza virus but transfected with plasmids expressing the viral PA, PB1, PB2 and NP, in addition to plasmids encoding the polymerase activity assay reporter genes [127]. Hence, *Bortz et al*. concluded that the requirement of HSPA8 for optimal polymerase function only in influenza virus infected cells, may be due to the role of HSPA8 in the cellular response to stress, rather than to a specific function for HSPA8 in influenza virus polymerase activity [127].

1.5 Mass spectrometry

Mass spectrometry is an analytical technique which allows for the identification, quantification and determination of chemical and structural properties of molecules. It can be used to analyze small molecule compounds, complex peptide and protein mixtures and even whole cellular proteomes. A proteome is defined as the complete set of proteins expressed by an organism or cell at a given time point under defined conditions [128]. The proteome is larger than the genome since proteins encoded by the same gene can undergo different post-translational modifications (PTMs) to generate several protein variants. In addition, the proteome of even a single cell can change dramatically in response to different stimuli, which further increases the complexity of proteome studies [129]. Mass spectrometry analysis can decipher this complexity and provides more detailed information compared to other techniques such as two-dimensional gel electrophoresis (2DE) [129]. Hence, mass spectrometry represents a powerful tool for the analysis of protein expression, modifications or interactions.

1.5.1 MS principles

Mass spectrometry (MS) analysis is based on the ionization of molecules and measurement of their mass-to-charge ratio (m/z). Hence, a mass spectrometer consists of an ion source, a mass analyzer and an ion detector. First the ion source ionizes the molecules. The most common techniques utilized for the ionization of peptides are electrospray ionization (ESI), where the sample is in a liquid phase, and matrix-assisted laser desorption/ionization (MALDI), where the sample is associated with a solid matrix. After ionization the molecules are guided through the mass analyzer where they are sorted according to their mass-to-charge ratios. There are different types of mass analyzers: ion trap, time-of-flight (TOF), Fourier transform-ion cyclotron (FTICMS), quadrupole and Orbitrap analyzers. Since each analyzer has its own advantages and disadvantages, the choice depends on the type of experiment that will be performed and the specific demands that come with it. Parameters like dynamic range, speed of analysis, sensitivity, mass accuracy and resolution need to be taken into account. The dynamic range of the instrument is the range over which ion signal and analyte concentration is directly proportional. Speed refers to the number of spectra that can be generated per unit of time. The sensitivity of a mass spectrometer is defined by the lowest amount of analyte that can be detected, whereas mass resolution describes the lowest difference in m/z ratios that can be distinguished. Mass accuracy is the discrepancy between the measured and the true m/z ratio.

For the analysis of proteins by MS, two different approaches can be used. In top-down proteomics (mainly used for the analysis of simple mixtures or individual proteins) the whole protein is analyzed, whereas in the bottom-up approach peptides of proteolytically digested proteins are introduced to the MS analyzer. Peptide identification is achieved by alignment of the received peptide spectra with a peptide spectral library, or by comparing the detected peptide masses with those predicted from a sequence database. Computational tools enable the assembly of identified peptides into protein sequences. Bottom-up proteomics is used for the analysis of complex protein mixtures and was employed in the experiments described in this thesis. An important aspect that needs to be considered is the possibility that peptides may have the same mass even if they have different sequences. To clearly identify peptides nonetheless, a technique called tandem mass spectrometry (MS/MS) can be employed. After a first MS scan (MS1) of peptide ions, a subset of peptides are selected based on their determined m/z ratio. These peptides are further fragmented by collision induced dissociation (CID) and analyzed in a second MS scan (MS2). The combination of spectra information from MS1 and MS2 allows for high accuracy peptide identification [130].

The tandem MS employed in this study was performed using the linear ion trap quadrupole (LTQ)-Orbitrap XL, a hybrid mass spectrometer with two sequential mass analyzers. The Orbitrap is used for the full scan of the peptide mixture (MS1) and is characterized by a high dynamic range, mass resolution and accuracy. The following scan (MS2) is conducted by the very sensitive and fast linear ion trap quadrupole. The technical process of tandem MS analysis by LTQ-Orbitrap starts with peptide ionization by ESI which results in the production of positively charged molecules. These peptide ions are trapped in the electrostatic field of the Orbitrap and start to oscillate around the central electrode. At this stage ions with different mass-to-charge ratios oscillate at different frequencies around the electrode, resulting in their separation. The oscillation amplitude represents the signal intensity which correlates with the amount of peptide. Fourier Transformation (FT) is then used to obtain the precursor ion spectrum (M1) from the detected signals [131].

The precursor ions with the five most intense peaks are selected for the second MS scan. These selected precursor ions are isolated, fragmented into smaller peptides by collision with inert gas molecules and then analyzed in the linear ion trap quadrupole, thereby generating the MS2 spectra.

As mentioned above, high-throughput MS/MS is employed for complex samples of proteolytically digested proteins. This technique results in millions of spectra which cannot be interpreted manually. Therefore, in order to process raw MS data a search engine

has to be used. The MS data obtained in this study were analyzed using MaxQuant software, a set of algorithms which enable the identification and quantification of proteins. After the correction of systemic inaccuracies in measured peptide masses and the assembly of the mass and intensity of the peptide peaks into 3D peak hills, the peptide and peptide fragment masses of MS1 and MS2, respectively, are searched in an organism specific sequence database [132]. To avoid false positives, a target-decoy-based false discovery rate (FDR) approach is applied [132]. The FDR represents the percentage of random identifications and indicates the quality of peptide identification [133]. In addition to the target sequences, the organism specific database also includes their reverse counterparts and contaminants to support correct peptide identification [132]. The assembly of peptide hits to protein hits results in the identification of proteins [132].

1.5.2 Stable isotopic labelling by amino acids in cell culture (SILAC)

Stable isotopic labelling by amino acids in cell culture (SILAC) is a method for quantitative MS and was developed by Matthias Mann and coworkers [134]. It enables the assignation of peptide signals to a specific sample set in a sample mixture and allows the difference in protein abundance between the different sample sets to be detected and relatively quantified (see figure 1.9). The method is based on the incorporation of non-radioactive amino acid isotopes into cellular proteins during cell growth. In order to achieve this, cells are grown in medium lacking specific natural amino acids, which are replaced by the same but isotopically labeled amino acids. To assure incorporation of isotopically labelled amino acids and complete labelling of cellular proteins, essential amino acids are isotopically labelled. Even though isotopically labelled forms of all 20 naturally occurring essential and non-essential amino acids are commercially available, L-lysine (K) and L-arginine (R) are the preferred choices. The most commonly used enzyme in proteomics (trypsin) cleaves proteins immediately after lysine and arginine residues. Therefore, except for the C-terminal peptide, labelling of all peptides is ensured when isotopically labelled arginine and lysine are used in combination with trypsin for proteolytic digestion.

Proteins from cells labelled with different combinations of isotopically distinguishable arginine and lysine are identical except for a small mass difference of a few Dalton. The cells themselves also behave the same and exhibit no differences in protein composition [134,135]. After complete labelling of cellular proteins, differently labelled cells are lysed and mixed in same protein proportions prior to further sample preparation for mass spectrometry.

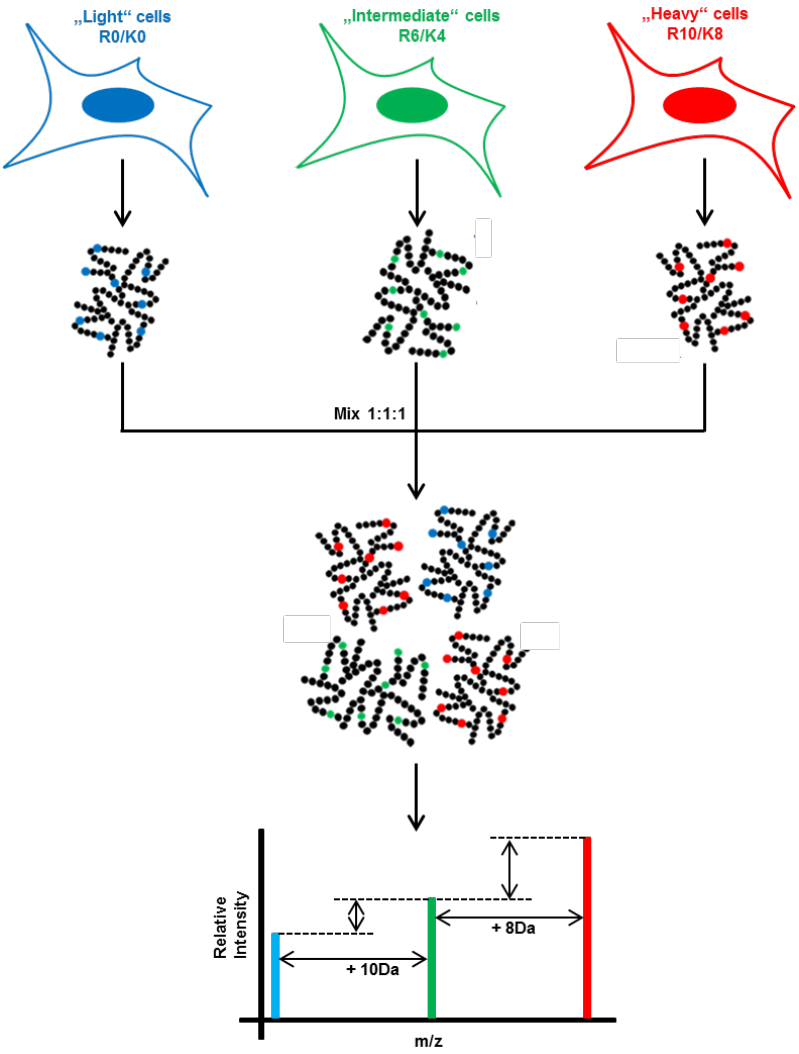

Figure 1.9. Principle of stable isotopic labeling by amino acids in cell culture (SILAC). Cells are grown in media containing different isotopically labelled amino acids. Proteins from differentially labeled cells (light, intermediate and heavy) are identical except for a small difference in mass. Lysates of cells in different states are mixed in equal proportions and the mass shift in peptides derived from different cells states is detected by MS. Comparison of signal intensities allows for relative protein quantification. In this example, the peptide is most abundant in cells containing ‘heavy’ (R10K8) labeled amino acids.

During MS, peptides that share the same aa sequence but originate from differentially labelled cells (also referred to as different states) appear in groups but exhibit a small shift of their mass-to-charge ratios. This mass shift enables the differentiation of these peptides, their assignment to their original state and the direct comparison of their signal intensities, thereby facilitating relative protein quantification [136]. In the experiments described in this thesis triplex-SILAC was employed. Cells were therefore either grown in medium containing light (R0K0), intermediate (R6K4) or heavy (R10K8) amino acid isotopes of L-lysine and L-arginine (see section 2.2.6 for further details).

1.6 Aim of this study

PB2 is part of the trimeric polymerase complex of influenza viruses. Together with PA, PB2 provides capped primers derived from cellular RNA which are indispensable for transcription of viral genes [57]. Hence, PB2 is a key factor in the replication process of influenza viruses and is furthermore known to be an important factor in the determination of influenza virus host range [57,71,137]. Hence, the interplay of PB2 with the cellular host proteome is of particular interest and has been previously investigated in several interaction studies. However, most of these studies either used laboratory/mouse-adapted influenza strains, which do not necessarily reflect characteristics of human influenza isolates, or were performed in the context of transiently transfected cells [138-144]. Studies performed in which viral proteins are expressed in non-infected cells do not also evaluate the influence of other viral proteins and of cellular proteins that are potentially differentially regulated and expressed in infected cells. Hence, the PB2 interactomes determined in previous studies may not reflect all aspects of the PB2-host proteome interplay in the context of naturally occurring strains in infected cells.

The main aim of this study was therefore to systematically identify cellular interaction partners of the PB2 protein of seasonal and highly pathogenic influenza virus strains in the context of infected cells. Therefore, a SILAC based affinity-purification mass spectrometry (AP-MS) screen was performed to determine the interactome of PB2 in seasonal A/Pan/99 (H3N2) or highly pathogenic A/Thai/04 (H5N1) infected human alveolar epithelial cells (A549). Selected proteins, preliminarily identified as PB2 interaction partners, were further validated and their impact on polymerase activity was examined.

It was hoped that new functional interactions of cellular proteins with PB2 could be described and that these findings may increase our understanding of the differences between seasonal and highly pathogenic influenza virus replication in human cells.

2. Materials and Methods

2.1 Materials

2.1.1 Chemicals and Consumables

1702 Plunger Assembly	Hamilton, Bonaduz (Switzerland)
0.5 ml reaction tubes	Sarstedt, Nümbrecht
1.5 ml reaction tubes	Sarstedt, Nümbrecht
15 ml reaction tubes	Roth, Karlsruhe
50 ml reaction tubes	TPP, Trasadingen (Switzerland)
6-well plates	TPP, Trasadingen (Switzerland)
12-well plates	PAA Laboratories, Cölbe
24-well plates	PAA Laboratories, Cölbe
96-well plates	BRAND GmbH, Wertheim
96-well PCR Plate, Skirted, Low-Profile, Natural	STARLAB, Hamburg
Acetic acid	Roth, Karlsruhe
Acetonitril	Roth, Karlsruhe
Acrylamide/Bis-acrylamide solution 30% (29:1)	Roth, Karlsruhe
Agarose NEEO Ultra Quality	Roth, Karlsruhe
Ammonium carbonate	Roth, Karlsruhe
Ammonium chloride	Roth, Karlsruhe
Ammonium peroxodisulfate (APS)	Roth, Karlsruhe
Ampicillin	Roche, Mannheim
Bacto-Agar	Becton-Dickenson, Heidelberg
B-Mercaptoethanol	Roth, Karlsruhe
Boric acid	Roth, Karlsruhe
Bovine albumin fraction V	Roth, Karlsruhe
BSA, 30%	PAA Laboratories, Cölbe
Calcium chloride	Merck, Darmstadt
Cell culture dishes	Greiner, Solingen
Cell culture dishes	Nunc, Roskilde (Denmark)
Cell culture flasks and dishes	TPP, Trasadingen (Switzerland)
Cell dissociation buffer	Gibco (Life Technologies), Darmstadt
Cell scraper	TPP, Trasadingen (Switzerland)
Clear view™ Snap-Cap microtubes, low retention	Sigma-Aldrich, Taufkirchen
CL-XPosure film	Thermo Fisher Scientific, Bonn
Coomassie brilliant blue R250	Roth, Karlsruhe
Corning Axygen® AM-96-PCR-RD AxyMat™ PCR Microplate Sealing Mat	Capitol Scientific, Austin (USA)

4',6-diamidino-2-phenylindole (DAPI)	Merck, Darmstadt
DEAE-Dextran	Sigma-Aldrich, Taufkirchen
Dialyzed FBS	Invitrogen (Life Technologies), Darmstadt
Dimethylsulfoxid (DMSO)	Sigma-Aldrich, Taufkirchen
Dithiothreitol (DTT)	Roth, Karlsruhe
DNA Fast Ruler	Fermentas, St. Leon-Rot
DNA Mass Ruler	Fermentas, St. Leon-Rot
DNA 6x loading buffer	Fermentas, St. Leon-Rot
EASY-Column, 2cm, C18-A1	Proxeon (Thermo Fisher Scientific), Dreieich
EASY-Column, 2cm, C18-A2	Proxeon (Thermo Fisher Scientific), Dreieich
EDTA	Roth, Karlsruhe
Embryonated chicken eggs	Valo Biomedia GmbH, Osterholz Scharmbeck
Empore™ Octadecyl C18 47mm extraction disc	Sigma-Aldrich, Taufkirchen
Ethanol	Roth, Karlsruhe
Ethidium bromide	Roth, Karlsruhe
Fetal bovine serum (FBS)	Biochrom, Cambridge (UK)
Formaldehyde 10 % (methanol-free)	Polysciences Inc., Eppelheim
Formaldehyde 37 %	Roth, Karlsruhe
Formic acid	Sigma-Aldrich, Taufkirchen
Glutamine	Roth, Karlsruhe
Glycerol	Roth, Karlsruhe
Glycin	Roth, Karlsruhe
HEPES	Roth, Karlsruhe
IGEPAL® CA-630	Fluka Biochemika, Milano (Italy)
Iodoacetamide	Sigma-Aldrich, Taufkirchen
Isopropanol	Roth, Karlsruhe
Kanamycin	Roth, Karlsruhe
L-Arginine (none labelled) Cat. #201004102	Silantes, München
L-Arginine ($^{13}C_6$) Cat. # 201204102	Silantes, München
L-Arginine ($^{13}C_6$, $^{15}N_4$) Cat. # 201604102	Silantes, München
L-Lysine (none labelled) Cat. # 211004102	Silantes, München
L-Lysine (D_4) Cat. # 211104112	Silantes, München
L-Lysine ($^{13}C_6$, $^{15}N_2$) Cat. # 211604102	Silantes, München
Lipofectamine® 2000	Invitrogen, Darmstadt
Lipofectamine® LTX	Invitrogen, Darmstadt
Lipofectamine® RNAiMAX	Invitrogen, Darmstadt
Magnesium sulfate	Roth, Karlsruhe
Methanol	Roth, Karlsruhe
Midori Green Advance	Biozyme Diagnostik, Oldendorf
Milk powder	Roth, Karlsruhe
Mowiol 4-88	Roth, Karlsruhe

Nitrocellulose-membrane	Whatman (GE Healthcare), Freiburg
Opti-MEM®	Gibco (Life Technologies), Darmstadt
Parafilm	American National Can, Chicago (USA)
Paraformaldehyde	Roth, Karlsruhe
Pefabloc	Roth, Karlsruhe
Penicillin/Streptomycin	PAA Laboratories, Cölbe
PicoTip emmiter silica tip	New Objective Inc., Woburn (USA)
Pierce™ 20X Tris-HEPES-SDS Buffer	Thermo Fisher Scientific, Bonn
Ponceau S	Sigma-Aldrich, Taufkirchen
Precise™ Tris-HEPES gels	Thermo Fisher Scientific, Bonn
Prestained protein ladder	Fermentas, St. Leon-Rot
Protein G Agarose	Roche, Mannheim
ProteoMass Cal Mix	Sigma-Aldrich, Taufkirchen
Rotisolv® Ultra LC-MS (MS grade water)	Roth, Karlsruhe
SimplyBlue™ SafeStain	Invitrogen™ (Thermo Fisher Scientific), Carlsbad (USA)
Sodium acetate	Roth, Karlsruhe
Sodium chloride	Roth, Karlsruhe
Sodium deoxycholat	Roth, Karlsruhe
Sodium dodecyl sulfate (SDS)	Serva, Heidelberg
Sodium orthovanadate	Sigma-Aldrich, Taufkirchen
Strep-Tactin® Superflow® 50 % suspension	IBA Lifesciences, Göttingen
Super Signal Dura chemiluminescence	Pierce, Bonn
TEMED	Serva, Heidelberg
TPCK-Trypsin	Sigma-Aldrich, Taufkirchen
Trifluoroacetic acid (TFA)	Roth, Karlsruhe
Tris	Roth, Karlsruhe
Triton-X 100	Serva, Heidelberg
Trypsin (cell culture)	Gibco (Life Technologies), Darmstadt
Trypsin (mass spectrometry)	Sigma-Aldrich, Taufkirchen
Tween® 20	Roth, Karlsruhe
Vivaspin® 500	Sartorius, Göttingen
Whatman paper	Whatman (GE Healthcare), Freiburg

2.1.2 Kits

BCA Protein Assay Kit	Pierce, Bonn
BigDye® Terminator 3.1 Kit	Applied Biosystems, Darmstadt
Cell Proliferation Kit I (MTT)	Roche, Mannheim
Dual-Luciferase® Reporter Assay System	Promega, Mannheim
Expand™ High Fidelity PCR System	Roche, Mannheim
Gateway™ LR Clonase™ II Enzyme mix	Thermo Fisher Scientific, Bonn
Invisorb® Spin DNA Extraction Kit	STRATEC Molecular GmbH, Berlin

Invisorb® Spin Plasmid Mini Two Miniprep Kit	STRATEC Molecular GmbH, Berlin
Phusion Green High-Fidelity DNA Polymerase	Thermo Fisher Scientific, Bonn
QIAamp Mini Elute Virus spin Kit	QIAGEN, Hilden
Qiagen® OneStep RT-PCR Kit	QIAGEN, Hilden
QIAfilter Plasmid Maxi Kit	QIAGEN, Hilden
QIAquick® PCR Purification Kit	QIAGEN, Hilden
RevertAid RT Reverse Transcription Kit	Thermo Fisher Scientific, Bonn

2.1.3 Enzymes

DpnI	Fermentas, St. Leon-Rot
RNasin	Promega, Mannheim
T4 DNA Ligase	Fermentas, St. Leon-Rot
T4 Polynucleotide kinase	Thermo Fisher Scientific, Bonn

2.1.4 Cell lines

A549 cells	Human alveolar epithelial cells
HEK293T cells	Human Embryonic Kidney cells
MDCKII cells	Madin-Darby Canine Kidney cells

2.1.5 Bacterial strains

Escherichia coli (E.coli), strain DH5α	fhuA2 lac(del)U169 phoA glnV44 Φ80`lacZ(del)M15 gyrA96 recA1 relA1 endA1 thi-1 hsdR17
Escherichia coli (E.coli), strain XL1-Blue (Stratagene)	recA1 endA1 gyrA96 thi-1 hsdR17 supE44 relA1 lac [F`proAB lac I^q ZδM15 Tn10 (Tet^r)]

2.1.6 Virus strains

A/Panama/2007/1999	H3N2	recombinant	
A/Panama/2007/1999 PB2-Strep	H3N2	recombinant	A/Panama/2007/1999 derived virus with a Twin-Strep-tag® at the C-terminal end of the PB2 protein

A/Thailand/1(KAN-1)/2004	H5N1	recombinant	
A/Thailand/1(KAN-1)/2004 PB2-Strep	H5N1	recombinant	A/Thailand/1(KAN-1)/2004 derived virus with a Twin-Strep-tag® at the C-terminal end of the PB2 protein

2.1.7 Plasmids

pCAGGS-A/Thailand/1(KAN-1)/2004-NP	V. Czudai-Matwich, Dept. of Medicine, Philipps Universität Marburg, Marburg
pCAGGS-A/Thailand/1(KAN-1)/2004-PA	V. Czudai-Matwich, Dept. of Medicine, Philipps Universität Marburg, Marburg
pCAGGS-A/Thailand/1(KAN-1)/2004-PB1	V. Czudai-Matwich, Dept. of Medicine, Philipps Universität Marburg, Marburg
pCAGGS-A/Thailand/1(KAN-1)/2004-PB2	V. Czudai-Matwich, Dept. of Medicine, Philipps Universität Marburg, Marburg
pCAGGS-EV	J.-I. Miyazaki, Institute for Medical Genetics, Kumamoto University Medical School, Kuhonji
pcDNA3.1 Flag YFP EV	U. Arnold, FG17, RKI, Berlin
pcDNA-A/PR8/33-PA	Ervin Fodor, Medical Sciences Division, University of Oxford, Oxford
pcDNA-A/PR8/33-PB1	Ervin Fodor, Medical Sciences Division, University of Oxford, Oxford
pcDNA-A/PR8/33-PB2	Ervin Fodor, Medical Sciences Division, University of Oxford, Oxford
pcDNA-A/PR8/33-NP	Ervin Fodor, Medical Sciences Division, University of Oxford, Oxford
pcDNA3.1 Flag YFP hNKCC1	Addgene Plasmid #49085
pcDNA5/FRT/TO V5 EV	U. Arnold, FG17, RKI, Berlin
pcDNA5/FRT/TO V5 HSPA2	Addgene Plasmid #19512
pcDNA5/FRT/TO V5 HSPA8	Addgene Plasmid #19460
pDONR221-AGR2	Harvard Medical School PlasmID Plasmid HsCD00042662
pDONR221-CAST	Harvard Medical School PlasmID Plasmid HsCD00043496
pDONR221-EPHX1	Harvard Medical School PlasmID Plasmid HsCD00044569
pDONR221-LXN	Harvard Medical School PlasmID Plasmid HsCD00296066
pDONR221-PABPC1	Harvard Medical School PlasmID Plasmid HsCD00045525
pDONR221-PABPC3	Harvard Medical School PlasmID Plasmid HsCD00044176

pENTR223-BAG2	Harvard Medical School PlasmID Plasmid HsCD00368116
pENTR223-GGH	Harvard Medical School PlasmID Plasmid HsCD00369546
pENTR223-RCN2	Harvard Medical School PlasmID Plasmid HsCD00383773
pESG-IBA 105	IBA Lifesciences, Göttingen
pEZYflag	Addgene Plasmid #18700
pEZYflag-AGR2	U. Arnold, FG17, RKI, Berlin
pEZYflag-CAST	U. Arnold, FG17, RKI, Berlin
pEZYflag-EPHX1	U. Arnold, FG17, RKI, Berlin
pEZYflag-LXN	U. Arnold, FG17, RKI, Berlin
pEZYflag-PABPC1	U. Arnold, FG17, RKI, Berlin
pEZYflag-PABPC3	U. Arnold, FG17, RKI, Berlin
pHW2000-A/Panama/2007/1999-NP	A. Martini, FG17, RKI, Berlin
pHW2000-A/Panama/2007/1999-PA	A. Martini, FG17, RKI, Berlin
pHW2000-A/Panama/2007/1999-PB1	A. Martini, FG17, RKI, Berlin
pHW2000-A/Panama/2007/1999-PB2	A. Martini, FG17, RKI, Berlin
pHW2000-A/Panama/2007/1999-PB2-Strep	U. Arnold, FG17, RKI, Berlin
pHW2000-A/Thailand/1(KAN-1)/2004-PB2	M. Schwemmle, Dept. for Medical Microbiology and Hygiene, Universitätsklinikum Freiburg, Freiburg
pHW2000-A/Thailand/1(KAN-1)/2004 PB2-Strep	U. Arnold, FG17, RKI, Berlin
pHW2000-EV	R. G. Webster, Dept. of Virology and Molecular Biology, St. Jude Children's Research Hospital, Memphis
pMAX-DEST	Addgene Plasmid #37631
pMAX-DEST-BAG2	U. Arnold, FG17, RKI, Berlin
pMAX-DEST-GGH	U. Arnold, FG17, RKI, Berlin
pMAX-DEST-RCN2	U. Arnold, FG17, RKI, Berlin
pPol-SapI-A-NS-Luc (Firefly)	J. Stärk, FG17, RKI, Berlin
pTK-Luc (Renilla)	Promega, Mannheim
pT7-V5-SBP-C1-EV	U. Arnold, FG17, RKI, Berlin
pT7-V5-SBP-C1-HshnRNPC1	Addgene Plasmid #64920

2.1.8 Antibodies

Primary antibodies

Identifier	Species/Feature	Source
α-A-NP	mouse/monoclonal	AbD Serotec (Bio-Rad), Hercules (USA)
α-A-PB2	goat/polyclonal	Santa Cruz Biotechnology, Dallas (USA)
α-A-PB2	rabbit/polyclonal	Thermo Fisher Scientific, Bonn
α-β-actin	mouse/monoclonal	Sigma-Aldrich, Taufkirchen
α-cMyc (9E10)	mouse/monoclonal	Santa Cruz Biotechnology, Dallas (USA)
α-Flag M2	mouse/monoclonal	Sigma-Aldrich, Taufkirchen
α-Hsc70	mouse/monoclonal	Abcam, Cambridge (UK)
α-Hsc70	rabbit/monoclonal	Abcam, Cambridge (UK)
α-Hsc70/HSP73	rat/monoclonal	Enzo Life Sciences GmbH, Lörrach
α-Strep	mouse/monoclonal	IBA Lifesciences, Göttingen
α-V5	mouse/monoclonal	AbD Serotec (Bio-Rad), Hercules (USA)

Secondary antibodies

Identifier	Species	Source
Alexa Fluor™ 488 α-rat IgG	donkey	Invitrogen™ (Thermo Fisher Scientific), Carlsbad (USA)
Alexa Fluor™ 594 α-rabbit IgG	goat	Invitrogen™ (Thermo Fisher Scientific), Carlsbad (USA)
α-mouse IgG-HRP	rabbit	Dako, Santa Clara (USA)
α-goat IgG-HRP	rabbit	Dako, Santa Clara (USA)
α-rabbit IgG-HRP	goat	Cell Signaling Technology®, Danvers (USA)

2.1.9 Primer

Identifier	Purpose of primer	Target sequence 5`→ 3`
A-PB2-Twin-Strep-tag For	Cloning	ATCAATTATAGCGCATGGAGTCATCCTCAATTCG
BD-uni-PB2 Rev	Sequencing	GGCCGCCGGGTTATTAGTAGAAACAAGGTCGTTT
B-PB2-Pan-Twin-Strep-tag Rev	Cloning	CCAATTAGCTTATTTTTCGAACTGCGGGTGGCTCC
B-PB2-Thai-Twin-Strep-tag Rev	Cloning	CCTATCAGCTTATTTTTCGAACTGCGGGTGGCTCC
CMV For	Sequencing	CGCAAATGGGCGGTAGGCGTG

C-Twin-Strep-tag-PB2-Pan For	Cloning	GAAAAATAAGCTAATTGGGCAAGGAGACG
C-Twin-Strep-tag-PB2-Thai For	Cloning	GAAAAATAAGCTGATAGGGCAAGGAGACG
D-pHW2000 Rev	Cloning	GAAAAATAAGCTAATTGGGCAAGGAGACG
hGH-pA-R Rev	Sequencing	CCAGCTTGGTTCCCAATAGA
LNCX For	Sequencing	AGCTCGTTTAGTGAACCGTCAGATC
M13 Rev	Sequencing	CAGGAAACAGCTATGAC
MB-CMV-seq For	Sequencing	AACAACTCCGCCCCATTGAC
Pan-intern-PB2 For	Sequencing	TTGTACAACAAAATGG
PB2-2333 Rev	Sequencing	CAAGGTCGTTTTTAAA
pCDNA3.1-inverse-fw	Cloning	TAATTAATTAAGTTTAAACCCGCTGATCAGCC
pCDNA3.1-inverse-rev	Cloning	CTTGTAGAGCTCGTCCATGCCG
pCDNA5-inverse-fw	Cloning	TAAGCGGCCGCTCGAGTCTAG
pCDNA5/pT7-inverse-rev	Cloning	CGTAGAATCGAGACCGAGGAGAG
pT7-inverse-fw	Cloning	TAAGAATTCTGCAGTCGACGGTACC
Thai-PB2-1751-1764 For	Sequencing	GGAGTTTGAACCG

2.1.10 siRNA

Identifier	**Source**	**Target sequence 5`→ 3`**
AllStars Negative Control siRNA	Qiagen FlexiTube	
siRNA HSPA8 #6*	Qiagen FlexiTube	AAGGACCTAAATTCGTAGCAA
siRNA HSPA8 #10*	Qiagen FlexiTube	GAGGTTGATTAAGCCAACCAA
siRNA HSPA8 #11*	Qiagen FlexiTube	TGGGCATTCTCAATACTTGAA
siRNA HSPA8 #12*	Qiagen FlexiTube	TTAAGCTGCTATAGTAAGTTA

* component of HSPA8-siRNA Mix

2.1.11 Cell culture media

DMEM/MEM culturing medium	FBS	10 %
	Glutamine	2 nM
	Pen/Strep	50 mg/mL
	DMEM or MEM	ad 500mL
Transfection DMEM/MEM	FBS	10 %
	Glutamine	2 nM
	DMEM or MEM	ad 500mL
Infection DMEM/MEM	BSA	0.2 %
	Glutamine	2 nM
	Pen/Strep	50 mg/mL
	DMEM or MEM	ad 500mL
SILAC DMEM	Dialyzed FBS	10 %
	Glutamine	2 mM
	Pen/Strep	50 mg/mL
	L-Lysine (non labelled), (D_4)or ($^{13}C_6$, $^{15}N_2$)	146 mg/L
	L-Arginine (non labelled), ($^{13}C_6$) or ($^{13}C_6$, $^{15}N_4$)	84 mg/L
	SILAC DMEM	ad 500mL
	filter 0.22 µm	
SILAC Infection DMEM	Glutamine	2 mM
	Pen/Strep	50 mg/mL
	L-Lysine (non labelled), (D_4)or ($^{13}C_6$, $^{15}N_2$)	146 mg/L
	L-Arginine (non labelled), ($^{13}C_6$) or ($^{13}C_6$, $^{15}N_4$)	84 mg/L
	SILAC DMEM	ad 500mL
	filter 0.22 µm	
Freezing Media	SILAC DMEM	
	Dialyzed FBS	20 %
	DMSO	10 %
Avicel overlay medium	2.5 % Avicel RC-581 in H_2O	4.86 mL
	2x MEM	4.86 mL
	30% BSA	66.7 µL
	5 % $NaHCO_3$	100 µL
	1 % DEAE-Dextran	100 µL

2.1.12 Media for bacteria

2x YT medium	Trypton	16 g/L
	Yeast extract	10 g/L
	NaCl	10 g/L
	pH 7.2	
SOC medium	Trypton	20 g/L
	Yeast extract	5 g/L
	NaCl	10 mM
	KCl	2.5 mM
	autoclaving	
	$MgCl_2$	20 mM
$MgCl_2$-Stock	$MgCl_2$ x 6 H_2O	1 M
	$MgSO_4$ x 7 H_2O	1 M
	Glucose	0.4 % (w/v)
2x YT-agar with antibiotics	2 x YT medium	
	Bacto-Agar	1.5 % (w/v)
	autoclaving and cooling down	
	Ampicillin or Kanamycin	100 g/L or 50 g/L

2.1.13 Buffer and solutions

PBS	NaCl	137 mM
	KCl	2.7 mM
	Na_2HPO_4	80.9 mM
	KH_2PO_4	1.5 mM
PBS^+	PBS	
	$MgCl_2$	0.1 g/L
	$CaCl_2$	0.13 g/L
$PBS^{+/+}$	PBS	
	BSA	0.2 %
	$MgCl_2$	0.1 g/L
	$CaCl_2$	0.13 g/L
PEI	Polyethylenimin	2,58 µg/µL
10x SDS buffer	Tris	250 mM
	Glycin	1.92 mM
	SDS	10 g/L

Separating gel buffer pH 8.8	Tris/HCl	1.5 mM
Stacking gel buffer pH 6.8	Tris/HCl	0.5 M
10x TBE buffer	Tris	0.89 M
	Boric acid	0.89 M
	EDTA, pH 8.0	10 mM
2x SDS sample buffer	H_2O	1.2 mL
	0.5 M Tris/HCl, pH 6.8	8.3 mL
	10 % SDS (w/v)	6 mL
	Glycerol	1.5 mL
	Bromphenolblue	9 g/L
	β-Mercaptoethanol	5 %
6 SDS sample buffer	H_2O	1.2 mL
	0.5 M Tris/HCl, pH 6.8	9.8 mL
	SDS	1.7 g
	Glycerol	5 mL
	0.5 mM EDTA, pH8	0.5 mL
	Bromphenolblue	9 g/L
	β-Mercaptoethanol	5 %
Semi-dry blotting buffer	Tris	40 mM
	Glycin	30 mM
	SDS	1.3 mM
	Ethanol	20 %
Coomassie staining solution	Coomassie Roti® Blue (5x)	20 %
	Ethanol	20 %
	H_2O	60 %
Coomassie destaining solution	Methanol in H_2O	10 %
Coomassie fixation solution	Acetic acid	10 %
	Ethanol	30 %
6x DNA sample buffer	Bromphenolblue	0.1 % (w/v)
	Xylencyanol	0.1 % (w/v)
	Glycerol	30 %
Mowiol	Mowiol 4-88	2.4 g
	Glycerol	6 mL
	H_2O	6 mL
	incubation over night	

	0.2 M Tris/HCl, pH 8.5	12 mL
	heating to 60°C while stirring	
	centrifugation for 15 min	1.300g
	DABCO	10 %
Cell lysis buffer (mass spectrometry)	Tris/HCl, pH 8.0	50 mM
	NaCl	300 mM
	$MgCl_2$	2 mM
	IGEPAL	0.3 %
	Dithiothreitol	1 mM
	Glycerol	10 %
	Sodium-Orthovanadat	2 mM
	Pefabloc	1 mM
Buffer W	Tris/HCl, pH 8.0	100 mM
	NaCl	150 mM
	EDTA	1 mM
Buffer E	Tris/HCl, pH 8.0	100 mM
	NaCl	150 mM
	EDTA	1 mM
	Desthibiotin	10 mM
1x Tris-HEPES SDS buffer	20x Tris HEPES buffer diluted in MS grade water	
Alkylation buffer	Iodoacetamide in MS grade water	50 mM
Destaining solution	NH_4HCO_3	200 mM
	Acetonitril	40 %
Enzyme reaction buffer	NH_4HCO_3	400 mM
	Acetonitril	9 %
Extraction buffer	Acetonitril	50 %
	Trifluoroacetic acid	0.1 %
Desalting buffer	Formic acid	0.5 %
	Acetonitril	80 %
IP-Lysis buffer	Tris/HCl, pH 7.4	25 mM
	NaCl	150 mM
	IGEPAL	1 %
	EDTA	1 mM
	Glycerol	5 %

2.1.14 Technical equipment

Centrifuges

Centrifuge 5417 R	**Eppendorf, Hamburg**
Heraeus™ Pico™ 17 Microcentrifuge	Thermo Fisher Scientific, Bonn
Labofuge 400R (rotor: 8179)	Heraeus (Thermo Fisher Scientific), Bonn
Megafuge 1.0R (rotor: 2704)	Heraeus (Thermo Fisher Scientific), Bonn
Multifuge 1S-R (rotor: 75002000)	Thermo Fisher Scientific, Bonn
Sorvall™ LYNX™ Superspeed-Centrifuge (rotors: F12-6x500, F14-6x250y, A27-8x50)	Thermo Fisher Scientific, Bonn
SpeedVac Univapo 150 H	Uniequip, Planegg

Thermocycler

Personal Cycler	Biometra, Göttingen
Primus 96	PEQLAB (VWR), Erlangen
Uno Thermoblock	Biometra, Göttingen

Microscopes

Eclipse TS100	Nikon, Tokyo (Japan)
Olympus CKX41	Olympus, Tokyo (Japan)
Confocal laser scan microscope LSM 780	Zeiss, Oberkochen

Other devices

ABI Prism 3100 Genetic Analyzer	Applied Biosystems, Foster City (USA)
Advanced Fluorescence Imager	Intas Science Imaging, Göttingen
Binder (incubator)	Thermo Fisher Scientific, Bonn
Ecotron (incubator shaker)	Infors HT, Bottmingen (Switzerland)
FLUOstar® Omega Plate Reader	BMG Labtech, Ortenberg
Haake DC10-P21 Open-Bath Circulators with Integral Bath (Water)	PSL Systemtechnik, Osterode am Harz
HeraSafe HSP15 clean bench	Heraeus (Thermo Fisher Scientific), Bonn
HeraSafe KS12	Heraeus (Thermo Fisher Scientific), Bonn
Curix 60 developer machine	Agfa, Mortsel (Belgium)
Easy Nano-LC2	Proxeon (Thermo Fisher Scientific), Dreieich
Gel chamber Mini-Sub Cell GT	Bio-Rad, Hercules (USA)
Gel documentation	Intas Science Imaging, Göttingen
LTQ Orbitrap Discovery mass spectrometer	Thermo Fisher Scientific, Bonn

Mini-PROTEAN® 3	Bio-Rad, Hercules (USA)
NanoDrop 8000	Thermo Fisher Scientific, Bonn
Power Pack 200 and 300	Bio-Rad, Hercules (USA)
Roto-Shake Genie	Scientific Industries, Bohemia (USA)
Spectrafluor Plus ELISA-Reader	Tecan, Männedorf (Switzerland)
Tecan Genios Pro ELISA-Reader	Tecan, Männedorf (Switzerland)
Thermomixer compact	Eppendorf, Hamburg
Trans-Blot SD Semi-Dry Transfer Cell	Bio-Rad, Hercules (USA)
TriStar LB941 Multimode Reader	Berthold Technologies GmbH & Co.KG, Schöneiche bei Berlin
Varocell 150 (incubator)	Varolab GmbH, Giesen

2.1.15 Software and web tools

Software

Adobe Photoshop CS6	image processing
ChemoStar Professional software (Intas)	gel documentation
DNASTAR Lasergene 10	sequence analysis
Endnote X7.4	reference manager
Geneious R10	sequence analysis
GraphPad Prism 7	tables and statistics
Intas-Capture	gel documentation
LabImage 1D	quantification of immunoblot protein bands
Magellan™	data analysis
MARS data analysis software	data analysis
MaxQuant 1.5.1.2	analysis of MS data
Microsoft Office 2010	text and presentations
MikroWin 2000	data analysis
Proteome Discoverer 1.4	analysis of MS data
Perseus 1.5.0.31	downstream biological analysis of MS data

Web tools

Bioinformatics & Evolutionary Genomics	http://bioinformatics.psb.ugent.be/webtools/Venn/
NCBI PubMed	https://www.ncbi.nlm.nih.gov/pubmed
PANTHER Gene List Analysis v11.1	http://pantherdb.org/
STRING: functional protein association networks v10.5	https://string-db.org/
UniProt Knowledgebase	http://www.uniprot.org/

2.2 Methods

2.2.1 Cell culture

Cell passaging

All cell types were cultured at 37°C and in 5 % CO_2 and manipulated under sterile conditions. Cells were subcultured every 3 – 4 days, depending on the cell line, when they reached 90 % to 95 % confluency. During subculture cells were washed in phosphate buffered saline (PBS) and detached by adding 1 mL trypsin-ETDA solution to a T75 cell culture flask. Detached cells were resuspended in fresh media and transferred into new flasks at the required density. MDCKII cells were cultured in complemented minimal essential medium (MEM) while A549 and HEK293T cells were cultivated in complemented Dulbecco's modified Eagle medium (DMEM). For the exact media composition see section 2.1.11.

Transfection of eukaryotic cells with Lipofectamine® 2000

The day prior to transfection, cells were subcultured to ensure they were still dividing when transfected. On the day of transfection, cells were washed once with PBS, detached with trypsin-EDTA solution and resuspended in transfection D-MEM). Cells were pelleted at 800 g for 3 minutes (min) and resuspended in 10 mL fresh transfection D-MEM. In each well of the 6-well plate, 800 µL of cells (corresponding to approximately 0.7 x 10^6 cells) were seeded and 1.2 mL of fresh transfection D-MEM was added. Meanwhile, Lipofectamine® 2000 was diluted in 100 µL Opti-MEM at a concentration of 1.5 µL per 1 µg of plasmid DNA, then the mixture was incubated at room temperature (RT) for 5 min. Plasmid DNA was diluted in 100 µL Opti-MEM then combined with the Lipofectamine® 2000-Opti-MEM mixture and incubated for 20 min at RT. The DNA-Lipofectamine® 2000-solution was added dropwise to the cells and distributed by shaking gently. Cells were incubated in 5 % CO_2 at 37 °C for 48 hours (h) before further analysis.

Transfection of eukaryotic cells with PEI

Cells were subcultured the day prior to transfection to ensure they were still dividing when transfected. On the day of transfection, cells were harvested, pelleted at 800 g for 3 min, resuspended in fresh transfection D-MEM and seeded corresponding to a confluency of ˜80 %. Plasmid DNA was diluted in Opti-MEM equivalent to 10 % of the seeding volume of the cells, and PEI was added at a concentration of 2 µL per 1 µg DNA. After 15 min of incubation at RT, the DNA-PEI mixture was added to the cells

and distributed by rocking the cell culture plate. Cells were incubated for 24 h before they were analyzed.

Transfection of siRNA

The effect of HSPA8 knock down was examined by transfecting A549 or 293T cells with HSPA8 FlexiTube siRNA mix using Lipofectamine® RNAiMAX according to manufacturers instructions. The siRNA mix was composed of 4 different, preselected siRNAs specific for the target gene (see section 2.1.10). Briefly, cells were seeded in transfection D-MEM such that they were~60 - 80 % confluent on the day of transfection. For each well of a 12-well plate, 25 pmol of siRNA was combined with Opti-MEM to a total volume of 50 µL, and in parallel 5 µL of Lipofectamine® RNAiMAX was combined with Opti-MEM also to a total volume of 50 µL. For each well of a 96-well plate, 2 pmol siRNA and 1µL of Lipofectamine® RNAiMAX was diluted in a total volume of 5 µL Opti-MEM each. In both cases, the solutions of siRNA and RNAiMAX were mixed and incubated for 5 min at RT before being added to the cells. 4 h after transfection, medium was replaced by fresh transfection D-MEM. Cells were transfected with either HSPA8 siRNA mix or non-target control siRNA. The efficacy of the knock down was evaluated at different time points post transfection (p.t.) by SDS-PAGE and immunoblotting.

2.2.2 Infectious work

All experiments involving infectious A/Thailand/1(KAN-1)/2004 influenza virus were performed under BSL3 conditions.

Infection of eukaryotic cells

For infection with influenza A viruses, cells were seeded such that their confluency was 80 - 90 % on the day of infection. Cells were either infected with a defined dilution (e.g. a 10^{-3} dilution) for viral titration or with a defined number of infectious virus particles per cell. To determine the amount of virus stock needed to reach a specific multiplicity of infection (MOI), the following formula was used:

$$\frac{number\ of\ cells\ \times MOI}{viral\ titer\ [\frac{PFU}{mL}]} = volume\ of\ virus\ stock\ [mL]$$

For infection, cells were washed once with PBS^{+} and then inoculated with the appropriate virus dilution in PBS^{++}. The total volume of the virus dilution was the minimum volume that could still cover the cells in the dish. After incubation for 45 min at RT under constant gentle shaking, in order to allow the viral particles to distribute evenly, cells were washed twice with PBS^{+} and infection media was added.

For monocyclic infections, the media was free of TPCK-Trypsin, however TPCK-Trypsin was added to the infection media in the case of multicyclic infections to assist cleaving of the viral HA and support virus propagation. The concentration of TPCK-Trypsin was dependent on the cell type used for the experiment: 1 µg/mL for MDCKII cells and 0.225 µg/mL for A549 cells.

For growth curve analysis, 10% of the total volume of media in the dish was removed at defined time points and replaced by fresh infection medium supplemented with TPCK-Trypsin. Supernatants were stored at -80°C until further analysis.

Viral titration by plaque-forming assay

Plaque-forming assay is a method for determining the amount of infectious virus particles in, for example, virus stocks or supernatants of infected cells. It is based on the cytopathic lytic effect of influenza viruses, which leads to the formation of visible plaques in an infected confluent cell monolayer. These plaques can be counted and the viral titer can be calculated.

Briefly, confluent MDCKII cells were washed once with PBS^{+} and infected with 10-fold serial dilutions of the virus solution in PBS^{++}. After a 45 min incubation at RT under constant gentle shaking, cells were washed twice with PBS^{+}, and then overlaid with Avicel medium containing 1 µg/mL TPCK-Trypsin and incubated at 37 °C. 48 h post infection (p.i.), Avicel medium was removed and cells were washed twice with PBS, and then stained for at least 15 min with 0.1 % crystal violet diluted in 10% formaldehyde. The staining solution was then removed and cells were washed thoroughly with water and dried at RT. Viral titers were calculated using the following formula:

$$viral\ titer\ [PFU/mL] = \frac{No.\ of\ plaques}{dilution\ factor} * \frac{1\ mL}{amount\ of\ virus\ solution\ used\ for\ infection\ [mL]}$$

Rescue of recombinant viruses

To generate recombinant A/Pan/99 (H3N2) and A/Thai/04 (H5N1) wild type (WT) and PB2-Strep viruses, cells were transfected with the corresponding pHW2000 plasmid system. The pHW2000 plasmid contains viral cDNA inserted between an RNA polymerase I (Pol I) promoter and terminator sequence, which are flanked by an RNA polymerase II (Pol II) promoter and a polyadenylation site [145]. The two transcription units are in opposing orientation on the plasmid, which allows for the synthesis of positive-sense mRNA and negative-sense vRNA, both necessary for virus rescue, from one viral cDNA template [145]. For A/Pan/99 rescue, 293T cells in a 6-well plate were transfected with a mixture of eight pHW200 plasmids, each representing one viral segment.

500 ng of each plasmid was used for transfection. For A/Thai/04 rescue, a mixture of 293T and MDCKII cells in a 6-well plate was transfected. In addition to the 500 ng of each of the 8 pHW200 plasmids, 4 helper plasmids were co-transfected. The helper plasmids were pcDNA expression plasmids encoding PA, PB1, PB2 or NP of the viral strain A/Puerto Rico/8/34 (H1N1). These plasmids only allow the synthesis of mRNA and not vRNA. The expressed A/PR8/34 proteins boost the production of A/Thai/04 viral particles in mammalian cells. 250 ng each of pcDNA-PA, -PB1 and -PB2, and 1 µg of pCDNA-NP were co-transfected into each well of a 6-well plate. For the rescue of A/Pan/99-PB2-Strep and A/Thai/04-PB2-Strep, the pHW2000-PB2-Strep plasmid for the corresponding virus was transfected instead of the WT plasmid. Transfected cells were incubated at 37 °C for 48 h before cell supernatants were collected.

Confluent MDCKII cells in a 6-well plate were infected with the 293T cell supernatant containing either A/Pan/99 or A/Thai/04 rescued virus. These MDCKII cells were washed once with PBS before inoculation with 250µL of 293T cell supernatant for 45 min at RT under constant gentle shaking. After removal of the supernatant, cells were washed twice with PBS^{+} and 2 mL of infection MEM containing 1 µg/mL TPCK-Trypsin was added to each well. After 48 h at 37 °C, MDCKII supernatant was collected and viral titers were determined by plaque-forming assay before being used for virus propagation in embryonated chicken eggs.

Infection of embryonated chicken eggs for virus propagation

Influenza viruses replicate well in the allantoic cavity of embryonated chicken eggs. Hence, A/Pan/99-WT, A/Pan/99-PB2-Strep, A/Thai/04-WT and A/Thai/04-PB2-Strep viral stocks were produced in 10 day old eggs. Each MDCKII supernatant was diluted to a concentration of 800 PFU in 100 µL PBS^{++} per egg. The diluted virus suspension was inoculated into the allantoic cavity with a needle (canula 0.55 x 25 mm). After 48 h

of incubation at 37 °C, eggs were cooled overnight (ON) at 4 °C. The shell around the air cell of the egg was removed with tweezers and the allantoic fluid was harvested with a stripette while the yolk sac was protected from lesions with a spatula. The harvested virus suspension was centrifuged (3.000 rpm, 5 min, 4 °C) and a hemagglutination assay was performed (see 2.2.2). Allantoic fluids of eggs with similar haemagglutination titers (HA titer) were pooled, aliquoted in cryovials and stored at -80 °C. Viral titers were subsequently determined by plaque-forming assay.

Hemagglutination assay

The hemagglutination assay allows for a rapid estimation of the amount of virus particles present in a solution. The technique is based on the ability of viral HA to bind sialic acids on the surface of erythrocytes, thereby cross-linking them to each other, which leads to agglutination. However, discrimination between infectious and non-infectious particles is not possible.

Virus containing solution was 1 in 2 serially diluted in a 96-well microtiter plate (V-bottom) in PBS. Equal amounts of a 1 % chicken erythrocyte solution were then added, solutions were mixed and the plate was incubated at 4 °C for at least 30 min. If an examined solution contains approximately 10^5 to 10^6 viral particles, erythrocytes agglutinate[146]. Whether the erythrocytes did or did not agglutinate can be determined by tilting the plate. If there are not enough viral particles for agglutination, red blood cells accumulated at the bottom of the well will stream in a “tear-drop” fashion. The reciprocal value of the dilution at which hemagglutination can still be observed (i.e no “tear-drop” stream of erythrocytes) represents the HA titer.

2.2.3 Molecular biology methods

Generation of pHW2000-PB2-Strep plasmids

For the rescue of A/Pan/99 and A/Thai/04 viruses expressing Strep-tagged PB2, the sequence of the Twin-Strep-tag® needed to be inserted into the corresponding pHW2000-PB2 plasmid. Based on the publication of *Rameix-Welti et al*. the tag sequence was fused to the sequence encoding the C terminus of PB2. To enable not only expression of the fusion protein but also packaging of the PB2 genomic segment into viral particles, a duplication of the last 109 nucleotides (nt) of the PB2 coding sequence was inserted between the stop codon of the tag sequence and the 5′ NCR [147]. This 143 nt long sequence represents the PB2 packaging sequence (figure 2.1.A). For the generation of the pHW2000-PB2-Strep plasmids a multi-step polymerase chain reac-

tion (PCR) procedure was applied (figure 2.1.B). First, the Twin-Strep-tag® sequence was amplified from the pESG-IBA 105 plasmid. The used forward (fw) primer contained a sequence homologous to the end of the PB2 non-coding region, not including the stop codon, at the 5'-end. The reverse (rev) primer contained a sequence homologous to the start of the PB2 packaging signal. In addition the packaging signal sequence was amplified from the pHW2000-PB2 plasmid, using a reverse primer homologous to the pHW2000 sequence downstream of the packaging signal and a forward primer that contained a sequence homologous to the 5' - end of the Twin-Strep-tag® sequence.

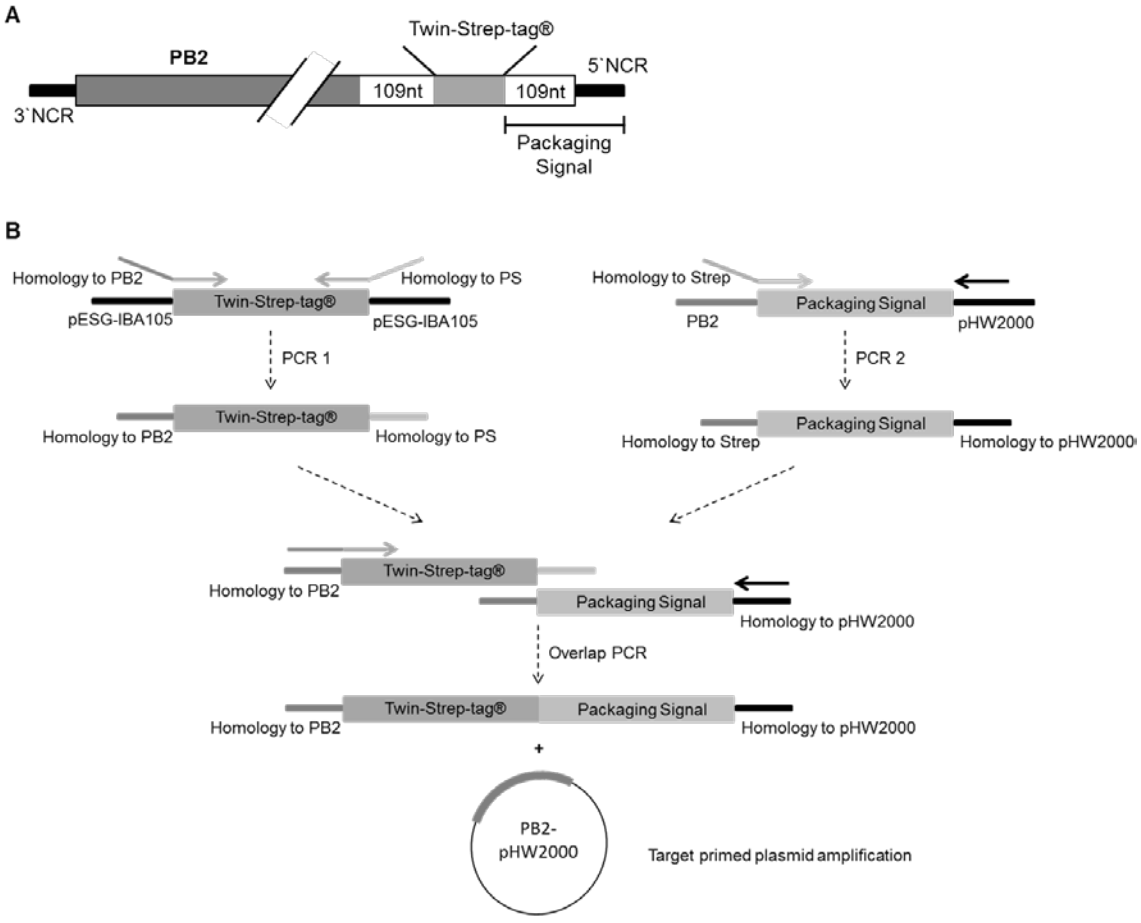

Figure 2.1. Generation of pHW2000-PB2-Strep plasmids. The Twin-Strep-tag® sequence was inserted between the PB2 coding region and the PB2 packaging signal of A/Pan/99 or A/Thai/04 (**A**) using a multi-step PCR procedure (**B**). The detailed procedure is described in the text.

The amplified sequences were fused by overlap PCR using both PCR products, the forward primer used for the amplification of the Twin-Strep-tag® sequence and the reverse primer used for the amplification for the packaging signal sequence.

The resulting fragment contained the sequence homologous to the end of the PB2 non-coding region followed by the Twin-Strep-tag® with a stop codon, the PB2 packaging signal and the sequence homologous to the pHW2000 plasmid sequence. Finally, the pHW2000-PB2-Strep plasmid was generated by target primed plasmid amplification using pHW2000-PB2 as template and the overlap PCR product as primer. The following reaction parameters were employed:

Conventional PCR:

Template DNA	100 ng
Fw Primer	1 µL (0.5 µM)
Rev Primer	1 µL (0.5 µM)
dNTPs	0.4 µL (200 µM)
5X Phusion Green GC Buffer	4 µL
Phusion Green High-Fidelity DNA Polymerase (2 U/µL)	0.2 µL
H_2O	ad 20 µL

Number of cycles	Temperature	Time
1x	98 °C	30 sec
35x	98 °C	10 sec
	69 °C	30 sec
	72 °C	30 sec
1x	72 °C	10 min
1x	4 °C	∞

Overlap PCR:

Template DNA 1 (PCR1)	10 ng
Template DNA 2 (PCR2)	10 ng
Fw Primer	1 µL (0.5 µM)
Rev Primer	1 µL (0.5 µM)
dNTPs	0.4 µL (200 µM)
5X Phusion Green HF Buffer	4 µL
Phusion Green High-Fidelity DNA Polymerase (2 U/µL)	0.2 µL
H_2O	ad 20 µL

Number of cycles	Temperature	Time
1x	98 °C	30 sec
35x	98 °C	10 sec
	71 °C	30 sec
	72 °C	30 sec
1x	72 °C	10 min
1x	4 °C	∞

Target primed plasmid amplification:

Template DNA	100 ng
Primer (Overlap PCR)	100 ng
dNTPs	1 µL (200 µM)
5X Phusion Green HF Buffer	10 µL
Phusion Green High-Fidelity DNA Polymerase (2 U/µL)	0.5 µL
H_2O	ad 50 µL

Number of cycles	Temperature	Time
1x	98 °C	1 min
35x	98 °C	10 sec
	66 °C	30 sec
	72 °C	95 sec
1x	72 °C	10 min
1x	4 °C	∞

Following the PCR reaction, a DpnI digestion was performed to degrade the remaining template DNA and transformation of bacteria was performed.

Gateway cloning

For fusion of human proteins of interest with a V5 or a FLAG tag, the gateway cloning method was used. Gateway cloning entry vectors encoding the protein of interest (pENTR223 or pDONR221, depending on availability) were acquired from Harvard Plasmid Information Database (PlasmID). Cloning into the destination vector pEZYflag or pMAX-DEST was performed using Gateway™ LR Clonase™ II Enzyme mix according to the manufacturer's instructions. 150 ng/µL of destination vector and 100 ng/µL entry clone were used per reaction.

Generation of control vectors by inverse PCR

If available, expression vectors encoding V5 or FLAG tagged proteins of interest were ordered. Since empty expression vectors coding only for the tag were needed for some experiments, the sequence of the protein of interest was deleted by inverse PCR. Primers adjacent to the protein sequence with the 3'-ends facing away from each other were designed and the expression vector was used as the template. The PCR product was the linearized tag vector lacking the sequence for the protein of interest. The following reaction parameters were employed:

Template DNA	250ng
DMSO	1.5µL
Fw Primer	2.5µL (0.5 µM)
Rev Primer	2.5µL (0.5 µM)
dNTPs	1µL (200 µM)
5X Phusion Green HF Buffer	10µL
Phusion Green High-Fidelity DNA Polymerase (2 U/µL)	0.5µL
H_2O	ad 50µL

Number of cycles	Temperature	Time
1x	98 °C	30 sec
25x	98 °C	10 sec
	72 °C	20 sec/kb
1x	72 °C	10 min
1x	4 °C	∞

Following the PCR reaction, a DpnI digestion was performed to degrade the remaining template DNA. For plasmid self-ligation, PCR products needed to be phosphorylated since the primers used for the inverse PCR lacked the 5'-end phosphate group.

DpnI digestion

The restriction enzyme DpnI specifically degrades methylated DNA. Therefore, it is widely used to remove the remaining template DNA after a PCR reaction. The template DNA is of bacterial origin and is thereby methylated, whilst the newly PCR-generated DNA does not have any methylation modification. For the restriction reaction, PCR product was mixed with 2 µL DpnI and incubated for 2 h at 37 °C.

Agarose gel electrophoresis

Agarose powder was boiled in 1x TBE buffer, cooled down, then 6 µL of Midori green was added per 100 µL of dissolved agarose. DNA samples were supplemented with 6x loading buffer, then loaded onto the agarose gel. Separation of samples was performed in 1x TBE buffer at a constant voltage of 120 V. DNA was visualized on a transillumina-tor with UV light and the size of the DNA fragments was determined by comparison to commercially available DNA ladders.

Purification of PCR products

PCR products were purified either immediately after the PCR reaction, or after analyzing the product by agarose gel electrophoresis, using QIAquick® PCR Purification Kit or Invisorb® Spin DNA Extraction Kit, respectively. Purification was performed according to the manufacturer's instructions and DNA was eluted with 40 µL double distilled (dd) H_2O.

5'-End phosphorylation and plasmid self-ligation

Purified inverse PCR products were phosphorylated employing following parameters:

Purified PCR product	40 µL
10x PNK Buffer A	5 µL
ATP (10 mM)	4 µL
T4 Polynucleotide kinase	1 µL

37 °C, 60 min

Next, 5'-end phosphorylation products were again purified and a self-ligation reaction was performed for 2 h at RT:

10x T4 ligase buffer	2 µ
100 ng purified PCR product	x µL
ATP (10 mM)	1 µL
PEG 4000	1 µL
T4 DNA Ligase	1 µ
H_2O	ad 20 µL

Transformation of bacteria

For transformation of bacteria, 50 µL of competent *E.coli XL-1 Blue* cells were thawed on ice and mixed with 5 µL of purified PCR product. After incubation for 30 min on ice, heat shock for the induction of DNA uptake was performed for 45 seconds (sec) at 42 °C. Bacteria were incubated for another 2 min on ice before being mixed with 500 µL

super optimal broth with catabolite repression (SOC) medium and incubated for 1 h at 37 °C under constant gentle shaking. Cells were plated on 2x YT agar plates supplemented with antibiotics (100 µg/mL Ampicillin or 50 µg/mL Kanamycin) and incubated at 37°C ON.

Plasmid preparation

Single colonies of transformed bacteria were picked and grown at 37 °C ON at 200 rpm in 5 mL (“mini culture”) or 200 mL (“maxi culture”) 2x TY medium containing the appropriate antibiotic (100 µg/mL Ampicillin or 50 µg/mL Kanamycin). Bacteria were pelleted and plasmid DNA was isolated employing the QIAfilter Plasmid Maxi Kit for maxi cultures, or the Invisorb® Spin Plasmid Mini Two Miniprep Kit for mini cultures, according to the manufacturer’s instructions. DNA was eluted with 50 µL ddH_2O (mini culture) or 200 µL ddH_2O (maxi culture). DNA concentration was determined using a NanoDrop 8000.

DNA sequencing

DNA was sequenced by Sanger sequencing using the BigDye® Terminator 3.1 Cycle Sequencing Kit under the following conditions:

Template DNA	200 ng
Primer	0.5 µL (0.5 µM)
BigDye 3.1 Mix	1 µL
5x ABI reaction buffer	1.5 µL
H_2O	ad 10 µL

Number of cycles	Temperature	Time
1x	96 °C	2 min
25x	96 °C	10 sec
	55 °C	5 sec
	60 °C	4 min
1x	4 °C	∞

2.2.4 Biochemical Methods

SDS polyacrylamide gel electrophoresis (PAGE)

Sodium dodecyl sulfate polyacrylamide gel electrophoresis (SDS PAGE) was performed to separate proteins according to their molecular weight. Gels were prepared using the Mini-PROTEAN® 3 gel casting equipment according to table 2.1.

After preparation and polymerization of the separation gel, the stacking gel solution was mixed and poured on top. Lanes were generated by insertion of a plastic comb with the designated number of teeth.

Table 2.1. Composition of SDS polyacrylamide gels. Volumes sufficient for a single 1.5 mm gel with the stated acrylamide concentration.

	separation gel			**stacking gel**
	7.5 %	10 %	12.5 %	5%
30% Acrylamide/ Bisacrylamide (29:1)	2.5 mL	3.3 mL	4.1 mL	0.83 mL
ddH_2O	4.8 mL	4.0 mL	3.2 mL	2.8 mL
1.5 M Tris/ Cl pH 8.8	2.5 mL	2.5 mL	2.5 mL	-
0.5 M Tris/ Cl pH 6.8	-	-	-	1.25 mL
10% SDS	100 µL	100 µL	100 µL	50 µL
10% APS	100 µL	100 µ	100 µ	50 µL
TEMED	6 µL	6 µL	6 µL	6 µL

Protein samples were mixed with 2x or 6x sample buffer and heated for 5 min at 95 °C prior to loading onto the gel. Separation of samples was performed in a vertical gel chamber in SDS-running buffer by application of an electric field with a current of 25 mA per gel.

Western transfer and immunoblot analysis

In order to detect specific proteins, separated proteins were transferred from the SDS polyacrylamide gel onto a nitrocellulose membrane by semi-dry western blotting.A Trans-Blot® SD Semi-Dry Transfer Cell was used for this purpose as follows: anode, 3x Whatman paper, SDS gel, nitrocellulose membrane, 3x Whatman paper, cathode. For protein transfer from a 1.5 mm gel, a constant current of 75 mA was applied for

80 min. Afterwards, membranes were blocked with 3 % milk powder in 1x TBST at RT for at least 30 min. Primary antibodies were diluted in 0.5 % milk powder in 1x TBST and incubation of membranes with primary antibody solution was performed ON at 4 °C under constant gentle shaking. Membranes were washed at least 3 times for 10 min with 1x TBST before incubation with the appropriate secondary horseradish-peroxidase conjugated antibody diluted in 0.5 % milk powder dissolved in 1x TBST. After 1 h, membranes were washed at least 6 times for 5 min each with 1x TBST prior to detection of the specific protein bands using an enhanced chemiluminescence protocol with SuperSignal™WestDura Extended Duration Substrate. Luminescence was detected using CL-XPosure™ x-ray films developed with a Curix 60 processor (Agfa) or with an Advanced Fluorescence Imager (INTAS) operated with the corresponding ChemoStar software (INTAS).

2.2.5 Cell biology Methods

Protein overexpression and endogenous co-immunoprecipitation

For the overexpression co-immunoprecipitation (co-IP) assay, 293T cells in a 10 cm dish were transfected with a plasmid expressing the FLAG or V5 tagged protein of interest, and with expression plasmids for PB1, PB2 and PA of either A/Pan/99 or A/Thai/04 using PEI (see section 2.2.1). In the case of the negative control samples, PB1, PB2, PA expression plasmids and the empty FLAG or V5 vector were transfected. 1.75 µg of each plasmid was used for transfection, resulting in a total DNA amount of 7 µg per 10 cm dish. Cells were lysed and further analyzed 24 h post transfection.

In the case of endogenous co-IP, A549 cells in a 10 cm dish were infected at an MOI of 5 with either A/Pan/99-WT or A/Thai/04-WT virus (see section 2.2.2). 16 hours post infection, cells were lysed and further analyzed.

For lysis, cells were washed once with ice cold PBS, then lysed for 10 min on ice with 500 µL IP-Lysis buffer per dish, transferred into a 1.5 mL reaction tube, and centrifuged for 10 min at 13.000 g at 4°C.

For each sample, one reaction tube containing 20 µL Protein G Agarose beads and one reaction tube containing 30 µL Protein G Agarose beads were prepared by washing 3 times with 500 µL IP-Lysis buffer. Centrifugation in-between washing steps was performed at 3.000 rpm for 3 min at 4 °C. After washing, the cell lysate was added to the 20 µL bead reaction tube for pre-clearing, while 500 µL IP-Lysis buffer containing 2 µg of either α-V5, α-FLAG M2, α-Hsc70 or α- cMyc antibody was added to the

30 µL bead reaction tube for coupling. Pre-clearing as well as coupling was performed at 4 °C on a rotating platform for at least 2 h.

Both bead mixtures were centrifuged at 3.000 rpm for 3 min at 4°C and the coupling solution was discarded. 50µL of the pre-cleared lysate was mixed with 6x SDS sample buffer, boiled at 95°C for 5 min and stored at -20 °C as a sample for whole cell lysate (WCL). The remaining 450 µL of pre-cleared lysate was added to the antibody-coupled beads and incubated ON at 4 °C on a rotating platform.

To remove non-bound proteins, Protein G Agarose beads were washed 3 times with ice cold PBS. For the last washing step, beads in PBS were transferred to a new reaction tube to avoid elution of proteins bound unspecifically to the reaction tube. Immunoprecipitated proteins and their interaction partners were eluted by incubation in 30 µL 2x SDS sample buffer for 10 min at 95 °C. Whole cell lysate and immunoprecipitate were analyzed by SDS PAGE and immunoblotting (see section 2.2.4).

Polymerase activity assay

For the polymerase activity assay, also known as minigenome or minireplicon assay, cells need to be transfected with expression plasmids encoding the polymerase proteins and the NP protein of the analyzed influenza strain (to enable the formation of a polymerase complex), a reporter plasmid under the control of the UTR of an influenza genome segment (for the determination of the polymerase activity) and a constitutively expressed reporter plasmid (to allow for normalization of protein expression). For this study, 293T cells were transfected in 12-well plates using PEI (see section 2.2.1). Per well, the amounts of expression plasmids specified in table 2.2 were transfected.

To determine the influence of proteins of interest on influenza polymerase activity by overexpression assays, either 100 ng or 500 ng of the plasmid encoding the investigated protein were additionally transfected per well. The total amount of transfected DNA in each experiment was kept constant using empty expression plasmids corresponding to those containing the analyzed protein. So for positive controls, 500 ng of the analogous empty vector was transfected. Cell lysis and luciferase activity measurement was performed 24 h p.t. using a Dual-Luciferase® Reporter Assay System Kit according to manufacturer's instructions. A/Thai/04 lysates were diluted 1:10 in the kit lysis buffer before measurement of luciferase activity.

To determine the influence of HSPA8 on influenza virus polymerase activity by siRNA knock down, 293T cells were transfected with 25 pmol per well of either NT siRNA or HSPA8 siRNA mix using Lipofectamine® RNAiMAX (see section 2.2.1) 24 hprior to transfection with the minigenome expression system (table 3.2). For negative controls, Lipofectamine® RNAiMAX was added to cells without siRNA (mock transfection) and in the second step the PB2 expression plasmid was replaced by the corresponding empty expression vector. 24 h after transfection of the minigenome expression system, determination of luciferase activity was performed as described above.

Table 2.2. Amount of expression plasmids transfected per well of a 12-well plate used for polymerase activity assay.

Expression Plasmid	Amount for A/Pan/99 [ng]	Amount for A/Thai/04 [ng]
pHW2000-A/Pan/2007/99-**PA**	50	-
pCAGGS-A/Thai/1(KAN-1)/04-**PA**	-	50
pHW2000-A/Pana/2007/99-**PB1**	50	-
pCAGGS-A/Thai/1(KAN-1)/04-**PB1**	-	50
pHW2000-A/Pan/2007/99-**PB2**	50	-
pCAGGS-A/Thai/1(KAN-1)/04-**PB2**	-	50
pHW2000-A/Pan/2007/99-**NP**	100	-
pCAGGS-A/Thai/1(KAN-1)/04-**NP**	-	50
pPol-SapI-A-NS-Luc	50	50
pTK-Luc	5	5

Cell viability assay (MTT test)

To identify possible effects of siRNA treatment on cell viability, a MTT test was performed. Cells were seeded in 96 well plates and transfected with 2 pmol/well of either NT siRNA or HSPA8 siRNA mix using Lipofectamine® RNAiMAX as described in section 2.2.1. Control cells were mock transfected and 4 hours p.t. medium was replaced by 100 %, 10 % or 1 % DMSO diluted in fresh transfection D-MEM. At 24, 48, 72, 96 and 120 hours p.t. cell viability was analyzed using the Cell Proliferation Kit I according to the manufacturer's protocol.

Immunofluorescence analysis

The subcellular localization of HSPA8 in influenza virus infected cells was visualized by indirect immunofluorescence analysis using fluorochrome-coupled antibodies. A549 cells were seeded on cover slips and infected with either A/Pan/99-WT or A/Thai/04-WT virus at an MOI of 1 (see section 2.2.2). 4 or 8 hours post infection cells were washed twice with PBS and fixed ON at 4 °C in 4 % PFA. After removal of PFA, cell permeabilization was performed for 20 min at RT with 0.1 % IGEPAL® CA-630 diluted in PBS. Cells were washed 3 times with PBS and blocked for 1 hour in 1 % milk powder in PBS, before being incubated with primary antibodies diluted in 1 % milk powder/PBS for 1 hour at 37 °C. Next, cells were washed three times with PBS, then incubation with suitable fluorophore-labelled secondary antibodies and DAPI, diluted in 1 % milk powder/PBS, was performed for 30 min at RT in the dark. Cells were washed 3 times with ddH_2O and cover slips were mounted on glass slides using Mowiol 4-88. Antibody-staining of specific proteins was visualized using a Zeiss 780 confocal laser scanning microscope (LSM) equipped with a 63x oil immersion objective, with a numerical aperture of 1.4. Images were captured and processed with Zeiss ZEN imaging software.

2.2.6 SILAC Mass spectrometry analysis

To identify the cellular interactome of influenza A/Pan/99 and influenza A/Thai/04, a stable isotopic labelling by amino acids in cell culture (SILAC) approach followed by high-resolution liquid chromatography (LC) tandem mass spectrometric analysis was utilized. The detailed workflow of the performed SILAC experiment is described in figure 3.2.

SILAC labeling of A549 cells

A549 cells were labelled with stable isotopic amino acids according to the protocol published by *Ong and Mann* [148]. A549 cells were grown in SILAC DMEM containing 10 % dialyzed FBS, 50 mg/mL Pen/Strep as well as light (L-lysine (K0) and L-arginine (R0)), intermediate (L-[D_4] lysine (K4) and L-[$^{13}C_6$] arginine (R6)) or heavy (L-[$^{13}C_6$, $^{15}N_2$] lysine (K8) and L-[$^{13}C_6$, $^{15}N_4$] arginine (R10)) labelled amino acids. Lysine was added at a concentration of 146 mg/L and arginine at a concentration of 84 mg/L. Cells were grown in cell culture flasks and passaged five times to ensure incorporation of labelled amino acids into cellular proteins (see section 2.2.1). To prevent integration of unlabelled L-lysine or L-arginine by the use of trypsin during cell passaging, Cell Dissocia-

tion Buffer was used for cell detachment. After five cell doublings, cells were frozen at -80 °C in SILAC DMEM containing 20 % dialyzed FBS and 10 % DMSO.

Monitoring labelling efficiency of cells

Protein lysates were generated from light, intermediate and heavy SILAC labelled A549 cells and prepared for, then analyzed by LC-MS as described below. Efficient labelling was demonstrated at the peptide level by use of Proteome Discoverer 1.4 software.

Infection of SILAC labelled cells with influenza A virus

Light, intermediate and heavy labelled A549 cells were seeded in SILAC DMEM at a density resulting in a confluency of 80 % to 90 % on the day of infection. For each cell type, 2x 10 cm dishes were infected at an MOI of 1.5 with either A/Pan/99-wt, A/Pan/99-PB2-Strep or A/Thai/04-PB2-Strep virus, diluted in PBS^+ (see section 2.2.2). Cells were then incubated for 16 h at 37 °C in SILAC infection DMEM.

Cell lysis, BCA test and co-precipitation

Infected cells were washed twice with PBS, detached from the dish in 1 mL ice cold PBS using a cell scraper, and transferred to a 2 mL reaction tube. The dish was flushed with an additional 0.75 mL PBS to collect the remaining cells, which were also transferred to the reaction tube. After centrifugation at 2.000 rpm for 5 min at 4 °C, the supernatant was discarded and the cells were lysed in 1 mL ice cold cell lysis buffer for 1 h at 4 °C on a rotating platform. After centrifugation at 13.000 rpm for 20 min at 4 °C the cleared lysates from the same SILAC and infection state were merged in a new 2 mL reaction tube. The protein concentration of each state was determined by BCA assay at dilutions of 1:2 and 1:10 in triplicates according to the manufacturer's protocol.

Lysates from the 3 SILAC states were mixed in a 1:1:1 protein ratio and 50 µL of the mixture was prepared as an input sample for immunoblot analysis (see section 2.2.5). The remaining lysate was used for co-precipitation of PB2 with Strep-Tactin resin. For co-precipitation, 4 mL Strep-Tactin® Superflow® 50 % suspension was washed 3 times with 5 mL cold Buffer W. Centrifugation in-between washing steps was performed at 3.000 rpm for 3 min at 4 °C. After the last washing step Buffer W was discarded, the cell lysate mixture was combined with the Strep-Tactin and precipitation was performed at 4 °C ON on a rotating platform.

On the next day, the sample was centrifuged at 3.000 rpm for 3 min at 4 °C and 50 µL of the supernatant was prepared for immunoblot analysis as the non-bound (NB) sample. The remaining supernatant was discarded and the Strep-Tactin and bound pro-

teins were washed 3 times with Buffer W. For the last washing step, Strep-Tactin in Buffer W was transferred to a new reaction tube to avoid elution of proteins bound unspecifically to the reaction tube. Elution was performed 3 times with 2 mL Buffer E for 1 h at 4 °C on a rotating platform. Eluate 1 to 3 were combined and concentrated at 12.500 rpm at 4 °C using Vivaspin® 500 columns. The concentrated eluate was mixed with 6x SDS sample buffer, discharged from the BSL-3 laboratory and boiled at 95 °C for 10 min.

Preparation of SILAC samples for LC-MS

The sample obtained after Co-precipitation was alkylated by incubating it with 50 mM Iodoacetamide (IAA) for 30 min at RT in the dark, before proteins were separated by SDS PAGE. The gel was washed 3 times with MS grade water and stained for 1 h with SimplyBlue™ SafeStain. After removal of the redundant stain by washing with MS grade water ON, the visualized protein lane was cut into 10 slices, each of them cut into smaller pieces of approximately 1 mm, and transferred into a low retention reaction tubes.

The small gel cubes were washed several times with destaining solution for 30 min at 37 °C until they were fully destained. Afterwards the gel pieces were dehydrated with 100 % acetonitrile (ACN) and in-gel digestion was performed. For this, one vial of MS grade trypsin was dissolved in 150 µL HCl and 1350 µL enzyme reaction buffer, before 75 µL trypsin solution was added to each of the reaction tubes containing the dried gel cubes. After 30 min at 4 °C the gel pieces had fully absorbed the trypsin solution and an additional 37.5 µL were added. The mixture was incubated for a total of 90 min at 4 °C, then 277.5 µL enzyme reaction buffer was added and in-gel digestion was performed at 37 °C ON. Supernatants were transferred into new low retention reaction tubes and residual peptides were extracted out of the gel cubes by incubation with 100 µL extraction buffer for 30 min at 37 °C whilst shaking. Combined peptide extracts were dried in a vacuum concentrator until samples were completely dry, then frozen at -20 °C.

After all 4experiments were conducted, dried samples were thawed and acidified to a pH of approximately 2, by resuspension in 1 % TFA. Desalting C18-Stage tips were prepared by stamping out round pieces out of an Empore™ Octadecyl C18 47mm Extraction Disc and packing them into 200 µL pipette tips by use of a 1702 Plunger Assembly. Desalting of peptides was conducted through the use of centrifugation steps at 2.000 g for 1 min (see table 2.3). Desalted peptides were dried in a vacuum concentrator, dissolved in 20 µL 0.1 % FA and loaded into a 96 well plate for MS analysis.

Table 2.3. Steps for desalting of peptides.

Step	Solution added to C18-Stage tip
Activation	100 µL MeOH
Equilibration	1. 100 µL 0.1 % FA, 80 % ACN
	2. 100 µL 0.2 % TFA
Loading	Samples dissolved in 1 % TFA
Washing	100 µL 0.2 % TFA
Elution	100 µL 0.1 % FA, 80 % ACN

Nano-LC and MS analysis

Peptide samples were separated by reverse phase EASY-nano-LC 2 using a C18-A column. The nano-LC setup was connected to a LTQ Orbitrap Discovery™ mass spectrometer equipped with a nanoelectrospray ion source.

Peptides were separated and eluted by applying a 65 min gradient from 2 % to 40 % between buffer A (0.2 % formic acid in water) and buffer B (0.2 % formic acid in acetonitrile) at a flow rate of 300 nl/min with a spray voltage of 1.8 kV and 200 °C capillary temperature.

Data dependent acquisition was performed using Xcalibur™ software 2.0 in positive ion mode. Full scan MS spectra (from m/z 300 to 1.700) were acquired in the FT-Orbitrap with a resolution of M/ΔM = 30.000. The 5 peptide ions with the highest intensity were sequentially isolated for fragmentation by collision induced dissociation (CID) in the linear ion trap. The Orbitrap lock mass feature was applied to improve mass accuracy.

Data processing and evaluation

Raw data acquired by MS analysis was processed using MaxQuant software version 1.5.1.2. Proteins were identified using following parameters: Labelling standard; Label multiplicity 3; the 4 SILAC labels K4, K8, R6 and R10; Variable modifications Acetyl (Protein N-term), Oxidation (M) and Deamidation (NQ); Digestion mode specific; Enzyme Trypsin/P; Max missed cleavages 2; Match type match from and to; Fixed modification Carbmidomethyl (C); Re-quantify; Match between runs; Decoy mode revert; Include contaminants. The false discovery rate (FDR) was set to 1 % and only protein groups identified by at least one unique peptide were kept for further analysis. Searches were performed against the Homo Sapiens data base of National Center for Biotechnology Information (NCBI) with 91.670 entries as of 08.10.2015 and against the influenza A/Pan/99 (Q1NZ46; Q1NZ48; Q1NZ45; Q1NZ38; Q1NZ39; Q8AZB6;

Q1NZ40; Q1NZ41; Q1NZ43;) and influenza A/Thai/04 (H8PF41; H8PF42; H8PF44; H8PF45; Q5L4F7; H8PF47; Q5QF2; Q5QF24; Q5L4F5) database. For quantification, only unique and razor peptides were used with a minimum ratio count of 2.

After retrieving a list of protein group identifications and quantifications from MaxQuant 1.5.1.2, additional data analysis steps were performed to help interpret the results. The reproducibility of biological replicates was evaluated by scatter plot analysis and calculation of the Pearson correlation using Perseus software, version 1.5.0.31. In addition, statistical tests were performed by volcano plot analysis to identify protein groups that were significantly changed between PB2-Strep samples and the internal control. Significantly altered protein groups were subjected to gene ontology (GO) term analysis with the PANTHER Gene List Analysis v11.1 online tool, in order to gain insight into their biological function.

To extract protein groups with the utmost probability of being PB2 interaction partners, the list of statistically significant protein groups was filtered based on the criteria that protein groups have to show a t-test difference of ≥ 1 in at least 2 out of the 4 experiments. The resulting protein hit list was further analyzed using STRING: functional protein association networks v10.5, to visualize relationships between hit proteins. The obtained interaction network for the hit proteins was clustered using the Markov Cluster algorithm (MCL) with the inflation parameter set to 2.

3. Results

As part of the influenza virus polymerase complex, PB2 plays a crucial role in the transcription and replication of the viral genome, as well as in the determination of the viral host range [57,71,137]. Consequently, the interaction of PB2 with the host cell proteome is of major interest. Preceding studies focusing on the host cell interactome of PB2 were either performed in the context of transiently transfected, non-infected cells, or with laboratory/mouse-adapted influenza virus strains [138-144]. In contrast, this study aimed to identify PB2 cellular interaction partners not only in the context of infected cells but also using non-laboratory adapted seasonal (represented by A/Panama/2007/99 (H3N2)) and highly pathogenic (represented by A/Thailand/(KAN-1)/04 (H5N1)) viral strains from human isolates.

Interactions of PB2 with cellular proteins were examined in a SILAC based affinity-purification mass spectrometry (AP-MS) approach. Mass spectrometry enabled the highly sensitive detection of protein-protein interactions (PPI) under physiological conditions in a relevant biological context [149], in this case human alveolar epithelial cells (A549) infected with influenza virus. Through the generation and use of influenza viruses carrying a Strep-tag at the C-terminus of their PB2 protein, affinity purification upstream of MS enriched PB2 and its interaction partners while non-specific contaminants were reduced. The use of triple SILAC labelling made it possible to perform a quantitative comparison between cells infected with PB2-Strep viruses and the internal control A/Pan/99-WT. This allowed the further exclusion of false positives and external protein contaminants and increased confidence in the identified interaction partners of PB2.

The interactome screen and subsequent validation experiments revealed new and already described interactions of PB2 with cellular proteins, and demonstrated the impact of these proteins on polymerase activity. The obtained data also hinted at differences in the importance of these identified proteins on the polymerase activity of seasonal and highly pathogenic influenza virus strains. Further analysis of the PB2 interactor HSPA8 revealed its relevance for replication, polymerase activity and the integrity of the PB2 protein of A/Pan/99.

3.1 Proteomic analysis of the PB2 interactome of influenza A/Panama/2007/99 (H3N2) and A/Thailand/(KAN-1)/04 (H5N1) viruses

3.1.1 Generation and functional characterization of PB2-Strep viruses for co-precipitation experiments

The PB2 protein sequence of A/Pan/99 (H3N2) and A/Thai/04 (H5N1) differs in 40 amino acids (aa) which correspond to 5.3 % of a total of 759 aa (figure 3.1.A). For example, one of the differences is located at position 627 which is known to play a role in the adaptation of avian influenza viruses to the mammalian host (see section 1.3.3). Interestingly, PB2 of the A/Thai/04 strain isolated from a human case contains the avian type glutamic acid and not the mammalian type lysine at this position.

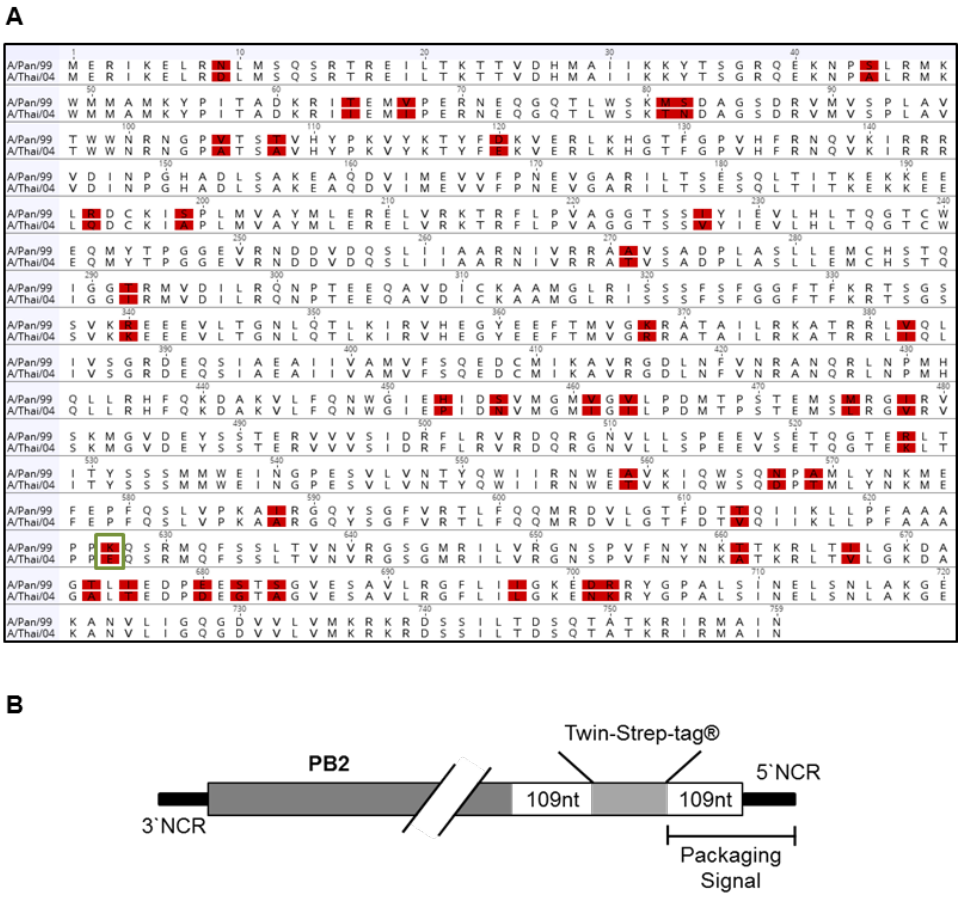

Figure 3.1. PB2 sequence information of constructed influenza A viruses. A Protein sequence comparison of A/Pan/99 and A/Thai04 PB2. Differences in aa sequence are highlighted in red. Host adaption relevant protein position 627 is framed in green. **B** Structure of the PB2 genetic constructs, used to generate recombinant viruses expression Strep-tagged PB2, which is described in detail in the text.

The plasmids encoding A/Pan/99 and A/Thai/04 PB2 were modified as described in section 2.2.3 to generate recombinant viruses that express Strep-tagged PB2. Thereby it is important to consider the packaging sequence of the genome segment coding for the protein to ensure not only expression of the fusion protein but also packaging of the genomic segment into viral particles. Thus, to generate recombinant A/Pan/99 (H3N2) and A/Thai/04 (H5N1) viruses that express a Strep-tagged PB2 protein the pHW2000 constructs need to contain the PB2 coding sequence followed by the Twin-Strep-tag® sequence, the 143 nt long packaging sequence for the PB2 segment (a duplication of the last 109 nt of the PB2 coding sequence followed by the 5′ NCR) and a stop codon (see figure 3.1.B). The accuracy of the PB2-Strep constructs was analyzed and confirmed by Sanger sequencing.

The use of recombinant A/Pan/99 (H3N2) and A/Thai/04 (H5N1) viruses that express a Strep-tagged PB2 protein has the advantage that protein specific antibodies are not needed for precipitation. Hence, interactions of host cell proteins with the epitope region of PB2 that would be interrupted by antibody binding are still intact and can be detected by downstream MS.

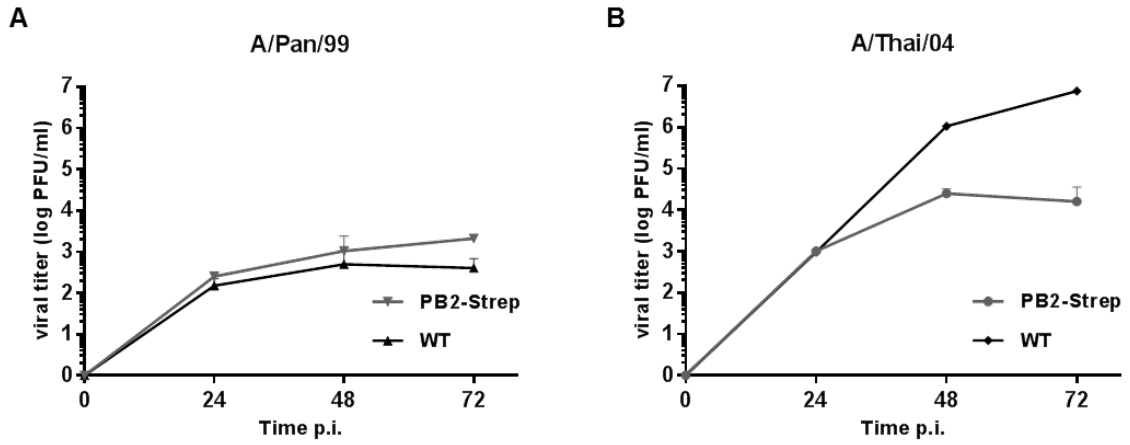

Figure 3.2. Growth characteristics of WT and Strep-PB2 viruses. A549 cells were infected with A/Pan/99-WT, A/Pan/99-PB2-Strep (**A**), A/Thai/04-WT or A/Thai/04-PB2-Strep (**B**) viruses. Viral titers (log PFU/ml) at 24, 48 and 72 h were determined by standard plaque titration assay. Displayed values represent the mean +SD of N=2.

After the successful rescue of recombinant viruses in 293T cells and subsequent virus propagation in embryonated chicken eggs, growth characteristics of the PB2-Strep viruses and the corresponding WT viruses were compared. Therefore A549 cells were infected and viral titers at 24, 48 and 72 h were determined by plaque-forming assay.

While A/Pan/99-PB2-Strep virus grew to similar but slightly higher titers (especially from 24 h onwards) as A/Pan/99-WT virus (see figure 3.2.A), growth of A/Thai/04-PB2-Strep was attenuated compared to the WT virus at 48 and 72 h (figure 3.2.B). However, given that the A/Thai/04-PB2-Strep virus did not replicate less efficient than the A/Pan/99-WT and A/Pan/99-PB2-Strep viruses, it was considered suitable for AP-MS analysis. In addition, this finding supported the decision to perform PB2 precipitation experiments at 16 h post infection, being in the time frame of monocyclic infection and ensuring the highest similarity between WT and PB2-Strep virus growth.

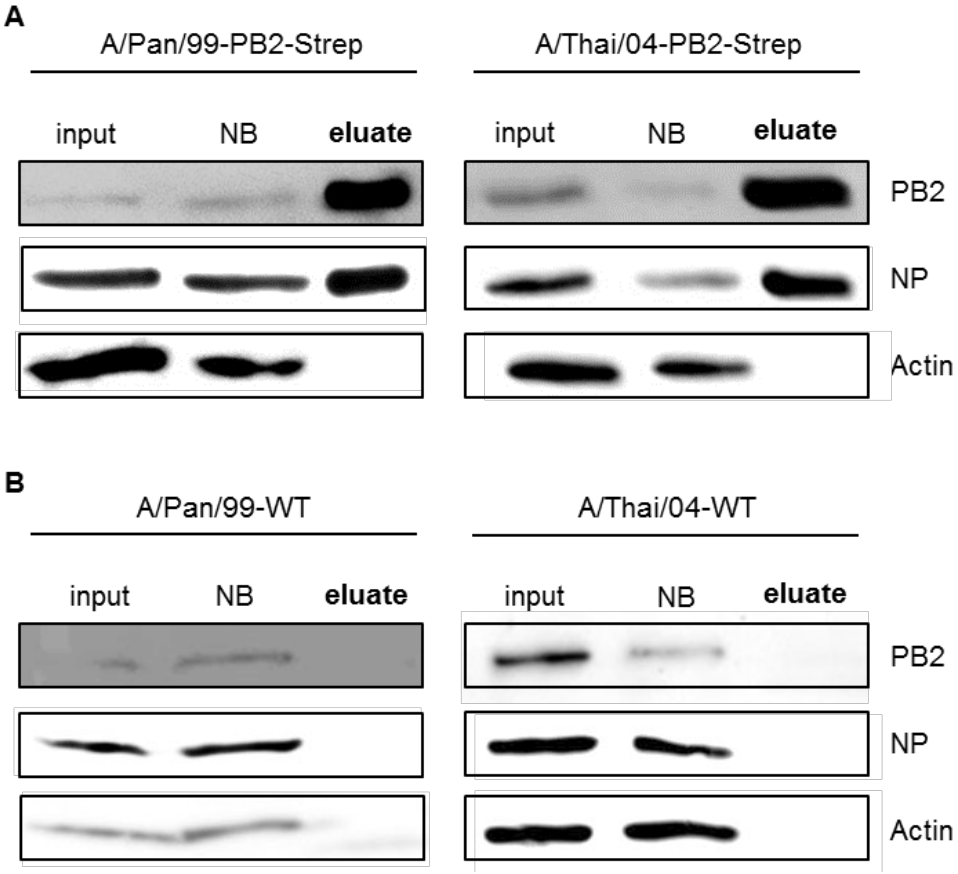

Figure 3.3. Recombinant PB2-Strep proteins co-precipitate viral NP. A549 cells were infected at an MOI of 1 with either A/Pan/99/-WT, -PB2-Strep, A/Thai/04-WT or -PB2-Strep viruses. 16 h p.i. cell lysates were combined with Strep-Tactin® Sepharose® and precipitation was performed overnight. The eluted proteins (eluate) of PB2-Strep (**A**) and WT (**B**) virus samples, as well as 5 % of the corresponding cell lysates (input) and non-bound (NB) proteins were analyzed by SDS PAGE. Immunoblotting analysis was performed with the indicated antibodies.

To test the functionality of the tag, A549 cells were infected with WT and PB2-Strep viruses at an MOI of 1. After 16 h of infection, cells were lysed and precipitation with Strep-Tactin® Sepharose® was performed. Figure 3.3 shows the precipitation of Pan-

PB2-Strep and Thai-PB2-Strep proteins (figure 3.3.A) whereas PB2-WT could not be detected in the IP fraction (figure 3.3.B), thus demonstrating the functionality of the tag in the context of infection. Viral NP, a known interaction partner of PB2, was used as a positive control for co-precipitation. NP was present in the eluate of Strep- but not WT-virus lysates, indicating the applicability of the constructed Strep-tagged proteins for co-precipitation experiments. In addition, the absence of the cellular protein actin after precipitation in PB2-Strep eluates underlined the specific precipitation of the tagged proteins and their interaction partners.

3.1.2 Experimental setup

To identify cellular interaction partners of the PB2 protein of the seasonal strain A/Pan/99 (H3N2) and the highly pathogenic strain A/Thai/04 (H5N1), a triple SILAC approach combined with high-resolution LC tandem mass spectrometry was employed. The workflow of the SILAC experiment is shown in figure 3.4.

A549 cells were cultured in medium containing light (R0/K0), intermediate (R6/K4) or heavy (R10/K8) arginine and lysine isotopes. The small mass differences between proteins derived from differentially labeled cells can be distinguished by MS. Hence, a peptide signal can be attributed to one SILAC state and thereby interaction partners of different viral strains can be distinguished.

3.1. Infection state of light, intermediate and heavy A549 cells in the 4 conducted SILAC experiments.

Experiment	Light state	Intermediate state	Heavy state
A	A/Pan/99-WT	A/Pan/99-PB2-Strep	A/Thai/04-PB2-Strep
B	A/Pan/99-WT	A/Thai/04-PB2-Strep	A/Pan/99-PB2-Strep
C	A/Pan/99-WT	A/Pan/99-PB2-Strep	A/Thai/04-PB2-Strep
D	A/Pan/99-WT	A/Thai/04-PB2-Strep	A/Pan/99-PB2-Strep

In total, 4 SILAC experiments were conducted, with each experiment representing a biological repeat. Labelled A549 cells were infected with A/Pan/99-WT (light state) as an internal control, A/Pan/99-PB2-Strep (intermediate state) or A/Thai/04-PB2-Strep (heavy state) at an MOI of 1.5. For replicates B and D, the virus used to infect cells in

each state was changed to account for differences caused by cell labeling. Thus, intermediate cells were also infected with A/Thai/04-PB2-Strep and heavy cells with A/Pan/99-PB2-Strep (see table 3.1). At 16 h post infection, cells were lysed and a sample from each state was taken and the protein concentration measured by BCA assay. Equivalent amounts of proteins from each state were then mixed and PB2-Strep was precipitated using Strep-Tactin® resin.

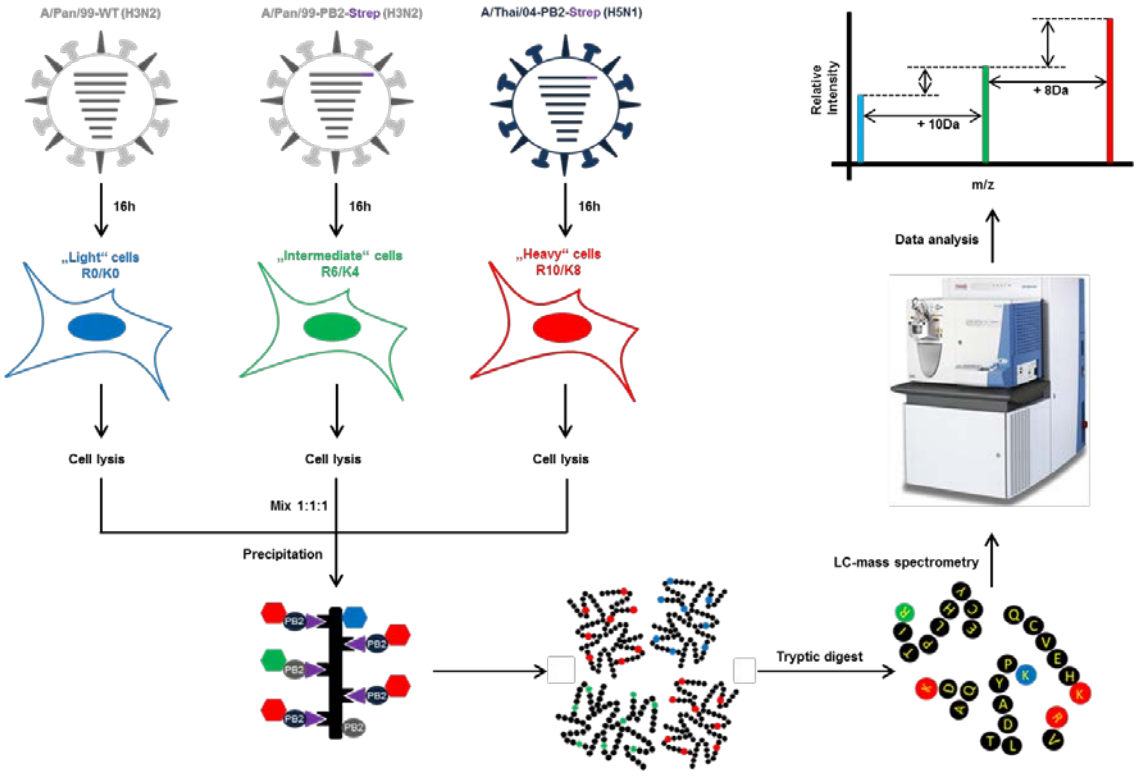

Figure 3.4. Workflow of SILAC experiments. A549 cells were differentially labelled by cultivation in medium containing light (R0/K0), intermediate (R6/K4) or heavy (R10/K8) amino acid isotopes. Cells were infected with A/Pan/99/-WT, A/Pan/99-PB2-Strep or A/Thai/04-PB2-Strep at an MOI of 1.5. At 16 hours p.i. cells were lysed, proteins were mixed in a 1:1:1 ratio and PB2-strep was precipitated with Strep-Tactin® resin. Eluted proteins were separated by size, digested with trypsin and the resulting peptides were analyzed using a LTQ-Orbitrap mass analyzer.

A sample of the input mix, the non-bound fraction and eluate 1 to 3 was analyzed by SDS PAGE and immunoblotting in order to monitor co-precipitation efficiency. This is shown in figure 3.5, where it can be seen that PB2 and its known interaction partner NP are specifically precipitated, whilst the negative control protein actin is absent from the eluate fraction. Eluted proteins were then concentrated by membrane ultrafiltration and disulfide bounds were broken by β-mercaptoethanol. After alkylation of free thiol groups on cysteine residues by treatment with iodacetamide, proteins were separated

by SDS PAGE and visualized by Coomassie staining. The protein lane was cut into ten slices and proteins were subjected to in-gel digestion by trypsin. The resulting peptide mixture was separated by high-performance liquid chromatography on a Nano-LC and analyzed using a LTQ Orbitrap Discovery™ mass spectrometer (see section 2.2.6).

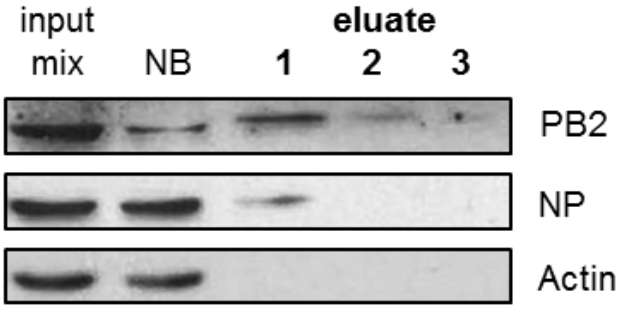

Figure 3.5. Precipitation control for SILAC experiments. Cell lysates from light, intermediate and heavy states were mixed in equal protein amounts and loaded onto Strep-Tactin® resin. After washing, proteins were eluted 3 times with elution buffer. Samples of input, non-bound and eluate 1 to 3 were analyzed by SDS PAGE and immunoblotting using the indicated antibodies. Shown is a single representative of the 4 SILAC replicates.

3.1.3 MS data evaluation

Evaluation of MS data was performed using MaxQuant software. In total, 2446 protein groups, including 18 viral proteins, were identified. A protein group consists of proteins which cannot be unambiguously identified by unique peptides, for example different protein isoforms. For quantification, only unique peptides and razor peptides (peptides which are shared between protein groups) were used with a FDR of 1% and a minimum ratio count of 2, leading to the quantification of 1842 protein groups. Intermediate to light (M/L) and heavy to light (H/L) ratios (representing the abundance of a protein group in A/Pan/99-PB2-Strep or A/Thai/04-PB2-Strep samples proportional to its abundance in the control sample A/Pan/99-WT) were calculated as the median of all peptide ratios assigned to a distinct protein group [150]. For further data analysis using Perseus software, peptide ratios were specified as log2 values.

Reproducibility between the 4 biological replicates A to D was verified by scatter plot analysis of M/L and H/L ratios (figure 3.6). The calculated Pearson correlation is a measure of linear correlation between two variables, in which 0 represents no linear correlation and 1 represents total positive linear correlation. In this study, the Pearson correlation ranged from 0.569 to 0.823 (figure 3.6.A) between replicates for A/Pan/99-PB2-Strep and from 0.858 to 0.922 for A/Thai/04-PB2-Strep samples (figure 3.6.B). To identify protein groups that were significantly changed in abundance between

PB2-Strep samples and the internal control, a one sample t-test of M/L and H/L ratios was performed, and displayed by volcano plot analysis (figure 3.7).

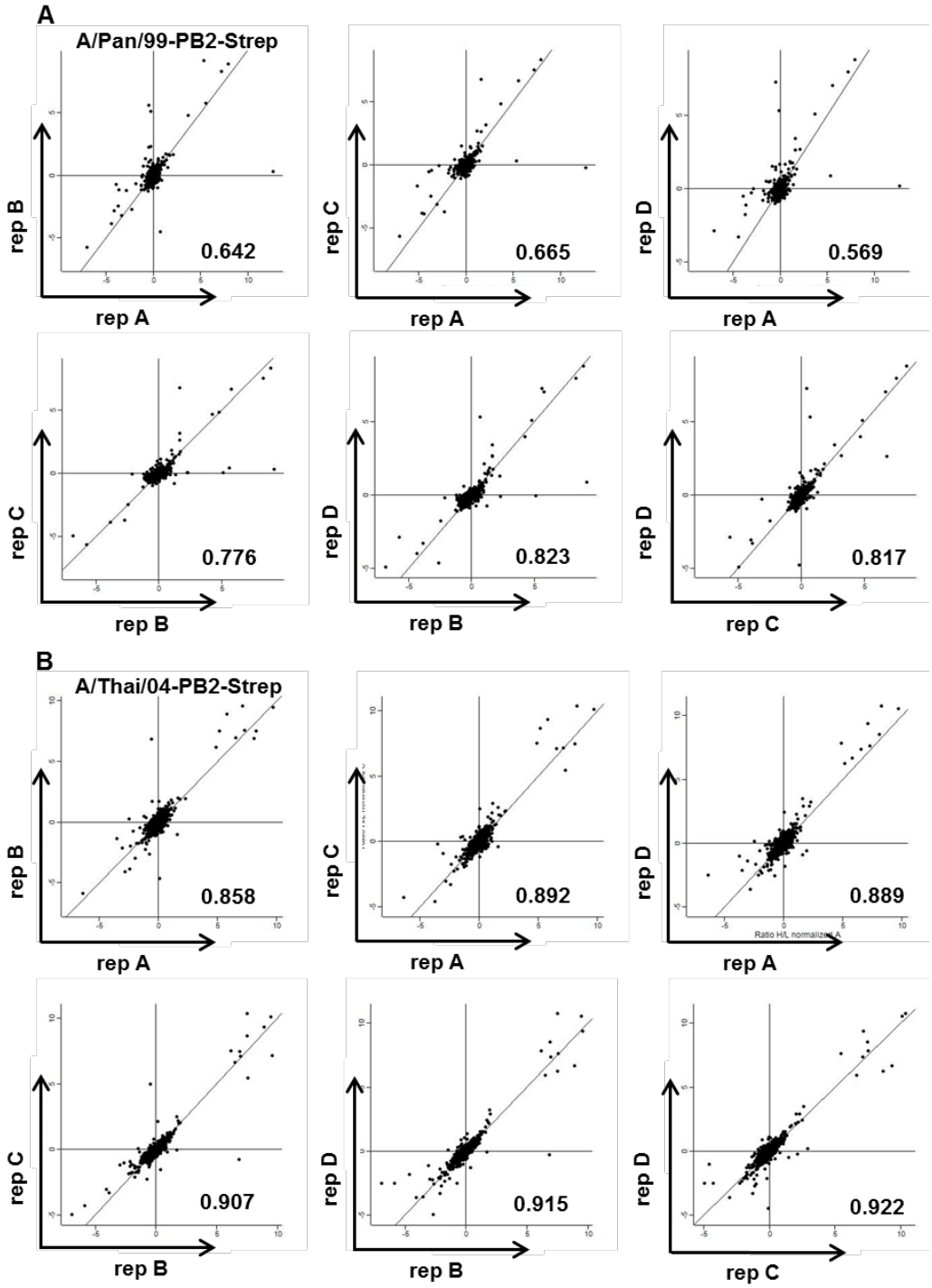

Figure 3.6. Correlation of protein ratios between replicates. Scatter Plot analysis of 4 biological replicates of **A** A/Pan/99-PB2-Strep and **B** A/Thai/04-PB2-Strep samples. Displayed are log2 values of M/L and H/L ratios of indicated replicates and the corresponding Pearson correlation. Dots represent protein groups.

Protein groups with a p-value of < 0.05 and a t-test difference of > 0 are depicted as blue dots. They represent protein groups that are significantly changed and are more abundant in A/Pan/99-PB2-Strep (189 cellular protein groups) and/or A/Thai/04-PB2-Strep (381 cellular protein groups) eluates compared to the A/Pan/99-WT control (see supplementary table S.1 for a complete list of significantly changed protein groups). For both viral strains, all viral proteins that were included in the MS data analysis were identified, and PB2 was the most significant and most abundant protein. For information about p values and t-test differences of viral proteins see supplementary tables S.2 and S.3.

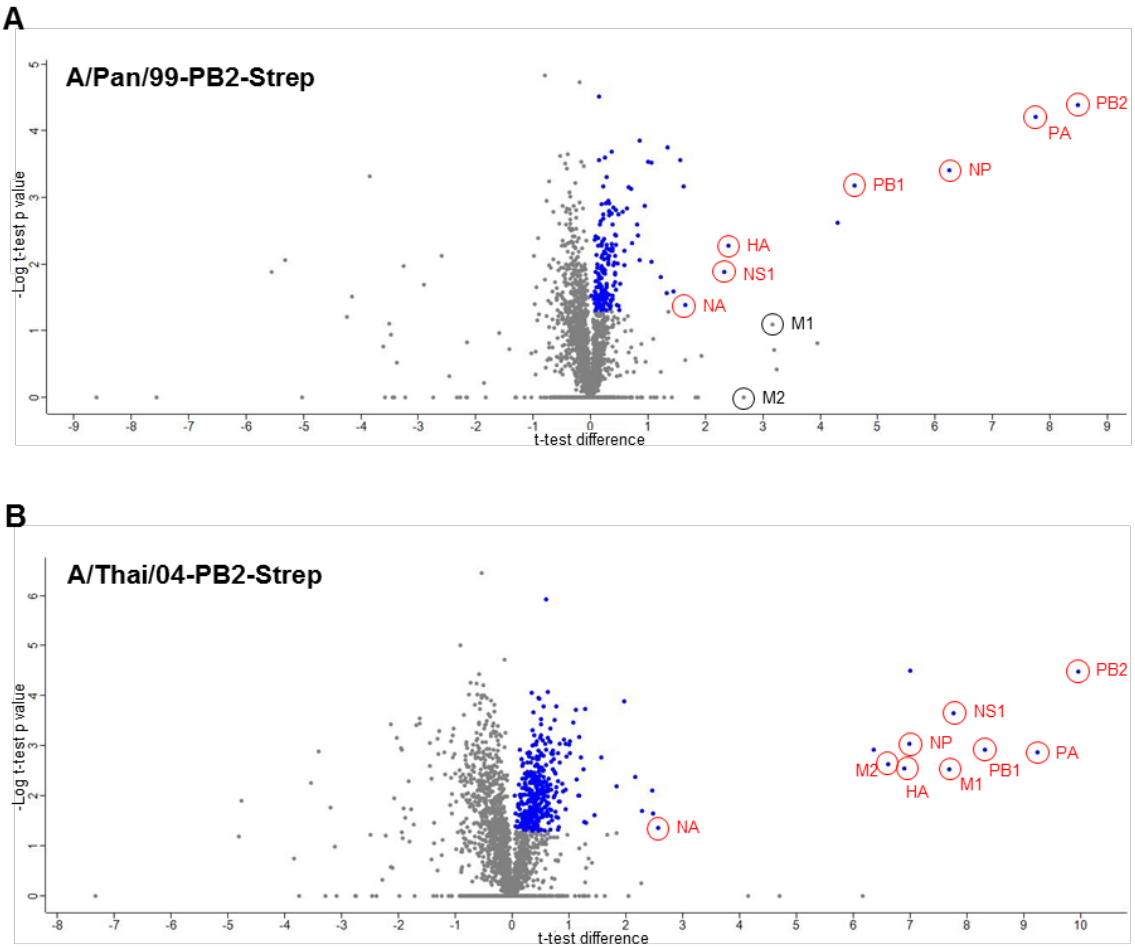

Figure 3.7. Significance and t-test difference of identified proteins. Volcano plot analysis for **A** A/Pan/99-PB2-Strep and **B** A/Thai/04-PB2-Strep samples was performed using Perseus software. One-sample t-test values were calculated for M/L and H/L ratios (log2) of 4 replicates and plotted as –log of p values on the y axis. The t-test difference was plotted on the x axis. Dots represent protein groups. Significantly changed protein groups with a t-test difference of >0 are depicted in blue. Detected viral proteins of A/Pan/99 and A/Thai/04 with a p-value of < 0.05 are encircled in red whereas viral proteins with a p-value of > 0.05 are encircled in black.

3.1.4 Protein classification

Evaluation of MS data revealed 487 protein groups significantly changed in abundance with a t-test difference of > 0 in A/Pan/99-PB2-Strep or A/Thai/04-PB2-Strep eluates (referred to as filtered list/filtered protein groups or UA, see supplementary table S.1 for a complete list of these protein group).

Out of these proteins, 131 (representing 26.9 %) were also found in other proteomic screens that looked for interaction partners of the PB2 protein of other influenza virus strains, either expressed alone or as part of the viral polymerase complex (figure 3.6) [138-142].

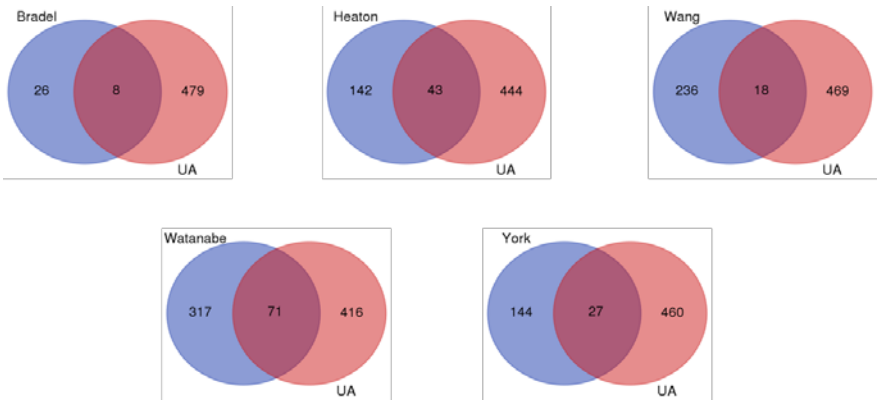

Figure 3.8. Comparison of MS data with different PB2/polymerase complex interactome screens. The list of significantly changed proteins with a t-test difference of > 0 (UA, depicted above in red) was compared to protein lists from other publications (depicted in blue) that focused on the interactome of influenza PB2 or polymerase complex. Studies used for comparison are: *Heaton et al.*, *Bradel-Tretheway et al.*, *Watanabe et al.*, *Wang et al*. and *York et al*. [138-142]. In the case of studies that were also investigating protein interactomes of other influenza virus proteins, comparison was performed only with AP-MS data of PB2- or "PB2 as part of the polymerase complex"-samples. Venn diagrams were generated ing http://bioinformatics.psb.ugent.be/webtools/Venn/. Numbers represent number of proteins.

The largest overlap of PB2/polymerase complex interactome proteins (71 proteins) was found with the *Watanabe et al.* screen (figure 3.8; Watanabe, UA). However, when the overlap between interactomes was calculated as the percentage of the number of proteins of the interactome screen used for comparison, the largest overlap was found with the *Bradel-Tretheway et al*. screen (figure 3.8; Bradel, UA). 8 proteins were detected in both screens, which represent 23.5 % of the 34 proteins identified as hit proteins in the *Bradel-Tretheway et al*. screen after stringent filtering. This screen aimed to identify interaction partners of the viral polymerase of A/Vietnam/1203/04 (H5N1).

Overall, the majority of proteins detected in all of the screens (925 out of 1192; 77.6 %) were identified in only one of the six compared screens.

To gain insight into the biological function of the filtered protein groups identified in this study, the protein list was subjected to gene ontology (GO) term analysis with the “Protein Analysis Through Evolutionary Relationships (PANTHER)” classification system online tool. For the 487 detected protein groups, 515 gene IDs were discovered and classified according to their protein class. The majority of the proteins in the filtered list (25.3 %) belong to a class of nucleic acid binding proteins, followed by proteins belonging to the class of oxidoreductase proteins (12.9 %) or hydrolase proteins (10.3 %) (figure 3.9).

The predominance of interactions with nucleic acid binding proteins was not unexpected since PB2, as part of the viral replication and transcription machinery, is a nucleic acid binding protein itself. In addition, interplay of cellular nucleic acid binding proteins with the polymerase complex has already been described (see section 1.2.3).

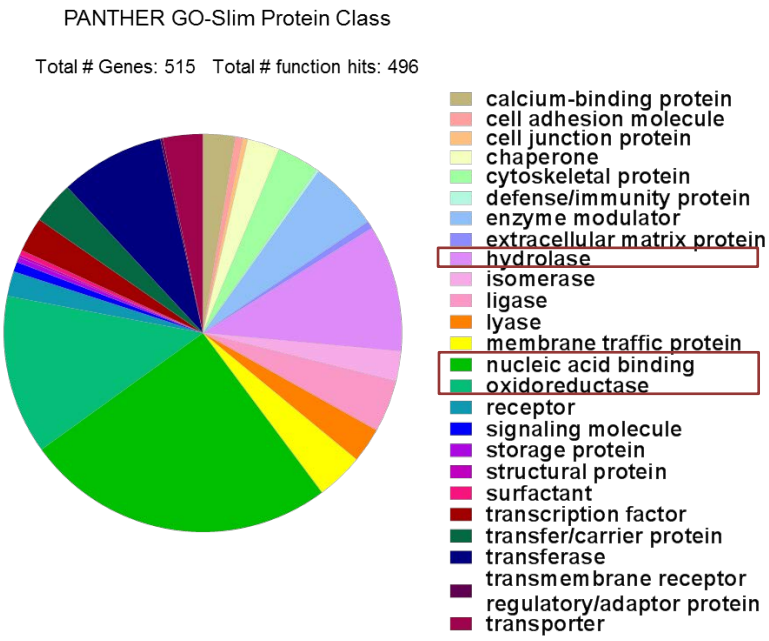

Figure 3.9. Functional classification of proteins in the filtered protein list. Filtered proteins were classified according to their protein class. GO term analysis was performed using the PANTHER classification system. The majority of proteins belong to the protein classes framed in red.

3.1.5. Hit protein classification and network analysis

In order to identify specific cellular interaction partners of PB2, first the filtered protein list with 487 protein groups was further condensed by adding another filter criterion as follows: in addition to being statistically significant and showing a t-test difference of > 0, protein groups needed to have a t-test difference of ≥ 1 in at least 2 out of 4 experimental replicates. A t-test difference of ≥ 1 (log2) equates to a fold increase in protein abundance of at least 2 compared to the A/Pan-99-WT control. Adding this criterion increased the likelihood of the further examined protein groups being specific binding partners of PB2 and shortened the list from 487 filtered protein groups to 20 hit protein groups. These 20 hit protein groups are detailed in table 3.2.

Table 3.2. List of hit proteins. Eluted proteins with a t-test difference of >0 in the 4 experimental replicate and a t-test difference of ≥ 1 in at least 2 replicates were defined as hit proteins. Bibliography: interactome screens of PB2/polymerase complex in which the protein was also identified in PB2 or "PB2 as part of the polymerase complex"-samples [138-142].

Gene name	Protein name	Function	Bibliography
AGR2	Anterior gradient protein 2 homolog	Required for MUC2 post-transcriptional synthesis and secretion	-
BAG2	BAG family molecular chaperone regulator 2	Co-chaperone for HSPA8 and HSP70	*Heaton et al./ Watanabe et al./ York* et al.
CAST	Calpastatin	Inhibition of Calpain	-
CKMT1A CKMT1B	Creatine kinase U-type	Catalyzes the transfer of phosphate between ATP and various phosphogens	- -
CPS1	Carbamoyl-phosphate synthase	Enzyme involved in the urea cycle	*Heaton et al./ Wang et al.*

Gene name	Protein name	Function	Bibliography
EPHX1	Epoxide hydrolase 1	Catalyzes the hydrolysis of epoxides to dihydrodiols	-
GGH	Gamma-glutamyl hydrolase	Hydrolyzes the polyglutamate sidechains of pteroylpolyglutamates	-
HIST1H2B	Histone H2B type 1	Core component of nucleosome	*Watanabe et al.*
HIST1H4A	Histone H4	Core component of nucle-osome	*Watanabe et al.*
HIST2H3A	Histone H3.2	Core component of nucle-osome	-
HNRNPC	Heterogeneous nuclear ribonucleoproteins C1/C2	Binds pre-mRNA and nucleates the assembly of 40S hnRNP particles	-
HSPA2	Heat shock-related 70 kDa protein 2	Molecular chaperone	*Watanabe et al.*
HSPA8	Heat shock cognate 71 kDa protein	Molecular chaperone	*Watanabe et al./ York et al.*
KCNJ8	ATP-sensitive inward rectifier potassium channel 8	Potassium channel	-
LXN	Latexin	Inhibitor of CPA1, 2, 4	-

Gene name	Protein name	Function	Bibliography
PABPC1 PABPC3	Polyadenylate-binding protein 1; 3	Binds the poly(A) tail of mRNA (1/3) Function in translational initiation regulation (1)	*Watanabe et al.* -
RCN2	Reticulocalbin-2	Calcium-binding protein	*Watanabe et al./ York et al.*
SLC12A2	Solute carrier family 12 member 2	Na-K-Cl cotransporter	-
SNRNP200	U5 small nuclear ribonucleoprotein 200 kDa helicase	Component of the U5 snRNP and U4/U6-U5 tri-snRNP complexe	-
TOP2A	DNA topoisomerase 2-alpha	Control of topological states of DNA	*Watanabe et al./ Bradel-Tretheway et al.*

For CKMT1A/B (Creatine kinase U-type A and Creatine kinase U-type B) and PABPC1/3 (Polyadenylate-binding protein 1 and Polyadenylate-binding protein 3), MaxQuant could not clearly differentiate between the two proteins. Even though encoded by different genes, the amino acid sequences are highly similar for CKMT1A and CKMT1B, and PBPC1 and PBPC3, respectively. Hence, all four proteins were included in the hit list which therefore contains 22 proteins (table 3.1).

Out of these 22 proteins, 13 proteins (GGH, CKMT1B, HIST2H3A, EPHX1, CKMT1A, PABPC3, SLC12A2, LXN, SNRNP200, CAST, KCNJ8, hnRNPC1, AGR2) were not found in the 5 previously published interactome screens used for comparison [138-142].

Since proteins interact with other proteins and usually work in complexes, a “Search Tool for the Retrieval of Interacting Genes/Proteins (STRING)” database network analysis was conducted in order to visualize relationships between hit proteins. STRING is an online database of predicted and known protein-protein interactions. It is based on

data from numerous sources such as the Molecular Interaction Database (MINT), Kyoto Encyclopedia of Genes and Genomes (KEGG) or GO. STRING also includes text mining, experimental data and computational predictions to create protein interaction networks.

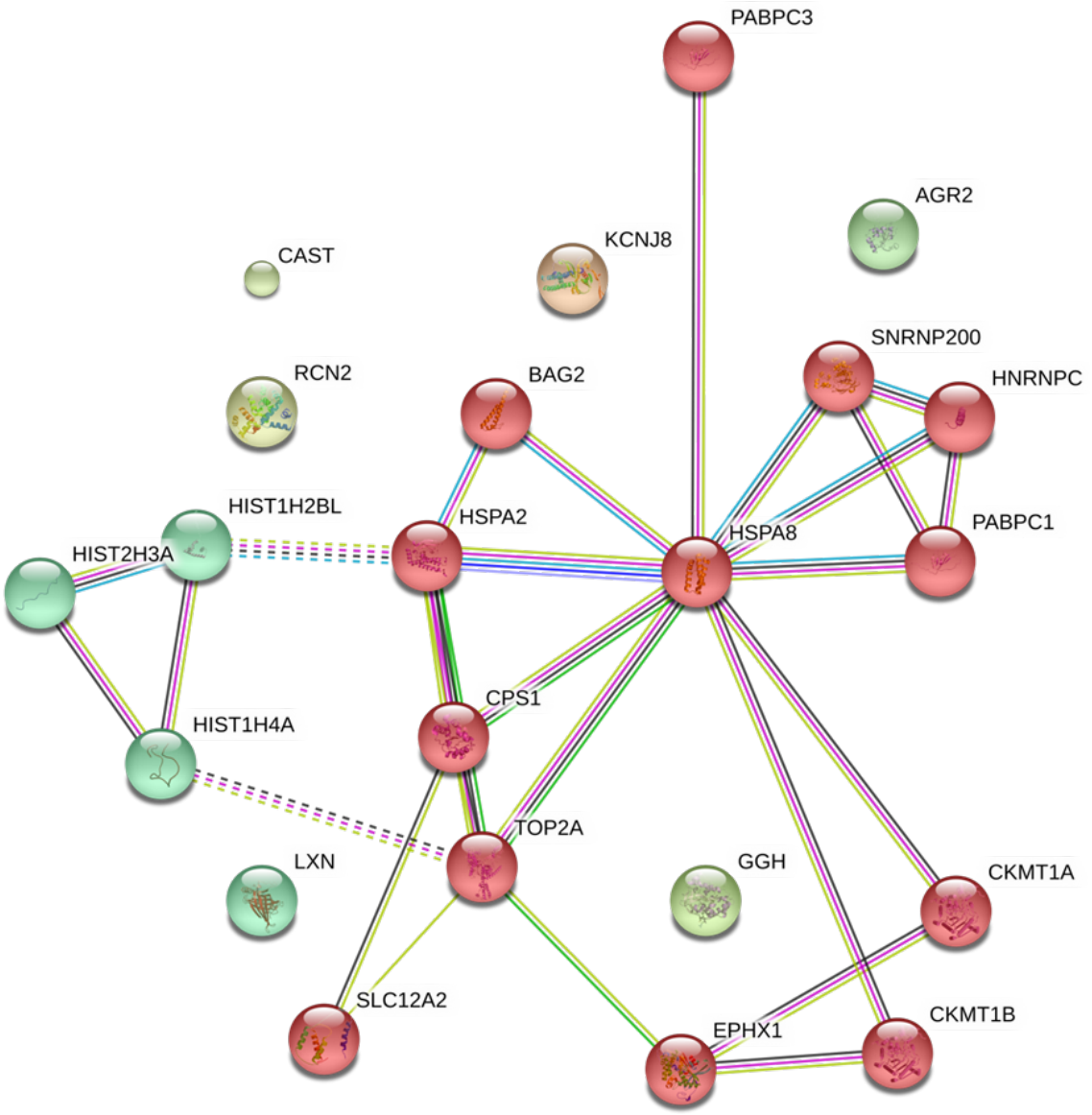

Figure 3.10. STRING network of PB2 interactome screen hit proteins. STRING database analysis (https://string-db.org/) of hit proteins from table 3.2. MCL inflation parameter for clustering of the network = 2. Line colors indicate: light blue = known interactions from curated databases; pink = known interactions experimentally determined; green = predicted interactions by gene neighborhood; dark blue = predicted interactions by gene co-occurrence; yellow = text mining; black = co-expression; light purple = protein homology.

The obtained interaction network for the hit proteins was clustered using the Markov Cluster algorithm (MCL) with the inflation parameter set to 2 (figure 3.10). Six proteins (CAST, RCN2, KCNJ8, AGR2, LXN and GGH) showed no relationship to other proteins while the remaining 16 proteins grouped together in two clusters. The smaller cluster comprised the three histone proteins (light green) while the second cluster encompassed the remaining 13 proteins (red). Except for BAG2, SLC12A2 and EPHX1 all proteins of the larger cluster could be assigned to the molecular function “nucleotide binding”.

Interestingly, for the majority of hit proteins (with the exception of SLC12A2 and the 6 proteins that showed no interactive relationship to other proteins) an experimentally determined protein interaction to at least one other hit protein is known. HSPA8 represents the clear center of the larger protein cluster with 10 experimentally determined protein interactions.

3.2 Data validation

To support the findings of the MS screen, 13 proteins from the hit list were selected and used for validation by polymerase activity assay (minigenome assay) and co-immunoprecipitation (co-IP). This selection was based on the molecular functions and reagent availability of the proteins. The following proteins were used for analysis: AGR2, BAG2, CAST, EPHX1, GGH, hnRNPC1, HSPA2, HSPA8, LXN, PABPC1, PABPC3, RCN2, SLC12A2.

3.2.1 Co-immunoprecipitation

To validate the co-precipitation of PB2 with selected hit proteins, 293T cells were transfected with expression plasmids for PB2, PB1 and PA of either A/Thai/04 or A/Pan/99 and the plasmid coding for the FLAG- or V5-tagged protein of interest.

In the case of control samples the empty vector, coding only for the tag sequence, was transfected in addition to PB2, PB1 and PA. 24 h post transfection, cells were lysed and proteins were immunoprecipitated by use of either α-V5 or α-FLAG antibodies coupled to protein G agarose beads. After washing and elution, co-immunoprecipitation of PB2 with the investigated protein was determined by immunoblot analysis.

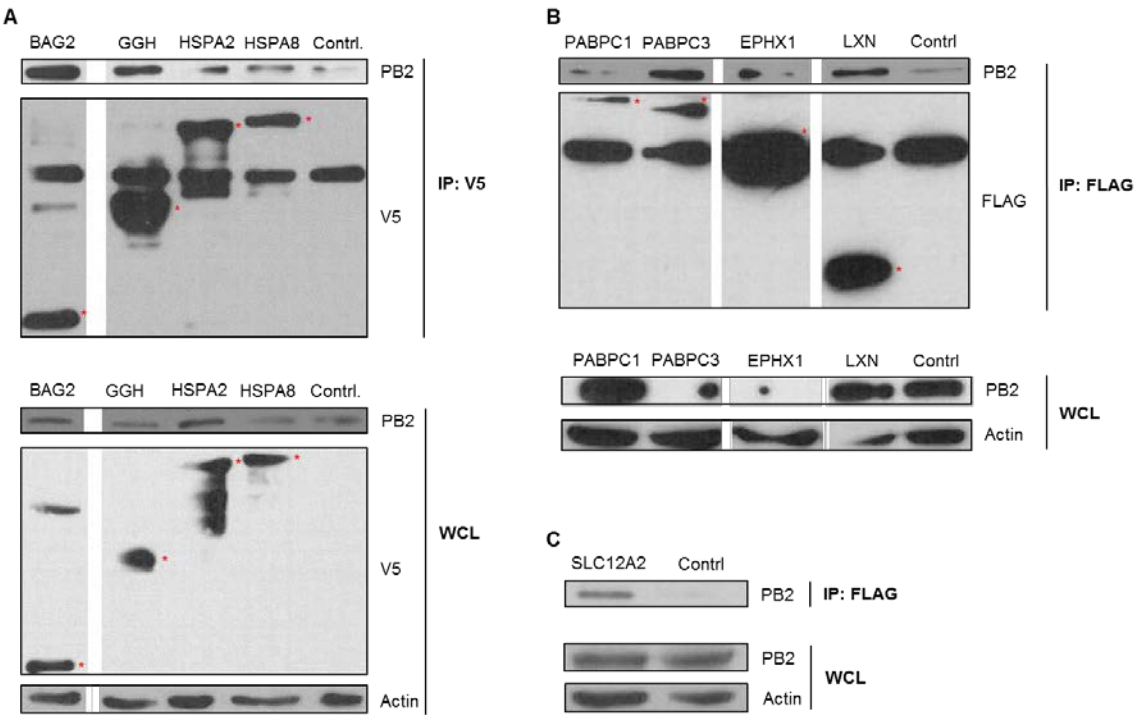

Figure 3.11. Validation of the co-precipitation of A/Thai/04 PB2 with selected hit proteins. 293T cells were transfected with plasmids encoding V5 or FLAG-tagged hit proteins, or the corresponding empty tag vector (control), and expression plasmids for A/Thai/04 PB2, PB1 and PA. 24 hours p.t., cells were lysed and immunoprecipitation was performed using protein G agarose beads coupled to **A** α-V5 or **B/C** α-FLAG antibodies. Bound proteins (IP) and cell lysates (WCL) were analyzed by SDS PAGE and immunoblotting using the indicated antibodies. Red asterisk indicate specific protein bands according to their calculated molecular masses. Representative experiment of N ≥ 2.

Co-IP analysis confirmed the co-precipitation of A/Thai/04 PB2 with BAG2, GGH, HSPA2, HSPA8, PABPC3, EPHX1, LXN and SLC12A2. The co-precipitation with PABPC1 could not be validated with certainty since the PB2 band was only slightly more increased compared to the control (figure 3.11). In case of A/Pan/99, co-precipitation with PB2 was verified for BAG2, HSPA8, PABPC1, PABPC3, EPHX1, LXN and SLC12A2 (figure 3.12). The A/Pan/99 PB2 band in the co-precipitate of GGH and HSPA2 samples was only slightly more intense compared to the control sample, indicating a possibly very weak interaction. Co-precipitation of A/Thai/04 or A/Pan/99 PB2 with AGR2, CAST, hnRNPC1 or RCN2 could not be confirmed under applied conditions.

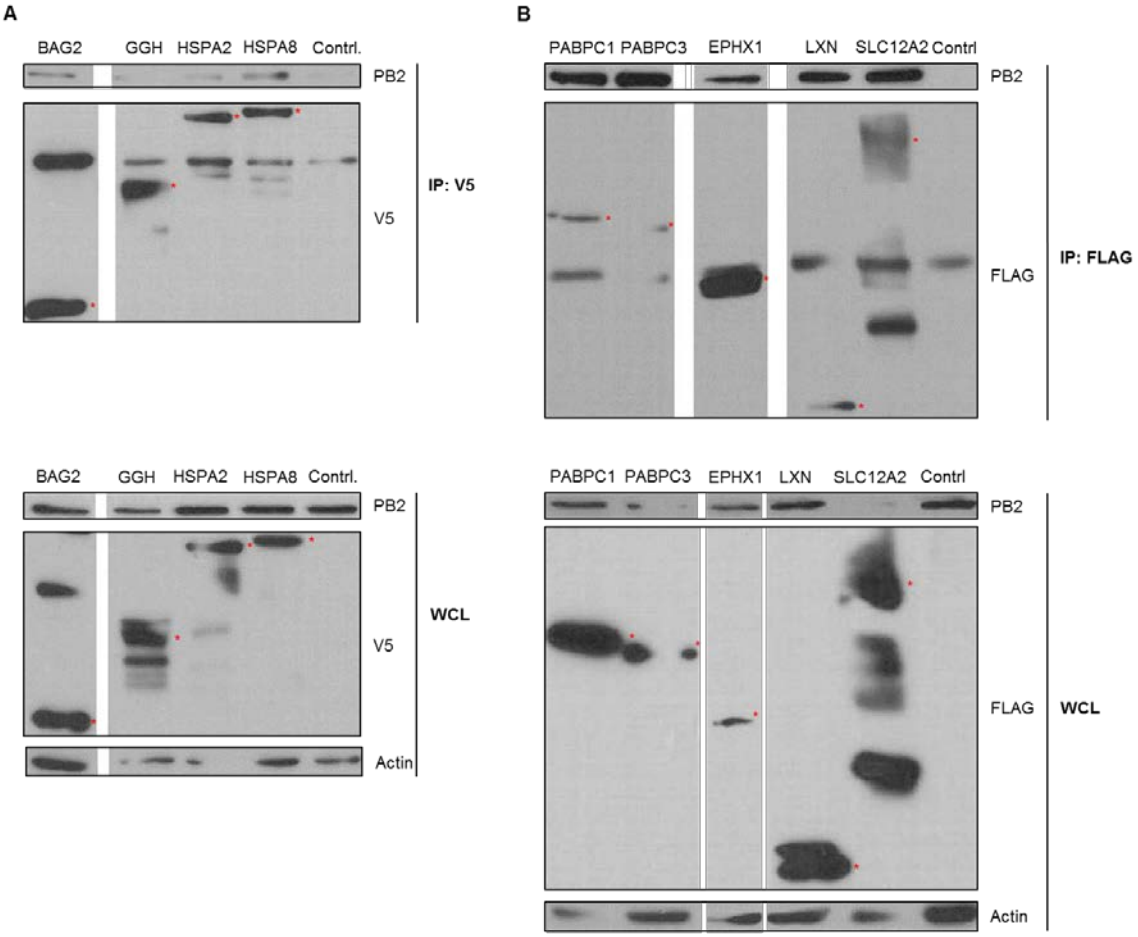

Figure 3.12. Validation of the co-precipitation of A/Pan/99 PB2 with selected hit proteins. 293T cells were transfected with expression plasmids for A/Pan/99 PB2, PB1 and PA, and plasmids encoding V5 or FLAG-tagged hit proteins, or the corresponding empty tag vector (control). After 24 h, cells were lysed and immunoprecipitation was performed using protein G agarose beads coupled to **A** α-V5 or **B** α-FLAG antibodies. Bound proteins (IP) and cell lysates (WCL) were analyzed by SDS PAGE and immunoblotting using the indicated antibodies. Red asterisk indicate specific protein bands according to their calculated molecular masses. Representative experiment of N ≥ 2.

3.2.2 Polymerase activity assay

The polymerase activity assay, also known as minigenome assay, is a reporter based assay that allows for determination of the influence of e.g. mutation, knock down or overexpression of proteins, on viral polymerase activity (see figure 3.13). The MS screen was conducted in order to identify cellular interaction partners of PB2 that have an impact on polymerase activity. Therefore, the minigenome assay was used to investigate the functional relevance of the PB2 cellular interaction partners on viral polymerase activity as it is a relatively fast screening method.

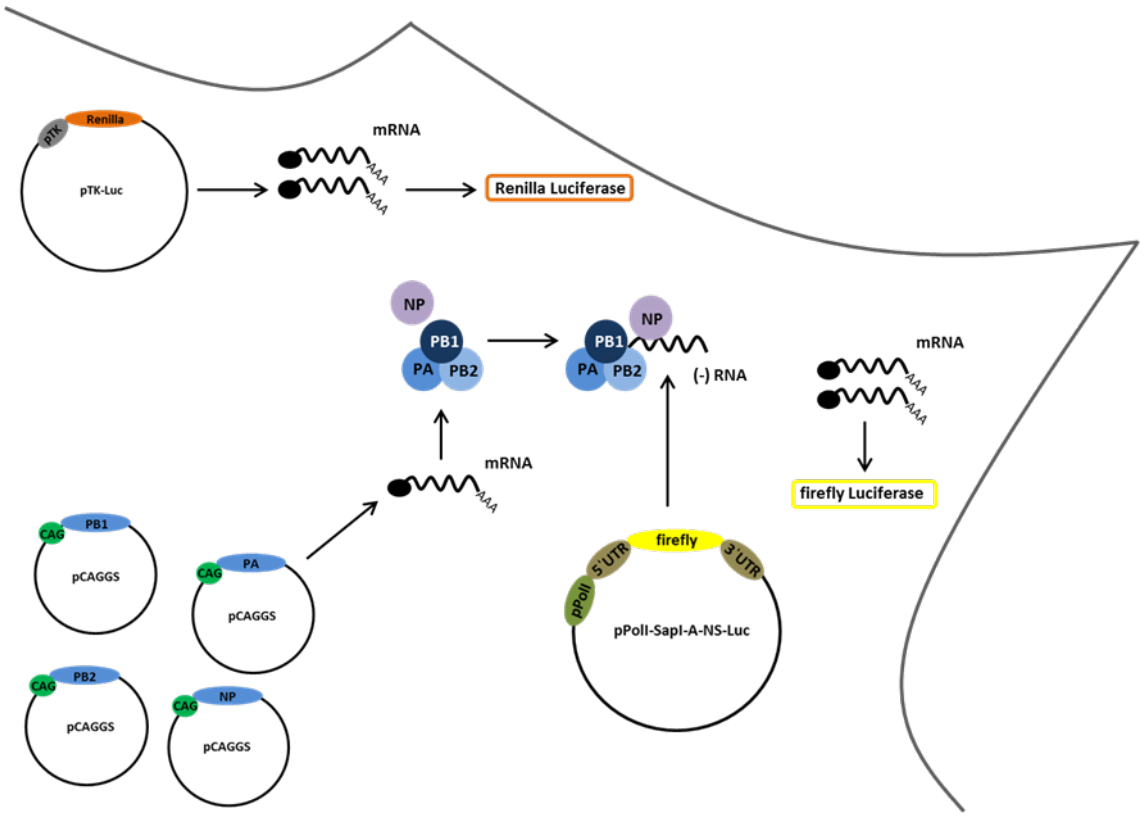

Figure 3.13. Schematic representation of the influenza polymerase activity assay. The minigenome plasmid (pPolI-SapI-A-NS-Luc) contains the firefly Luciferase gene flanked by the 5` and 3`untranslated region of an influenza genomic segment (in this case the NS segment) and the intracellular synthesis of the firefly RNA in negative orientation is driven by pPolI. The viral proteins PA, PB1, PB2 and NP, their expression enabled by a constitutive promoter (for example the CAG-promoter), bind the (-) RNA and facilitates transcription. An increase in firefly Luciferase activity, based on viral polymerase induced protein expression, indicates influenza polymerase activity. The constitutively expressed Renilla Luciferase (encoded on the pTK-plasmid) allows for normalization of transcription levels and protein expression.

293T cells were transfected with expression plasmids encoding PB2, PB1, PA and NP of either A/Pan/99 or A/Thai/04, a firefly luciferase reporter plasmid under the control of the UTRs of the NS segment of Influenza A, and a constitutively expressed Renilla luciferase reporter plasmid as an internal transfection and expression control. In addition, either 100 ng or 500 ng of the plasmid encoding the investigated cellular protein was co-transfected. The total amount of DNA between samples was kept constant with empty expression plasmids corresponding to the analyzed protein. For positive controls, 500 ng of the analogous empty vector was co-transfected.

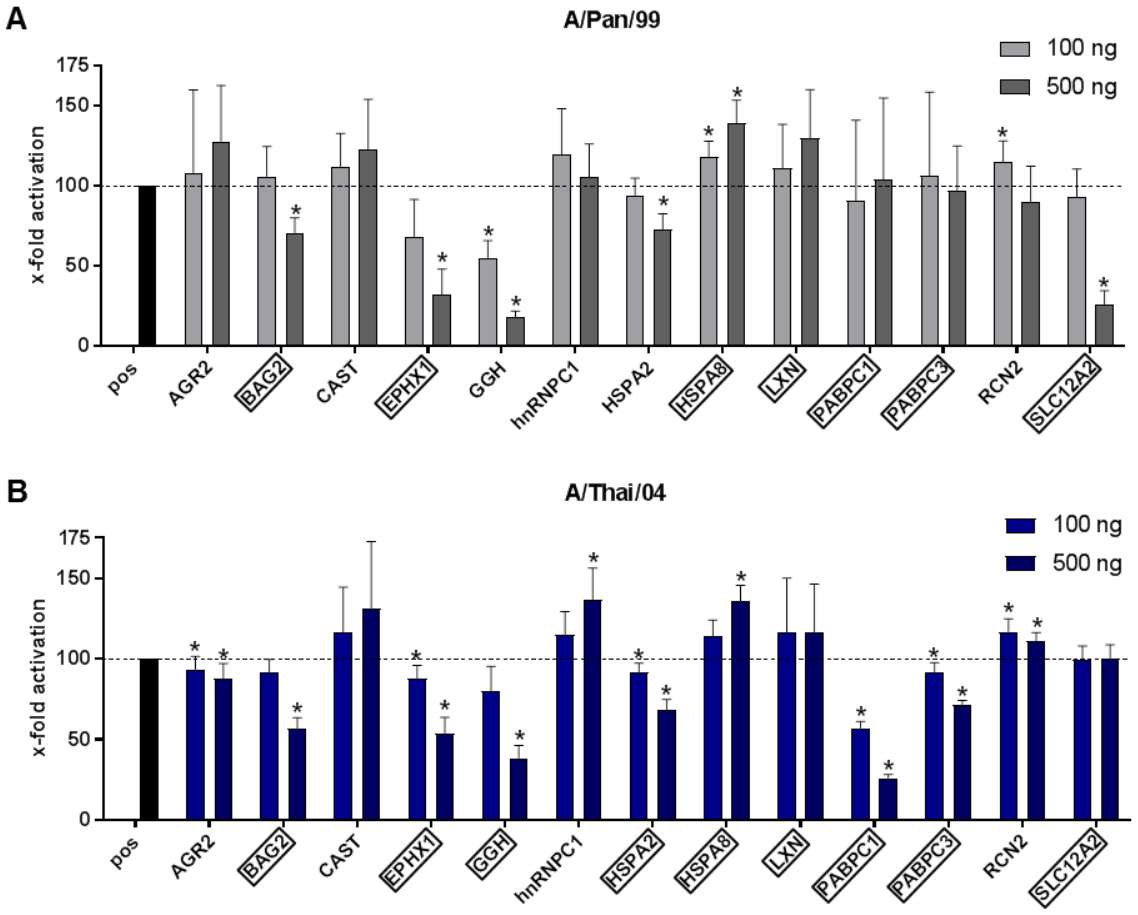

Figure 3.14. Functional investigation of MS data by polymerase activity assay. 293T cells were transfected with expression plasmids encoding the components of the minigenome assay and the cellular proteins of interest: **A** A/P**a**n/99 or **B** A/Thai/04 PB2, PB1, PA and NP, the firefly luciferase reporter plasmid as well as 100 ng or 500 ng of plasmids coding for the proteins of interest. In case of the 100 ng samples, 400 ng of the corresponding empty vector was co-transfected to keep the total amount of DNA constant. The constitutively expressed Renilla luciferase reporter plasmid was also co-transfected and served as an internal control. For the positive control samples, empty expression vectors corresponding to the investigated proteins were co-transfected. 24 h after transfection, cells were lysed and luciferase activity was measured. The displayed values are the mean + SD of 3 independent experiments conducted in duplicates. The p values were determined by the Wilcoxon signed rank test. Proteins framed by boxes were verified for PB2 interaction by Co-IP (figure 3.9 and 3.10).

After 24 h, cells were lysed and luciferase activity was measured. The activity of the firefly luciferase was normalized to the activity of the Renilla luciferase, then the normalized luciferase activity was calculated as an x-fold activation in comparison to the corresponding positive control (set to 100 %). These results are shown in figure 3.14.

Overexpression of AGR2, CAST, hnRNPC1, LXN, PABPC1 and PABPC3 had no significant effect on the polymerase activity of A/Pan/99 (figure 3.14.A). In contrast, overexpression of AGR2, PABPC1 and PABPC3 led to a dose dependent decrease in

A/Thai/04 polymerase activity, while overexpression of hnRNPC1 increased polymerase activity (figure 3.14.B). On the other hand, while overexpression of SLC12A2 had no significant effect on A/Thai/04 polymerase activity, it led to a decrease in A/Pan/99 polymerase activity when transfected in the same quantities. The effect of overexpression of the remaining cellular proteins was similar for both viral strains (see figure 3.14).

BAG2, EPHX1, GGH and HSPA2 overexpression had a negative effect on polymerase activity of both influenza virus strains while overexpression of RCN2 and HSPA8 increased polymerase activity. The impact on polymerase activity was dose dependent for each protein except for RCN2, which had a significant influence on A/Pan/99 only when 100 ng was transfected and a stronger significant effect on A/Thai/04 also when 100 ng was transfected. Overall, the results of the minigenome assay strongly supported the functional relevance of the MS data since overexpression of all proteins except for CAST and LXN had an impact on the polymerase activity of at least one viral strain.

Results of the co-immunoprecipitation and polymerase activity assay validation experiments are summarized in table 3.3.

Table 3.3. Combined results of the co-immunoprecipitation and polymerase activity assay experiments. Listed are the investigated proteins, whether or not they co-precipitated A/Pan/99 or A/Thai/04 PB2, and if their overexpression significantly increased (↑) or decreased (↓) viral polymerase activity or had no significant effect (-).

Protein	**Co-precipitation with PB2 confirmed by co-IP**		**Significant effect on polymerase activity**			
	A/Pan/99	A/Thai/04	A/Pan/99		A/Thai/04	
			100 ng	500 ng	100 ng	500 ng
AGR2	No	No	-	-	↓	↓
BAG2	Yes	Yes	-	↓	-	↓
CAST	No	No	-	-	-	-
EPHX1	Yes	Yes	-	↓	↓	↓
GGH	Weak	Yes	↓	↓	-	↓

Protein	Co-precipitation with PB2 confirmed by co-IP		Significant effect on polymerase activity			
	A/Pan/99	A/Thai/04	A/Pan/99		A/Thai/04	
			100 ng	500 ng	100 ng	500 ng
hnRNPC1	No	No	-	-	-	↑
HSPA2	Weak	Yes	-	↓	↓	↓
HSPA8	Yes	Yes	↑	↑	-	↑
LXN	Yes	Yes	-	-	-	-
PABPC1	Yes	No	-	-	↓	↓
PABPC3	Yes	Yes	-	-	↓	↓
RCN2	No	No	↑	-	↑	↑
SLC12A2	Yes	Yes	-	↓	-	-

3.3 Characterization of HSPA8 as a novel PB2 interaction partner

The SILAC based MS analysis of A/Pan/99-PB2-Strep and A/Thai/04-PB2-Strep precipitations resulted in a hit list of 22 PB2 interaction partners. Co-immunoprecipitation analysis then confirmed the interaction of PB2 with 9 out of 13 proteins selected for data validation. Overexpression of 11 out of these 13 proteins also had an impact on polymerase activity as determined by minigenome assay. Hence, the MS data was confirmed to be of functional relevance. In a final set of experiments a target interacting protein of PB2 was selected for further exemplary analysis. Among hit proteins, HSPA8 was especially of interest. Not only could the interaction of HSPA8 with PB2 of both viral strains be confirmed by co-immunoprecipitation, HSPA8 was also one of only

three tested proteins whose overexpression had a positive effect on viral polymerase activity. In addition, HSPA8 was the center of the hit protein network (figure 3.10).

HSPA8, also known as Hsc70, belongs to the heat shock protein family HSP70 and carries out a wide range of biological functions. For example, HSPA8 plays a role in clathrin-mediated endocytosis, protein folding, and nuclear import and export of proteins [118]. In addition to its importance for *Turnip mosaic virus* and herpes simplex virus type 1 (HSV-1) replication, it has been reported to interact with the influenza A virus M1 protein and is believed to play a role in the nuclear export of the influenza virus ribonucleoprotein complex [62,122,125,151]. HSPA8 was also found to be a potential PB2 interaction partner of the lab adapted influenza viral strain A/WSN/33 (H1N1) in the MS screens of *York et al.* and *Watanabe et al*. [141,142]. However, both studies did not confirm this interaction with additional experiments.

3.3.1 Co-precipitation of PB2 with Endogenous HSPA8

To further characterize and confirm the co-precipitation of PB2 with HSPA8, co-IP analysis of the endogenous protein expressed in A549 cells was employed. A549 cells infected with A/Pan/99-WT or A/Thai/04-WT virus were lysed and endogenous HSPA8 was immunoprecipitated by use of protein G agarose beads coupled to α-HSPA8 antibody. As a negative control, α-c-Myc antibody coupled protein G agarose beads were used. The Co-IP of PB2 was determined by immunoblot analysis.

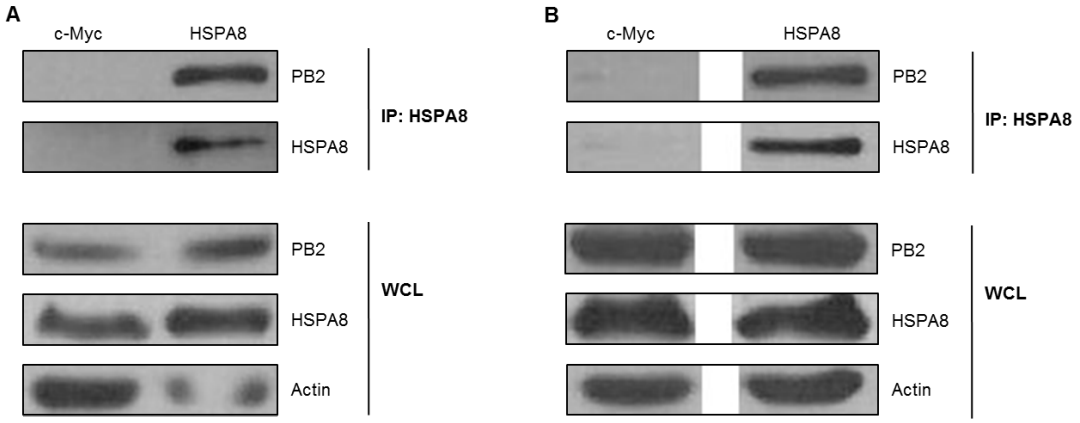

Figure 3.15. Co-precipitation of PB2 with endogenous HSPA8. A549 cells were infected with A/Pan/99-WT (**A**) or A/Thai/04-WT virus (**B**) at an MOI of 5. 16h p.i. cells were lysed and Co-IP was performed with α-HSPA8 or α-c-Myc (control) antibodies coupled to protein G agarose beads. Precipitated proteins (IP) and 10 % of whole cell lysates (WCL) were analyzed by SDS PAGE and immunoblotted using the indicated antibodies. Displayed data is from a representative experiment of N ≥ 2.

Co-IP experiments showed the co-precipitation of A/Pan/99 and A/Thai/04 PB2 with endogenous HSPA8 in infected A549 cells (figure 3.15.A and B, respectively). These data therefore confirm the results of co-IP in hit protein overexpressing cells (figure 3.11 and 3.12) and MS analysis.

3.3.2 HSPA8 relocates into the nucleus in infected cells

HSPA8 is constitutively expressed and mainly localized in the cytoplasm of cells under physiological conditions. Under stress conditions such as e.g. heat shock, HSPA8 concentrates in the nucleus [152]. *Watanabe et al*. demonstrated that HSPA8 also relocates into the nucleus of influenza virus infected cells at late time points of infection [125]. However, in the study conducted by *Watanabe et al*. the relocation of HSPA8 during influenza virus infection was only shown for the lab adapted strain A/WSN/33. To determine if this relocation also occurs in cells infected with A/Pan/99 and A/Thai/04 strains, which have unlike A/WSN/33 not been subjected to multiple passages, and to thereby further characterize the role of HSPA8 in influenza virus infected cells, the localization of HSPA8 was analyzed by immunofluorescence staining during A/Pan/99 and A/Thai/04 infection.

A549 cells were infected with A/Pan/99-WT or A/Thai/04-WT at an MOI of 1. After 4 h or 8 h p.i. cells were fixed and HSPA8 was visualized by staining with an α-HSPA8 antibody and fluorescently labelled secondary antibody. Since staining of PB2 with all commercially available antibodies tested under different conditions was unfortunately not successful, staining with α-NP antibodies and fluorescently labelled secondary antibodies was used to locate influenza virus infected cells. The sub-cellular localization of HSPA8 was then determined using confocal microscopy.

At 4 h p.i., HSPA8 was almost equally distributed in the cytoplasm and the nucleus of uninfected cells as well as of cells infected with A/Pan/99-WT or A/Thai/04-WT (figures 3.16.A and 3.17.A, respectively). This is illustrated in the corresponding intensity profiles of the HSPA8, NP and DAPI channels (see bottom left corner of the panels in figure 3.13 and 3.14). If one follows the green line, representing the HSPA8 signal, a similar intensity of the signal in the nucleus (characterized by an increase in intensity of the blue DAPI signal) and the cytoplasm can be seen. This equates to the distribution of HSPA8 in cells 0 h after infection (data not shown). The red influenza virus NP signal peaked in the nuclear region of the infected cells at 4 h post infection.

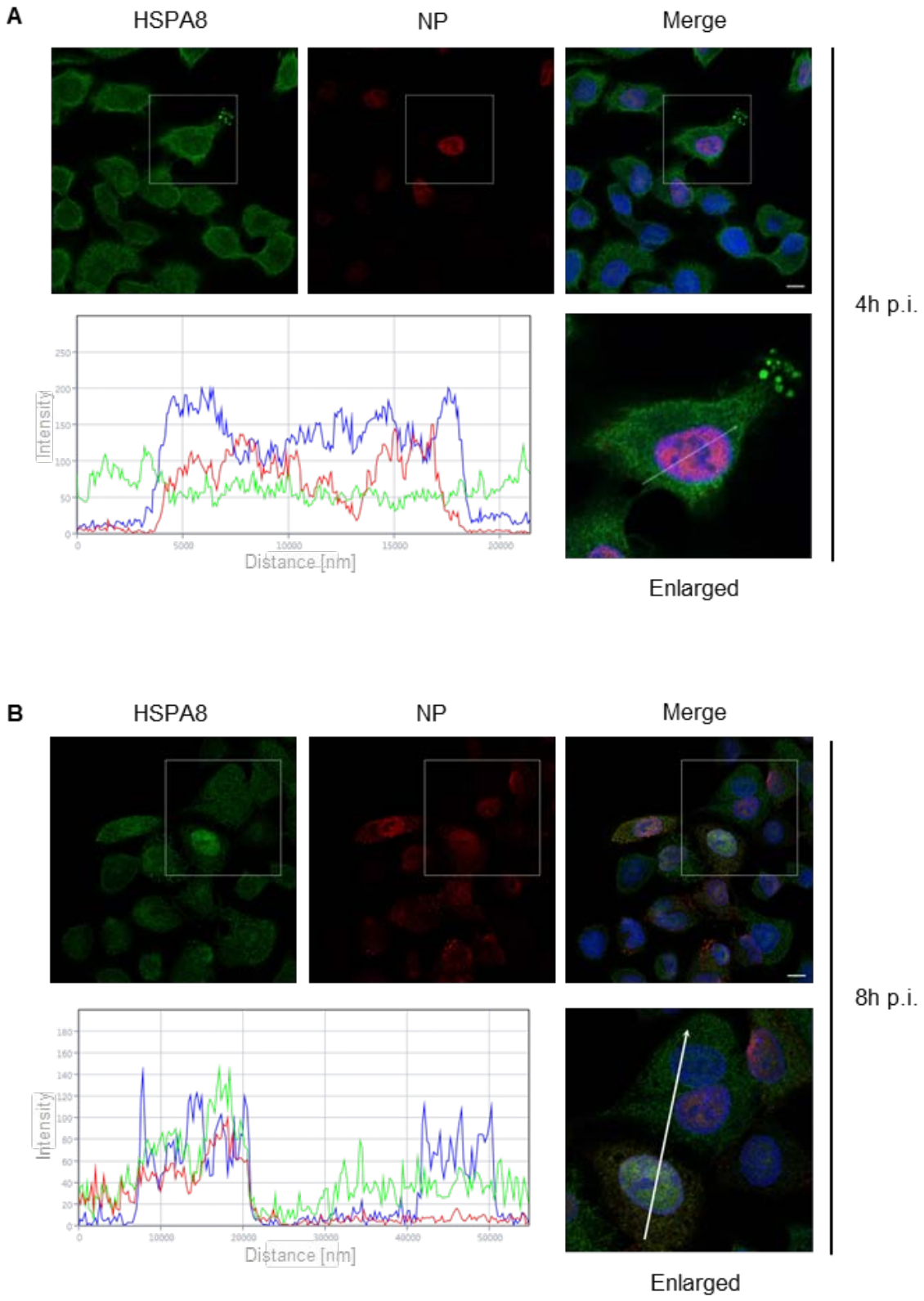

Figure 3.16. HSPA8 relocates into the nucleus at late time points of A/Pan/99-WT infection. A549 cells were infected with A/Pan/99-WT at an MOI of 1. **A** 4 h or **B** 8 h p.i. cells were fixed and HSPA8 and influenza virus NP visualized by staining with antibodies for the indicated proteins. The square area of the inset is digitally magnified (enlarged). The white arrow indicates the area used for intensity profiles of the green (HSPA8), red (NP) and blue (DAPI) channel. Scale bar =10 µm.

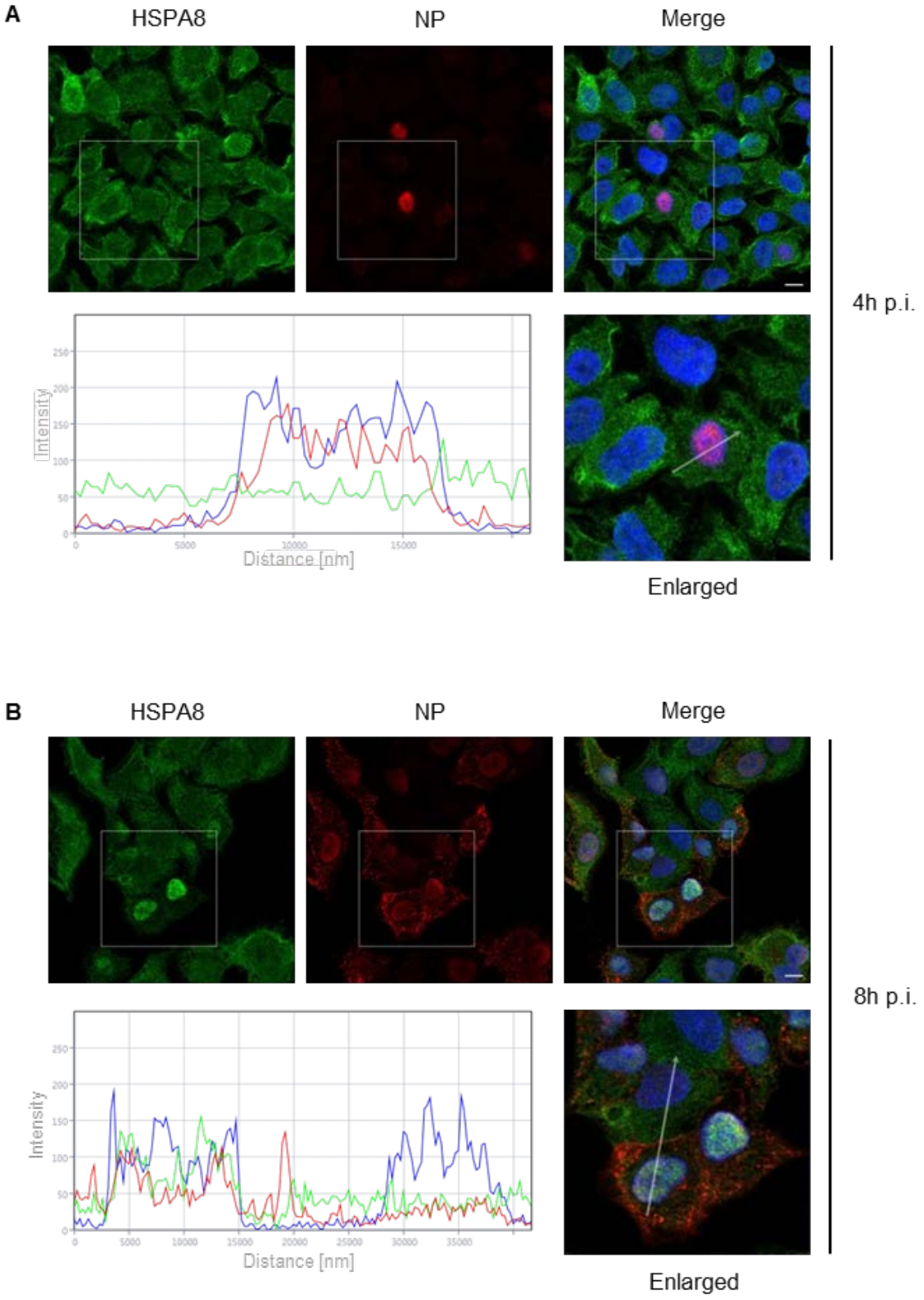

Figure 3.17. HSPA8 relocates into the nucleus at late time points of A/Thai/04-WT infection. A549 cells were infected with A/Thai/04-WT at an MOI of 1. **A** 4 h or **B** 8 h p.i. cells were fixed and HSPA8 and influenza virus NP were visualized by staining with antibodies for the indicated proteins. The square area of the inset is digitally magnified (enlarged). The white arrow indicates the area used for intensity profiles of the green (HSPA8), red (NP) and blue (DAPI) channel. Scale bar =10 µm.

8 h post infection, a relocation of HSPA8 into the nucleus of A/Pan/99-WT and A/Thai/04-WT infected cells was observed (figure 3.16.B and 3.17.B, respectively). The intensity profiles showed a clear increase of the green HSPA8 signal in the nucleus of infected cells (characterized by an increase of the red influenza virus NP signal) when compared to the intensity of the cytoplasmic HSPA8 signal. In contrast, the green HSPA8 signal in neighboring uninfected cells remained constant in nuclear and cytoplasmic areas of the cell. NP was located in the nucleus as well as in the cytoplasm at 8 h post infection.

Hence, confocal microscopy analysis revealed that HSPA8 also relocates into the nucleus of A549 cells infected with non-lab adapted influenza virus strains of the subtypes H3N2 and H5N1. This HSPA8 relocation was also observed at late time points of infection (16 h p.i., data not shown).

3.3.3 siRNA mediated depletion of HSPA8 expression influences A/Panama/2007/99 and A/Thailand/(KAN-1)/04 replication

To investigate the role of HSPA8 in viral replication, viral growth curve analysis was performed in A549 cells after siRNA mediated HSPA8 depletion.

A549 cells were transfected with an HSPA8 siRNA mix, composed of four individual HSPA8 siRNAs, or non-target (NT) control siRNA, then infected with A/Pan/99-WT or A/Thai/04-WT viruses at an MOI 0.1, 48 hours post siRNA transfection. The time point for infection was previously determined in optimization experiments (data not shown). In addition cell viability was monitored over the time frame of the experiment by MTT assay.

The viability of HSPA8 knock down cells was stable over time and similar to cells transfected with non-target siRNA (figure 3.18.A). Therefore, it could be excluded that the effects of the HSPA8 knock down on viral growth were due to changes in cell viability.

To ensure that the depletion in HSPA8 protein expression remained stable during the course of the experiment, cell lysates were taken for analysis at 0 h and 72 h post infection (48 h and 120 h post siRNA transfection). These time points represent the start and end point of viral growth curve analysis, where HSPA8 protein depletion was confirmed by immunoblot analysis (figure 3.18.B).

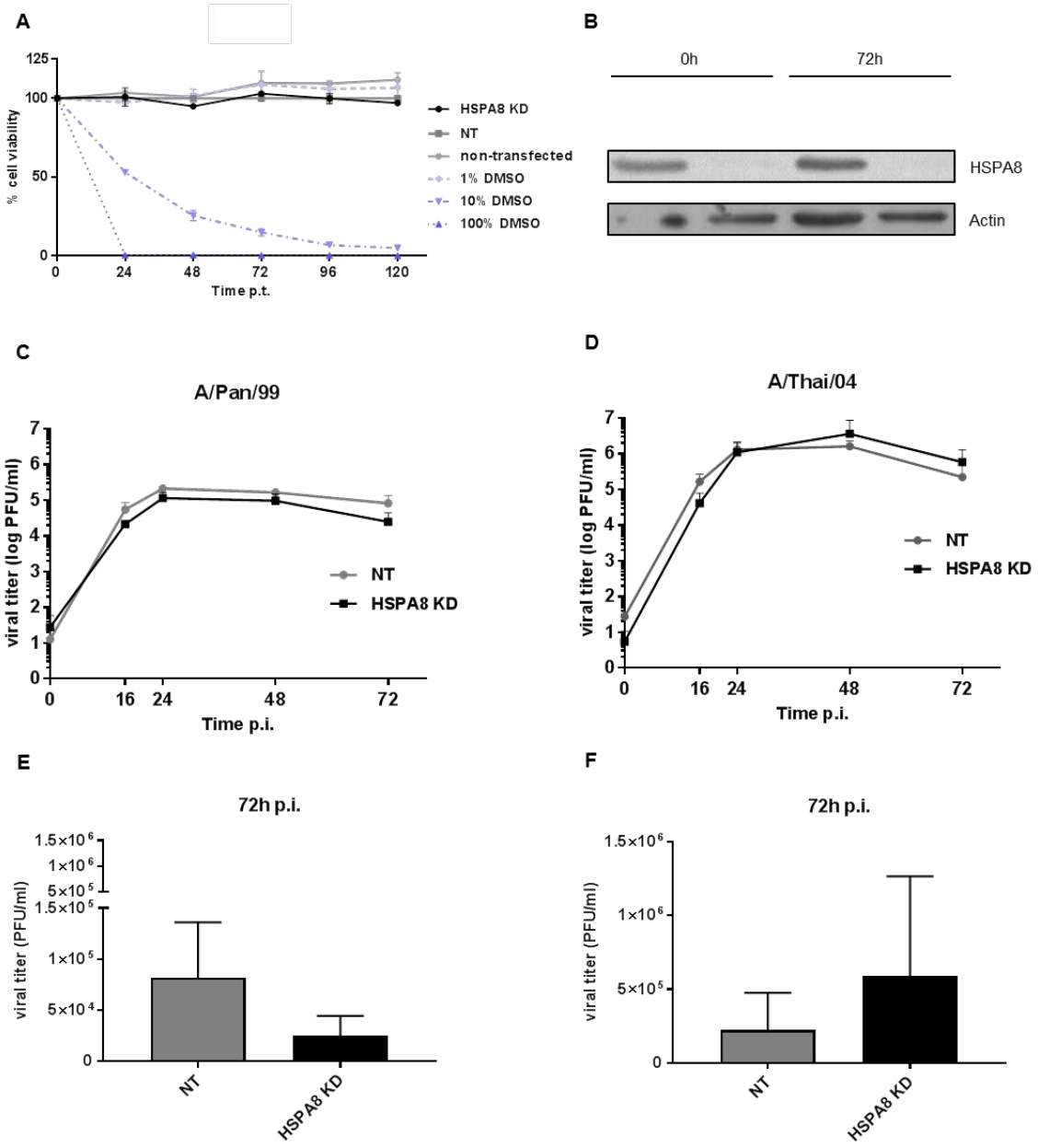

Figure 3.18. Depletion of HSPA8 influences A/Pan/99-WT and A/Thai/04-WT replication. A549 cells were transfected with NT siRNA or a HSPA8 siRNA mix. After 48 h, cells were infected with A/Pan/99-WT or A/Thai/04-WT viruses at an MOI of 0.1. **A** Influence on cell viability of HSPA8 depletion monitored by MTT assay. Displayed values represent the mean +SD of N=2 in duplicate. **B** The integrity of the HSPA8 depletion at 0 h and 72 h p.i. was confirmed by immunoblot analysis. Viral titers (log PFU/ml) of **C** A/Pan/99-WT and **D** A/Thai/04-WT strains over time were determined by standard plaque titration assay. Displayed values represent the mean +SD of N=2 in duplicates. Viral titers of **E** A/Pan/99-WT and **F** A/Thai/04-WT strains at 72 h p.i. were also depicted as absolute values.

siRNA mediated depletion of HSPA8 led to a slight decrease in A/Pan/99-WT viral growth from 16 h p.i. onwards (figure 3.18.C). Viral titers were decreased between 41.7 % and 69.6 % compared to viral titers from non-target A549 cells. The strongest

effect was observed at 72 h post infection. While A/Pan/99-WT virus grew to a mean of 81.875 PFU/mL in non-target siRNA transfected cells, it grew only to a mean of 24.875 PFU/mL in HSPA8 knock down cells (figure 3.18.E).

Viral growth of A/Thai/04-WT in HSPA8 knock down cells was slightly decreased at 0 h and 16 h p.i. (figure 3.18.D). However, while titers were almost identical at 24 h p.i., at 48 h and 72 h p.i. viral titers from HSPA8 depleted cells were marginally increased in comparison to virus titers from non-target siRNA transfected cells. Hence, no clear trend for the influence of HSPA8 depletion on A/Thai/04-WT growth during the time course of infection could be observed, while HSPA8 depletion showed a negative effect on A/Pan/99-WT growth from 16 h to 72 h post infection. The effect of HSPA8 depletion on viral growth was however not statistically significant.

3.3.4 Knock down of HSPA8 leads to a depletion of A/Panama/2007/99 PB2

Since the knock down of HSPA8 had a slight effect on viral growth, and overexpression of HSPA8 led to an increase in polymerase activity of A/Pan/99 and A/Thai/04 (see section 3.2.2), the minigenome assay was also performed in siRNA knock down cells to further investigate the role of HSPA8 in the viral replication cycle.

293T cells were transfected with NT siRNA or the HSPA8 siRNA mix. After 24 h, cells were transfected with expression plasmids encoding PB2, PB1, PA and NP of either A/Pan/99 or A/Thai/04, a firefly luciferase reporter plasmid under the control of the UTR of the NS segment of influenza A virus, and a constitutively expressed Renilla luciferase reporter plasmid. For the negative control, the PB2 expression plasmid was replaced by the corresponding empty plasmid. 24 h later, cells were lysed and luciferase activity was measured. Normalized luciferase activity was calculated as x-fold activation in comparison to non-target siRNA transfected samples (set to 100 %).

The polymerase activity of the A/Thai/04 strain was slightly increased to 111.7 % in HSPA8 depleted cells (figure 3.19. B). In contrast, depletion of HSPA8 led to a 39.8 % reduction in A/Pan/99 polymerase activity in comparison to NT siRNA transfected cells (figure 3.19.A). These data correlate well with the overexpression (figure 3.14.A) and virus growth curve analysis data (figure 3.18.C and E).

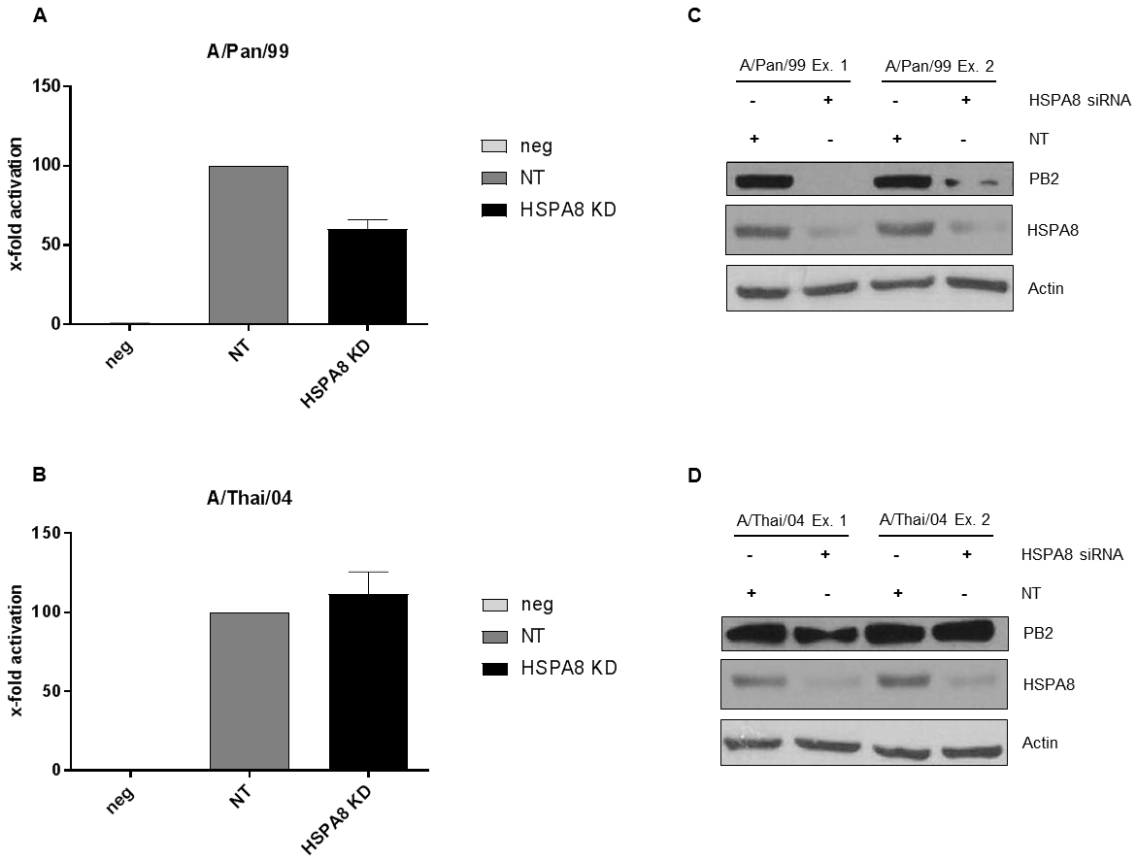

Figure 3.19. Knock down of HSPA8 leads to a depletion of A/Pan/99 PB2. 293T cells were transfected with the siRNA mix for HSPA8 or NT siRNA. After 24 h cells were transfected with expression plasmids encoding **A** A/Pan/99 or **B** A/Thai/04 PB2, PB1, PA and NP, as well as the firefly luciferase minigenome plasmid. The constitutively expressed Renilla luciferase reporter plasmid served as the internal control. The PB2 expression plasmid was replaced by the corresponding empty vector in negative control samples. 24 h after minigenome transfection, cells were lysed and luciferase activity was measured. Displayed values represent the mean + SD of 3 independent experiments. Expression levels of the indicated proteins were determined by immunoblot analysis of minigenome lysates of **C** A/Pan/99 and **D** A/Thai/04 samples. Depicted are immunoblot data representing 2 out of 3 experiments.

Depletion of HSPA8 was confirmed by immunoblot analysis of minigenome expressing lysates. While HSPA8 depletion was similar for A/Pan/99 and A/Thai/04 samples (figure 3.19.B and D, respectively), expression levels of PB2 differed dramatically between strains. While A/Thai/04 PB2 expression levels were similar in NT and HSPA8 siRNA transfected cells, A/Pan/99 PB2 protein was strongly depleted in HSPA8 knock down cells. This effect was not due to differences in whole protein amounts, as measured actin levels were similar between NT and HSPA8 siRNA transfected cells in A/Thai/04 and A/Pan/99 samples. This observation hints at a role for HSPA8 in A/Pan/99 PB2 protein stability.

4. Discussion

4.1 Mass spectrometric analysis revealed the PB2 interactome of non-laboratory adapted seasonal and highly pathogenic avian influenza virus strains

All viruses are obligate intracellular parasites, meaning they are entirely reliant on their host cell and its resources for their own reproduction. Hence, to understand the replication cycle of a virus it is essential to not only analyze viral proteins but viral proteins in their host cell environment. This includes the identification of cellular binding partners of viral proteins. Only the interaction with cellular proteins enables the virus to access cellular pathways and thereby allows for effective virus replication. In addition the control of viral replication by the innate or adaptive immune system is based on the interaction of viral and cellular factors.

The influenza virus protein PB2 is part of the trimeric viral polymerase complex. It is crucial for viral genome transcription and replication and was shown to be linked to the viral host range [57,71,137]. Hence, the host cell interactome of PB2 has been the subject of several studies focusing on influenza virus polymerase activity or host range determinants. However, many of these studies were performed with laboratory-adapted influenza strains, e.g. A/PR8/34 or A/WSN/33 [139,141,142]. To enable efficient replication in mice (which are not natural hosts for influenza virus but represent a low-cost, easy-husbandry and well established model) these viruses underwent multiple passages in mice [153]. Hence, the PB2 interactomes determined in studies using A/PR8/34 or A/WSN/33 do not necessarily reflect the PB2 interactome of human isolates and thereby the natural situation. Other studies have analyzed the PB2 interactome of human isolates of seasonal and highly pathogenic influenza virus strains, however these studies were carried out not in the context of infected cells, but in cells in which PB2 or the complete polymerase complex was expressed by transient transfection [138,143,144]. Viral proteins that are expressed in non-infected cells are not in the environment of a complete virus replication cycle and lack the influence of other viral and cellular proteins that are expressed or differentially regulated in infected cells. This thesis represents the first study in which the PB2 interactome of viral strains representing human isolates was determined in infected cells. We aimed to identify the PB2 interactome, including direct as well as indirect interaction partners of PB2, of seasonal (represented by A/Pan/99 (H3N2)) and highly pathogenic (represented by A/Thai/04 (H5N1)) viral

strains and to characterize the effect of selected interaction partners on viral replication.

Mass spectrometric analysis

Protein interactions of PB2 were identified in a SILAC based affinity-purification mass spectrometry (AP-MS) approach. AP-MS was selected due to several different characteristics of this approach. Firstly, mass spectrometry allowed for the highly sensitive detection of protein-protein interactions (PPI) under physiological conditions in a relevant biological context [149], in this case human alveolar epithelial cells (A549) infected with influenza virus. By means of affinity purification upstream of MS, PB2 and its cellular interaction partners were enriched and non-specific contaminants were reduced. Secondly, the use of SILAC labeled cells made it possible to perform a quantitative comparison between cells infected with A/Pan/99-PB2-Strep, A/Thai/04-PB2-Strep and the internal control A/Pan/99-WT. This enabled the further exclusion of false positives and external protein contaminants, which increased confidence in the identified interaction partners of A/Pan/99- and/or A/Thai/04-PB2 proteins.

The experimental setup of the MS screen needed to take several important factors into account. For example, the choice of influenza virus strains, the cell type used for infection, and the time period cells were infected for prior to affinity purification of PB2-strep. The human influenza virus strain A/Pan/99 (H3N2) was chosen because it represents a classical seasonal influenza virus, it was part of the influenza vaccine from 2000 to 2004 [154], and the eight-plasmid-based rescue system of this strain was established in the laboratory. Of the available rescue systems for a highly pathogenic influenza virus strain that originated from a human isolate, the A/Thai/04 strain was chosen because its PB2 protein harbors a glutamic acid residue at position 627, and therefore represents an avian-type PB2. Even though it was shown that A/Thai/04 acquired an adaptive mutation in its NEP protein to compensate for the lack of a mammalian-type K-627 PB2 [155] in order to enhance its polymerase activity, it is not yet known whether avian-type PB2 of highly pathogenic human isolates interacts with host factors different to the mammalian-type PB2 of seasonal strains. Therefore, the comparison of these influenza virus strains was of particular interest. Both recombinant WT and Strep-tagged viruses were propagated in embryonated chicken eggs. Due to the need for responsible handling of animal material, virus stocks were limited. To allow for a maximum number of biological replicates cells could only be infected at an MOI of 1.5 and no experimental set-ups using A/Thai/04-WT as internal control was included. In order to maximize the amount of PB2 protein available for affinity purification, whilst still being within the time frame of a monocyclic infection, cell lysis was performed 16 hours post infection. In

addition, growth analysis showed a major attenuation of the A/Thai/04Strep-PB2 virus compared to the WT virus from 24 h on (see figure 3.2.B). Even though it cannot be explained why the virus showed attenuation only from 24 h onwards, this observation reinforced the decision to infect cells for 16 h. Human alveolar epithelial cells (A549 cells) represent an *in vitro* model for type II pneumocytes, the primary target cells for influenza viruses in the human lung [95], and are widely used in influenza virus research; therefore they were selected as the host cell line of choice in the MS study.

In total, data from 4 experimental replicates were collected in order to identify cellular interaction partners of A/Pan/99 and A/Thai/04 PB2 proteins, resulting in the detection and quantification of 1842 protein groups.

Evaluation of MS data

Replicates showed a relatively strong Pearson correlation of 0.569 to 0.823 for A/Pan/99-PB2-Strep, and from 0.858 to 0.922 for A/Thai/04-PB2-Strep samples (figure 3.6.A-3.6.B). Hence, M/L and H/L ratios of protein groups were very similar between replicates, indicating stable proportions of the individual protein groups between A/Pan/99-PB2-Strep; A/Thai/04-PB2-Strep and the internal A/pan/99-WT control were affinity purified and detected across the 4 experiments.

Volcano plot analysis revealed 487 cellular protein groups that were significantly more abundant in PB2-Strep samples compared to the internal WT control (see supplementary table S.1). Of these, 83 protein groups were significantly more abundant in both A/Pan/99-PB2-Strep and A/Thai/04-PB2-Strep eluates, while 106 and 298 protein groups were solely significantly more abundant in either A/Pan/99-PB2-Strep or A/Thai/04-PB2-Strep eluates, respectively. This could lead to the assumption that PB2 of the A/Thai/04 strain specifically interacts with a greater number of cellular proteins. However, analysis of the H/M ratio of PB2 peptides in the 4 replicates revealed that A/Thai/04 PB2 was 2.7 to 10.9 times more abundant than A/Pan/99 PB2 (data not shown). This correlated with the observation that PB2 expression levels were higher in A/Thai/04 infected A549 cells compared to A/Pan/99 infected cells (see figure 3.1 as an example). In addition, A/Thai/04 infection led to more profound cytopathic effects (CPE) at 16 hours post infection and viral titers were up to 3 times higher compared to A/Pan/99 (see figure 3.2 as an example). Over a 72 h time course of infection, A/Thai/04 viral titers were increased by up to 7 times compared to the A/Pan/99 strain, indicating a more potent replication of A/Thai/04 influenza virus in A549 cells, an observation that has also been described before by *Matthaei et al*. and *Gabriel at al*. [156,157]. Hence, even though equal overall protein amounts of the 3 cell states infect-

ed with the 3 different viral strains were mixed together and then used for co-precipitation, the proportion of viral proteins was supposedly higher in the A/Thai/04-PB2-Strep than in the A/Pan/99-PB2-Strep lysates. Therefore, it is likely that binding sites on the Strep-Tactin resin were relatively stronger occupied by A/Thai/04-PB2-Strep protein and its interaction partners, leaving less space for A/Pan/99-PB2-Strep protein and its interaction partners to bind. This could have shifted the M/L; H/L ratio equilibrium in the direction of A/Thai/04 PB2. Subsequently, protein groups that were found to be significantly more abundant only in A/Thai/04-PB2-Strep eluates cannot generally be excluded as potential A/Pan/99 PB2 binding partners. As a result, the filtered protein group list was considered as a whole, rather than being divided into A/Thai/04 and A/Pan/99, in the analyses that followed. Hence, the experimental conditions were not optimal for a comparative analysis of A/Pan/99 and A/Thai/04 PB2 interaction partners using mass spectrometry.

Regarding future AP-MS studies, an adjustment of tagged-protein levels, or the application of two separate affinity purifications, one for each viral strain in combination with its internal control, would be strongly advisable.

The limited amount of available binding sites on the Strep-Tactin resin, highlighted by the fact that PB2 protein was also found in the non-bound fraction (see figure 3.5), combined with the unequal amounts of A/Thai/04 and A/Pan/99 PB2 proteins applied to the resin, could also explain the slightly lower Pearson correlation of the A/Pan/99-PB2-Strep data. The likelihood that a protein will bind to the Strep-Tactin resin in similar amounts across 4 individual experiments decreases with decreasing numbers of available binding sites.

All viral proteins that were included in the database used for protein identification by MaxQuant were found to be more abundant in Strep eluates compared to the WT control (see figure 3.7). Except for the M1 and M2 protein of A/Pan/99, the change in protein abundance was significant for all proteins (see supplementary table S.2 and S.3). PB2 showed the highest significance and fold-change in A/Pan/99-PB2-Strep (t-test difference 358.29) as well as in A/Thai/04-PB2-Strep (t-test difference 992.55) eluates compared to the internal control, confirming the functionality of the experimental setup and the significance of data evaluation. Overall, viral proteins were at least 3 times more abundant in Strep eluates, indicating that they co-purified with PB2-Strep. PB2 forms vRNPs together with PA, PB1, NP and vRNA [13]. Hence the co-purification of these proteins with PB2-Strep in an infectious context could be predicted, while the co-purification of PB2 with e.g. the transmembrane proteins NA and HA was less expected. However, the M1 protein is presumed to interact with the cytoplasmic tails of

NA, HA and M2 as well as with NEP and vRNPs [48,158-160]. Given that all viral proteins are present at 16 hours post infection, M1 presumably served as a linker and the whole protein complex was precipitated. The same mechanism could explain the abundance of NS1, which is known to interact with NP [161], in the PB2-Strep eluates.

The filtered list of cellular proteins significantly more abundant in PB2-Strep eluates was compared to data from 5 other previously published proteome screens that looked for interaction partners of PB2, either expressed alone or as part of the viral polymerase complex (figure 3.8) [138-142]. The largest data overlap (71 of the same cellular proteins identified in both studies) was found with the *Watanabe et al*. screen (figure 3.8; Watanabe, UA). This is probably due to the fact that the *Watanabe et al*. protein list, generated by MS analysis, was not subjected to a stringent data filtering process before additional experimental analyses were performed [141]. Hence, this list of 388 potential PB2 interaction partners was the longest used for comparison, which thereby facilitated the observed largest data overlap.

However, when the data overlap was calculated as a percentage of the number of proteins of the interactome screen used for comparison, the largest overlap was found with the *Bradel-Tretheway et al.* screen (figure 3.8.A; Bradel, UA). The same 8 proteins were detected in both screens which represent 23.5 % of 34 hit proteins of the *Bradel-Tretheway et al.* screen, which aimed to identify interaction partners of the viral polymerase of A/Vietnam/1203/04 (H5N1) [138]. Two of these proteins, ANP32A and B, are known to be crucial for viral polymerase activity. Especially a 33 long aa sequence present in avian but not mammalian ANP32A plays a role in the suboptimal polymerase activity of avian H5N1 or H7N9 polymerase in mammalian cells (see section 1.2.4) [68]. The fact that this screen also analyzed the interactome of a H5N1 strain presumably contributes to the number of overlap proteins. In addition, strict filter criteria were applied, thus lowering the likelihood of false positives, which promotes the number of proportional overlap proteins.

The majority of all compared protein groups, namely 925 out of 1192 (77.6 %), were found in only 1 screen. The discrepancy between various studies using AP-MS and other systems-level technologies like RNAi screens to identify host-pathogen interactions has been shown to be high [162]. Possible reasons for this low overlap include different experimental setups, false positives and negatives, divergent applications of statistical analysis [163] and individual filter criteria. As shown in Table 4.1, even though AP-MS techniques were used to identify interaction partners of PB2 or the polymerase complex, each experimental setup was unique in the combination of cell type, viral strain e.t.c, all of which contributes to differences in the obtained results.

Table 4.1. Experimental setups of proteome screens used for comparison with our filtered protein list. The AP-MS screens aimed to identify interaction partners of the influenza virus PB2 protein expressed in isolation (*Heaton et al.*, *Wang et al.*, *Watanabe et al.* and *York et al.*) or as part of the polymerase complex (*Bradel-Tretheway et al.*).

	Heaton et al.	**Bradel-Tretheway et al.**	**Wang et al.**	**Watanbe et al.**	**York et al.**
Cell type	A549	A549	293T	293T	293T
Viral Strain	A/PR/8/34 (H1N1)	A/VN/1203/04 (H5N1)	A/PR/8/34 (H1N1); A/WSN/33 (H1N1); A/NY/18/2009 (H1N1); A/VN/1203/04 (H5N1)	A/WSN/33 (H1N1)	A/WSN/33 (H1N1)
Tag	FLAG	TAP	FLAG	FLAG	Strep
Transfection	-	PA-TAP + PB2 PA-TAP + PB1 + PB2	PB2-FLAG	PB2-FLAG	-
Infection	MOI 3 10 hours	-	MOI 1 16 hours (no VN/04 inf.)	-	MOI 5 7 hours

Nonetheless, 2 proteins were found in our filtered protein list and in the *Heaton et al*.; *Watanabe et al*. and the *York et al*. screens. SLC25A6, also known as ANT3, is known to interact with the viral protein PB1-F2, which triggers the intrinsic apoptosis pathways in the host cell [164]. The second protein, BAG2, is known to stimulate the ADP/ATP exchange rate of HSPA8 and to act as an inhibitor of its CHIP-dependent ubiquitin ligase activity[165]. However a role for BAG2 in the influenza virus replication cycle has not yet been described.

A total of 30 proteins (6.2 %) were also found in 2 out of 4 previously published screens. Among them are proteins that have not yet been described in the context of

influenza virus infection, as well as proteins that are known to be required for the efficient polymerase activity of H1N1 and H5N1 subtypes, e.g. DDB1 and DDX5 [127]. While an additional 98 proteins were also found in 1 of the compared screens (20.1 %), the majority of identified proteins (356; 73.1 %) were only found in the screen performed in this study. This comparative analysis on one hand highlights the significance of the retrieved data by displaying proteins that were found in multiple screens and are known to play a role in the influenza virus replication cycle. On the other hand, the comparison also points out the need for further data filtering to decrease the number of false positives, and to increase the likelihood of identifying specific interaction partners of PB2.

GO term analysis of the protein list using the PANTHER online tool to gain further insight into the biological functions of the identified protein groups led to the same conclusion (figure 3.9). Classification according to their protein class showed that the majority of proteins (25.3 %) belong to the class of nucleic acid binding proteins. This was consistent with expectations, since PB2 is part of the viral RNA replication and transcription machinery; hence, it is plausibly that PB2 might interact with cellular proteins also involved in nucleic acid binding. The interaction of PB2 with representatives of the third most prominent protein class, hydrolysis proteins (10.3 % of interaction partners identified in our screen), was less predictable. However, nucleases belong to a class of hydrolases, which could explain the occurrence of this protein class in an interactome screen of a viral polymerase protein. The cellular proteins MCM2/3/4/6 and 7 identified in our screen, also belong to a class of hydrolase proteins, and form the minichromosome maintenance complex, which has previously been shown to interact with influenza virus PA protein and to regulate virus genome replication, thus supporting the relevance of the data set [67]. On the other hand, proteins belonging to the second most prominent protein class, oxidoreductase proteins (12.9 %), as well as to other categories revealed in PANTHER analysis (such as extracellular matrix proteins and cell junction proteins), highlight the need to apply more stringent filter criteria, even though the involvement of these proteins in PB2 function cannot be excluded with absolute certainty.

In order to obtain a more stringent list of potential PB2 interaction partners, another filter criterion was added to the analysis. In addition to being statistically significant, protein groups needed to have a t-test difference of ≥ 1 (log2) in at least 2 out of 4 experiments, equating to a fold increase in protein abundance of at least 2 compared to the A/Pan-99-WT control. This shortened the list from 487 filtered protein groups to 22 protein hits (hit list; table 3.2) and increased the ratio of proteins overlapping with the other proteome screens from 22.4 % to 40.9 %. The proteins GGH, CKMT1B,

HIST2H3A, EPHX1, CKMT1A, PABPC3, SLC12A2, LXN, SNRNP200, CAST, KCNJ8, hnRNPC1, and AGR2 were, not found to interact with PB2 in the 5 published interactome screens used for comparison and thereby represent potential novel binding partners of PB2 [138-142]. For example, it is known that the ubiquitously expressed protein hnRNPC1 associates with pre-mRNAs in the nucleus and potentially influences splicing regulation[166]. The influenza virus proteins NEP and M2 are produced by splicing of the NS1 and M1 mRNAs, a process which is controlled by the cellular proteins RED and SMU1. This protein complex is recruited by PB2 and PB1 to splicing sites of viral mRNA [167]. Hence, the interaction of PB2 with other cellular splicing regulators is possible, and may have functional relevance to the influenza virus replication cycle. In addition, the importance of hnRPC1 for the replication of other viruses has already been shown in the context of dengue, hepatitis C and poliovirus infection [168].

GO term analysis assigned 11 of 22 hit proteins to the molecular function “nucleotide binding”, indicating the relevance of hit proteins. A STRING database network analysis revealed 2 clusters of protein interaction networks (see figure 3.10). The smaller cluster comprised 3 histone proteins while the second cluster encompassed 13 proteins with HSPA8 as the center. All of the 10 connections of HSPA8 shown in figure 3.10 represent experimentally determined protein interactions. This could lead to the assumption that a single large complex of interacting proteins has been precipitated with PB2. However, since HSPA8 is a member of the heat shock protein 70 (HSP70) family and plays a role in nascent protein folding and cellular transport of proteins [118] it is likely that it binds to a wide variety of proteins. Therefore, this large cluster does not necessarily represent a single large protein complex, but potentially reflects the chaperone function of HSPA8 and/or a network of smaller protein complexes that are not all physically linked inside cells, but that all contain HSPA8 (see section 4.2 for further discussion of HSPA8 and its role in the influenza replication cycle). The fact that some of the proteins are mainly located in the nucleus (for example SNRNP200 and TOP2A) while others are located in the cytosol (for example BAG2), the mitochondrion (CKMT1A/B) or the endoplasmic reticulum (EPHX1) also speaks against a single large protein complex. The possible precipitation of several small protein complexes is supported by the fact that for the majority of hit proteins (excluding SLC12A2, PABPC3 and the 6 proteins that showed no relationship to other proteins) an experimentally determined protein interaction to at least one other hit protein in addition to HSPA8 is known. Overall, these results were in line with expectations. The overlap with other proteome screens, the assigned molecular functions of identified proteins and the identification of known PB2 interaction partners such as PABPC1 [61] indicated the functional relevance of the AP-MS data. Nevertheless, the performed interactome screen enabled the identifica-

tion of potentially novel PB2 interaction partners which, until now, have not yet been reported.

Validation of protein hits

To further support the findings of the MS screen, 13 proteins from the hit list were selected for validation based on their molecular functions and reagent availability. AGR2, CAST, EPHX1, GGH, hnRNPC1, LXN, PABPC3 and SLC12A2 were selected as candidates representing potentially novel PB2 interaction partners. In addition BAG2, HSPA2, HSPA8 and RCN2 served as representatives of proteins already found in other PB2 interactome screens, but not yet further investigated in terms of their potential role in polymerase interaction or function. For example, the BAG2 protein was not only found in 3 out of the 4 proteome screens used for comparison [139,141,142] but is also known to have a regulatory function within the chaperone activity of Hsp70 family members, of which 2, HSPA2 and HSPA8, were also found in the AP-MS screen. Hence, further investigation of these interacting proteins seemed logical.

The 13th protein selected for validation, PABPC1, is a known interaction partner of PB2 [61] and served as a positive control for the Co-IP validation experiment. This 3'-poly(A) tail binding protein is known to be part of the translation pre-initiation complex. PABPC1 interacts with the translation initiation factor eIF4G which is, in turn, part of the cap-binding complex which is recruited to mRNA through interaction of the complex component eIF4E with the 5'-cap [169]. Hence, the interaction of PABPC1 and eIF4G forms a protein bridge between 3′- and 5′-mRNA-termini [170]. The formation of this so called "closed loop structure" promotes recruitment of the small ribosomal subunit to the mRNA 5′ terminus [171]. It has been shown that the influenza virus NS1 protein not only interacts with PABPC1 and eIF4G, but is also associated with viral but not cellular mRNA, suggesting that NS1 promotes the specific recruitment of the translation initiation complex to viral mRNAs [172]. However, viral mRNAs are nonetheless selectively translated in influenza virus mutants lacking the NS1 protein, hinting at an additional mechanism for selective translation of viral mRNAs [173]. Even though the interaction of the viral polymerase with viral mRNAs that have already been transported to the cytoplasm is highly controversial, *Yángüez et al.* showed that PB2 interacts with eIF4G and proposed a model in which PB2 mediates the association of the 5'-cap with the cap-binding complex in an eIF4E independent manner [174]. Since infection with influenza leads to the dephosphorylation and inactivation of eIF4E [175], it was suggested that PB2 promotes the formation of the "closed-loop" structure, thereby helping to initiate viral mRNA translation. Since the interaction of PB2 with PABPC1 has also been shown [61], the formation of the "closed-loop structure" is potentially even independent of the inter-

action of NS1 with PABPC1, supporting the hypothesis of an additional role for PB2 in the influenza virus replication cycle. Alternatively, the interaction of PB2 with PABPC1 could also occur in the nucleus where the cellular protein is known to bind un-spliced and partially spliced pre-mRNA [176]. The role of PABPC1 in nuclear events is however still unclear [177]. The Co-IP analysis showed co-precipitation of A/Pan/99 PB2 with over-expressed, tagged PABPC1 protein, verifying the functionality of the MS experimental setup (see figure 3.12). Interestingly, PABPC1 overexpression had however only a significant influence on the activity of the A/Thai/04 polymerase for which co-precipitation of PB2 could not be verified with certainty (see figure 3.11. and 3.14). However, the fact that overexpression had an effect on polymerase activity supports an interaction of PABPC1 with PB2. A decrease in polymerase activity of A/Thai/04 was not only observed after PABPC1 overexpression but also after overexpression of the second poly(A)-binding protein analyzed, PABPC3. The inhibitory effect of PABPC1/3 overexpression on A/Thai/04, but not on A/Pan/99 polymerase activity hints at an inhibitory effect of PABPC proteins on the activity of avian-type viral polymerases. It would be worthwhile testing if the same difference in effects of PABPC proteins on polymerase activity can be observed in other seasonal and highly pathogenic avian/avian-type influenza virus strains.

Overall, the co-precipitation of A/Thai/04 PB2 with 8 (BAG2, GGH, HSPA2, HSPA8, PABPC3, EPHX1, LXN, SLC12A2), and the co-precipitation of A/Pan/99 PB2 with 7 (BAG2, HSPA8, PABPC1, PABPC3, EPHX1, LXN, SLC12A2) out of 13 examined hit proteins could be verified in overexpression experiments (see figures 3.11 and 3.12). This validation rate is very high for a high-throughput screen, indicating the robustness of the chosen method. Moreover, minigenome assay revealed an effect with 11 out of 13 overexpressed proteins on the polymerase activity of either A/Pan/99 or A/Thai/04 strains (figure 3.14). In addition to PABPC1 and 3, AGR2, hnRNPC1 and SLC12A2 overexpression had different effects on the viral polymerase activity of the 2 influenza virus strains. While AGR2 overexpression slightly inhibited A/Thai/04 polymerase activity whilst not affecting A/Pan/99 polymerase activity, SLC12A2 only showed an inhibitory effect on the activity of the A/Pan/99 polymerase, leaving the A/Thai/04 polymerase unaffected. The membrane protein SLC12A2 transports sodium (Na), potassium and chloride into cells [179]. It has been shown that an increase in intracellular Na^+ leads to a decline in influenza virus titers [180]. Given that overexpression of SLC12A2 leads to a decrease in A/Pan/99 polymerase activity, an inhibitory effect of Na^+ is feasible while the A/Thai/04 polymerase is maybe less sensitive to elevated Na^+ concentrations.

The ribonucleoprotein hnRNPC1 had a positive effect on polymerase activity, however this was only observed for A/Thai/04 strain. Interestingly, the interaction of hnRNPC1, as well as the interaction of the polymerase influencing proteins AGR2 and RCN2 with PB2 could not be verified by co-IP (see table 3.3.). This may hint at a possible role of NP in the interaction with some of these proteins since NP was present in the MS experiment as well as in the minigenome assay, but not during the Co-IP with the tagged, overexpressed cellular proteins. For example, the NP interacting splicing factor UAP56 has been shown to facilitate the NP-RNA interaction that likely serves as the viral polymerase template. Hence, it was suggested that the UAP56-NP interaction could lead to enhanced viral RNA synthesis [178]. A potentially similar function for the splicing factor hnRNPC1 in A/Thai/04 replication represents an interesting topic for further investigation.

The co-precipitation of the polymerase inhibiting proteins GGH and HSPA2 (detrimentally influences both A/Pan/99 and A/Thai/04 polymerase activity) with A/Pan/99 PB2 protein could not be verified with certainty. The PB2 bands in these eluates were only slightly more prominent than in the control eluate. However, when combined with the results of the minigenome assay, an interaction of these proteins (as it was shown for A/Thai/04 PB2) with A/Pan/99 is plausible. Furthermore, the inhibitory effect of HSPA2 on the polymerase activity of A/Pan/99 and A/Thai/04 is similar to findings regarding HSPA1A of the Hsp70 family: HSPA1A was shown to interact with PB2 as well as with PB1 of the A/WSN/33 influenza strain, and its overexpression also inhibited viral polymerase activity. This resulted in significantly reduced transcription and replication of viral RNA due to the interference of HSPA1A with RNP integrity, which is thought to be achieved by HSPA1A blocking the interaction of PB1 with vRNA [181].

Overall, validation experiments confirmed the co-precipitation of PB2 with a large number of the cellular proteins identified in the SILAC AP-MS screen, which had been further streamlined through the appliance of stringent filter criteria. The question of whether the interaction of these proteins with PB2 is direct or mediated through viral PB1, PA or additional cellular proteins could not be clarified in this experimental setup and should be the subject of further investigation. Proteins usually work in complexes and the MS setup was designed to identify cellular factors influencing viral polymerase function. Hence, the focus of this study was not on details of the protein interaction itself, but on the functional influence of these interacting cellular proteins on viral polymerase activity. The observation that overexpression of 11 out of 13 proteins selected for validation had a significant influence on the polymerase activity of A/Thai/04 and/or A/Pan/99 strains indicates the suitability of the MS analysis for this purpose. Several of

these proteins, for example HSPA2 and hnRNPC1, have not yet been reported to have an influence on influenza virus polymerase activity. Hence, this study has uncovered variety of cellular proteins for further experimental trials investigating the influenza virus polymerase and its interplay with host cell factors. The obtained data also suggests differences in the impact of these identified proteins on the polymerase activity of seasonal and highly pathogenic influenza virus strains.

4.2 HSPA8 is a novel regulator of the non-laboratory adapted seasonal influenza virus polymerase

HSPA8, also known as Hsc70 or HSP73, belongs to the 70 kDa heat shock protein (HSP70) family [119]. In addition to its various cellular functions in protein folding [182], protein degradation [183] and protein transport into organelles [184] (amongst other functions, see figure 4.1), HSPA8 has also been shown to play a role in regulating the replication of a variety of different viruses. For example, HSPA8 functions as a receptor for Japanese encephalitis virus [123], is important for formation of the pre-replicative site of herpes simplex virus type 1 (HSV-1) [122] and interacts with the RNA-dependent RNA polymerase of turnip mosaic virus [124].

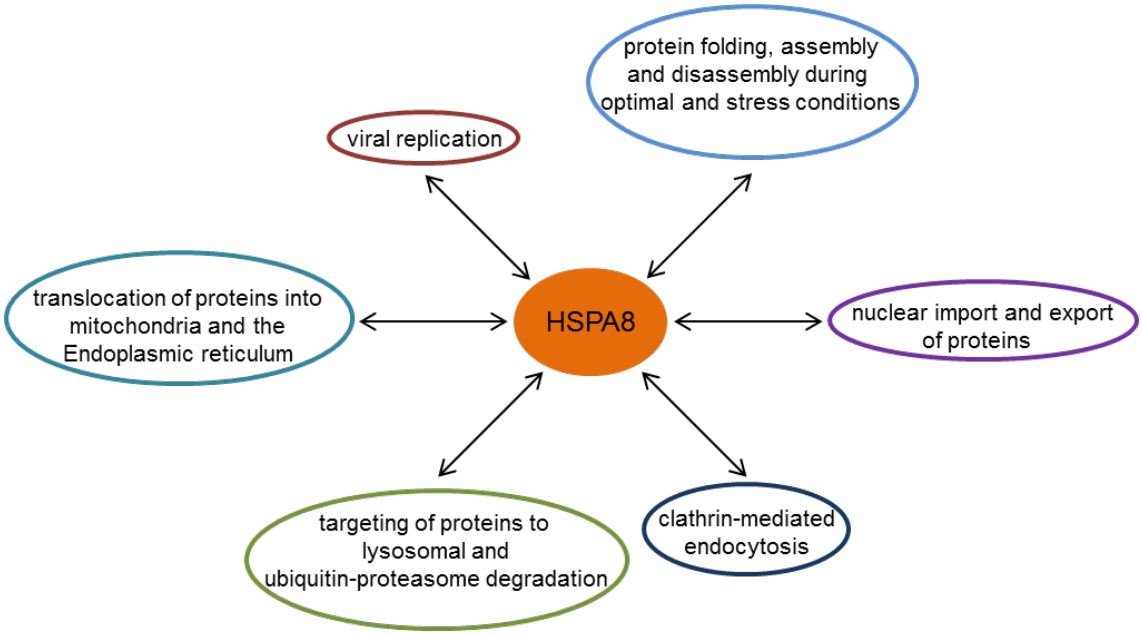

Figure 4.1. Cellular functions of HSPA8. The heat shock protein HSPA8 has a large variety of cellular functions during optimal as well as during stress conditions. For more detailed information on HSPA8 and its cellular functions see section 1.4.

In addition, HSPA8 has also been described in the context of the Influenza virus replication cycle. *Watanabe et al.* showed that the depletion of HSPA8 leads to reduced titers of A/WSN/33 in HeLa cells, presumably due to its interaction with the influenza virus M1 protein, and the potential role of this interaction in the nuclear export of vRNPs [62,125,126]. Furthermore, *Bortz et al.* identified HSPA8 as an enhancer of A/WSN/33 and A/VN/1203/04 (H5N1) polymerase activity in 293T cells [127]. However, this was only observed in the infection-based minigenome assay and not in the conventional minigenome assay, leading them to the conclusion that the influence of HSPA8s on viral polymerase activity was due to its function in the cellular stress response.

In contrast, our study showed a positive effect of HSPA8 overexpression on A/Pan/99 as well as A/Thai/04 polymerase activity in minigenome expressing, non-infected A549 cells (see figure 3.14), suggesting a non-stress related role for HSPA8 in polymerase function. Already interesting in itself, it was also observed that overexpression of BAG2 (a co-factor of HSPA8) resulted in the downregulation of both A/Pan/99 and A/Thai/04 polymerase activity. BAG2 belongs to the Bcl-2-associated athanogene (BAG) family of proteins which are characterized by the presence of at least one BAG domain located at the C-terminus [185]. The BAG domain mediates the binding of these proteins to the ATPase domain of Hsp70 family members, which accelerates the chaperones ADP/ATP exchange rate and thereby encourages substrate release [118]. The family member BAG2, identified in this and in 3 other PB2/polymerase interactome screens, binds the ATPase domain of HSPA8 with high affinity in a 2:2 stoichiometry [186]. Given that endogenous HSPA8 is present in BAG2 overexpression cells, it is plausible that additional, overexpressed BAG2 proteins throws the BAG2-HSPA8 equilibrium out of balance, leading to reduced HSPA8 function and therefore inhibited viral polymerase activity. The presence of an HSPA8 co-factor in the hit list and an effect on this factor on viral polymerase activity supported the decision to analyze HSPA8 and its role in viral replication in more detail

Role of HSPA8 in the replication cycle of A/Pan/99 and A/Thai/04

To further investigate the role of HSPA8 in the context of an influenza virus infection in more detail, co-IP of PB2 with cellular HSPA8 was performed. The co-precipitation of A/Pan/99 and A/Thai/04 PB2 with endogenous HSPA8 from infected A549 cells was confirmed (see figure 3.15). This is in keeping with observations concerning other heat shock proteins. *Li et al.* described the interaction of HSPA1A, another member of the HSP70 family, with PB2 and PB1 of the A/WSN/33 influenza strain [181] and an interaction with the same viral proteins, in this case of the A/PR8/33 influenza strain, was

shown for Hsp90 by *Naito et al.* [64]. The question whether HSPA8 interacts only/directly with PB2 or also with/through other proteins of the viral polymerase complex needs to be further investigated. However, the co-precipitation of PB2 with HSPA8 in PA/PB1/PB2 and HSPA8 transfected 293T cells indicated that the heat shock protein interacts with the viral polymerase complex without the need of additional viral proteins (see figure 3.11 and 3.12). Taken together with the minigenome assay results in HSPA8 overexpressing cells (figure 3.14), the direct involvement of HSPA8 in viral polymerase functionality is plausible.

Unlike HSPA1A, HSPA8 is constitutively expressed and only mildly induced during cellular stress [118]. Even though mainly located in the cytosol, HSPA8 shuttles between the nucleus and cytoplasm under normal conditions and concentrates in the nucleus under stressful conditions [118]. *Watanabe et al.* showed an accumulation of HSPA8 in the nucleus of A/WSN/33 and A/PR8/33 infected MDCK and HeLa cells, respectively [125]. To determine if the concentration of HSPA8 in the nucleus is a common feature of influenza virus infected cells, the localization of HSPA8 was analyzed by immunofluorescence staining in A549 cells infected with the seasonal A/Pan/99 and the highly pathogenic A/Thai/04 strains of influenza virus. In both cases HSPA8 was evenly distributed between the cytoplasm and the nucleus of infected cells 4 hours p.i., while HSPA8 was then observed to be concentrated in the nucleus of infected cells after 8 hours of infection (see figure 3.16 and 3.17). This is in agreement with the results from *Watanabe et al.* which showed a relocation of HSPA8 into the nucleus at 9 h but not 3 h post infection [125]. *Watanabe et al.* proposed a regulatory role for HSPA8 in the nuclear export of newly formed vRNPs through its interaction with the viral M1 protein [62]. In terms of viral polymerase activity, the presence of HSPA8 in the nucleus at late time points of infection indicates an influence of this heat shock protein on newly formed polymerase proteins, rather than on polymerase complexes that are part of the incoming vRNPs.

HSPA8 depletion using a mixture of 4 different siRNAs slightly decreased A/Pan/99 titers from 16 h p.i. onwards, with a peak of viral titer decline at 72 h p.i. (figure 3.18.C and E), compared to negative control siRNA treated cells. These results are in accordance with the effect of overexpression of HSPA8 on viral polymerase activity (figure 3.14.A) and the observation by *Watanabe et al.* that HSPA8 depletion results in a decrease in viral titer of A/WSN/33 in HeLa cells [125]. Interestingly, the influence of HSPA8 on A/Thai/04 replication was less clear. Viral titers were decreased at 16 h p.i. in HSPA8 depleted cells, however titers were almost identical at 24 h p.i., and then increased at 48 h and 72 h p.i. in comparison to negative control siRNA treated cells (see

figure 3.18.D and F). These data could hint at different functions for HSPA8 in early and late time points of the A/Thai/04 viral replication cycle, or alternatively could be a result of the unintentional use of lower viral titers for the initial infection of cells treated with HSPA8 specific siRNA. Even though complications during infection of A549 cells cannot be excluded, the same pipetting error in 2 experiments performed in duplicates is very unlikely. Therefore it is more plausible to suspect that the lower titers at 0 h and 16 h p.i. in HSPA8 depleted cells were perhaps due to an impact of HSPA8 depletion on viral attachment and/or endocytosis. It has been shown that influenza virus H5N1 can enter host cells through clathrin mediated endocytosis [187], during which HSPA8 acts as a clathrin-uncoating ATPase [119]. In this case, the depletion of HSPA8 could result in a reduction in clathrin mediated endocytosis, which could in turn lead to a reduction in virus entry, and reduced viral titers.

The reason for the enhancing effect of HSPA8 depletion on A/Thai/04 replication at late time points of infection (48 h and 72h p.i.) is a subject of speculation. One possible explanation could be related to the function of HSPA8 in protein degradation through the ubiquitin-proteasome pathway [119]. The interaction of HSPA8 with STUB1/CHIP leads to the coupling of ubiquitin side chains to the chaperones protein substrate and the substrates subsequent degradation. Hence, decreased HSPA8 levels may result in the rescue of viral proteins from HSPA8/ubiquitin dependent proteasomal degradation, thus resulting in enhanced viral titers. The involvement of increased viral polymerase activity in elevated viral replication in HSPA8 depleted cells seems unlikely, given the stimulating effect of HSPA8 overexpression on A/Thai/04 polymerase activity. However, siRNA depletion of HSPA8 in 293T cells did lead to a slight increase in viral polymerase activity to 111.7 % (figure 3.19.B) which is maybe also due to decreased HSPA8 mediated viral protein degradation. Unfortunately, a clear conclusion regarding the influence of HSPA8 on A/Thai/04 polymerase activity and viral replication cannot be made based on these results.

Results concerning the involvement of HSPA8 in the A/Pan/99 replication cycle were however, more in agreement with each other. While HSPA8 overexpression increased viral polymerase activity, HSPA8 depletion decreased A/Pan/99 replication to 30.4 % and viral polymerase activity down to 60.2 % in comparison to cells treated with negative control siRNA (figure 3.19.A). Intriguingly, HSPA8 depletion led to a strong depletion of A/Pan/99 PB2 protein (figure 3.19.C). Given that HSPA8 functions as a molecular chaperone for a variety of proteins, it is likely that PB2 is also dependent on HSPA8 for proper folding and protein stability. The lack of HSPA8 presumably leaves PB2 in a premature state, resulting in the reduced activity of PB2 and/or its degradation by the

cellular ubiquitin-proteasome system (UPS) or by lysosomal degradation. A small amount of PB2 was however still detectable by immunoblot analysis, perhaps explaining the remaining activity of the viral polymerase complex, and was presumably due to the fact that small amounts of HSPA8 were still present inside cells. To test whether reduced viral polymerase activity is linked to inaccurate folded PB2, HSPA8 knock down cells could be treated with inhibitors of the lysosomal or ubiquitin-proteasome degradation system. This should lead to a rescue of PB2 protein amounts in immunoblot assay while the polymerase activity should still be decreased. To further characterize the influence of HSPA8 on viral polymerase activity, the minigenome assay was performed in the presence of the HSP70 inhibitor YM-01 (data not shown). Addition of the inhibitor resulted in a concentration dependent increase in viral polymerase activity. Even though this seems to be contradictory to the knock down results, one has to consider that YM-01 not only modulates the activity of HSPA8, but also of other Hsp70 family members such as HSPA1A, which has previously been shown to have an inhibitory effect on influenza virus polymerase activity [181]. Hence, it could not be determined which HSP70 member led to the increase in viral polymerase activity when cells were treated with YM-01. Moreover, it cannot be excluded that the inhibitor has previously undocumented off target effects that interfere with viral replication. Given that siRNA treatment is much more specific when investigating the role of individual HSP70 family members in viral replication and polymerase activity, these results were considered to have more relevance.

Role of HSPA8 as a PB2 chaperone

As previously mentioned, the relocation of HSPA8 to the nucleus at late time points of infection does not support a role for this chaperone on incoming viral polymerase proteins. Early transcription from incoming vRNPs leads to expression of the early gene products PA, PB1, PB2 and NP which are then subsequently transported into the nucleus after translation in the cytoplasm [62]. PB1 and PA form a dimeric complex in the cytoplasm which is imported into the nucleus by RanBP5, while PB2 is imported into the nucleus separately by the importin α/β pathway [63]. In the nucleus, PB2 and the PB1-PA dimer assemble to form the polymerase complex which in turn forms new vRNPs together with viral RNA and NP. Newly formed vRNPs then serve as a template for transcription of the late genes HA, NA, NEP, M2 and M1 [62]. *Watanabe et al.* proposed that the nuclear export of newly formed vRNPs is regulated by HSPA8 via the formation of a CRM1-HSPA8-M1-vRNP complex mediated by the HSPA8 nuclear export sequence (see figure 1.7), thus supporting a role for HSPA8 at later time points during influenza virus infection [62].

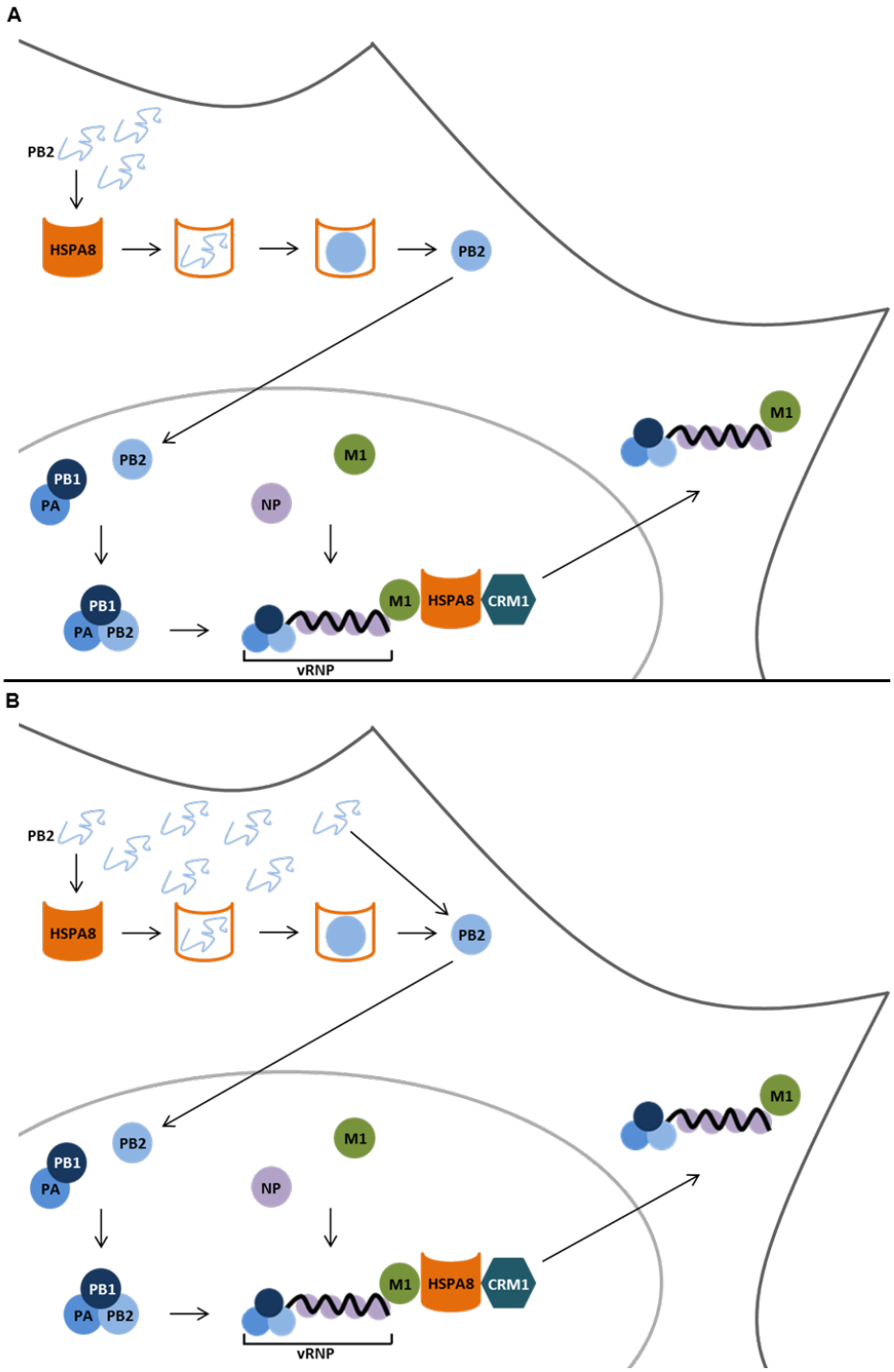

Figure 4.2. Proposed model for the role of HSPA8 in the influenza virus replication cycle. The polymerase protein PB2 is expressed early in influenza virus infection. After translation, cytosolic HSPA8 acts as a chaperone to promote A/Pan/99 PB2 maturation and stability which is necessary for efficient viral replication (**A**). Even though HSPA8 can presumably also act as a chaperone for A/Thai/04 PB2, the high expression rate of PB2 allows for the generation of sufficiently high concentrations of correctly folded protein even in the absence of the chaperone protein (**B**). Hence, A/Thai/04 is less dependent on HSPA8 for viral replication. Correctly folded PB2 and the PB1-PA dimer are separately transported into the nucleus where they form the trimeric polymerase complex. After formation of vRNPs together with newly synthesized vRNA and NP, HSPA8 (which relocates into the nucleus at late time points of infection) regulates the nuclear export of vRNPs via the formation of a CRM1-HSPA8-M1-vRNP complex [62].

The data presented in this thesis combined with the results from *Watanabe et al.* hint at a dual role for HSPA8 in the replication cycle of seasonal influenza viruses (see figure 4.2). It is thought that cytosolic HSPA8 acts as a chaperone for newly translated polymerase protein PB2, facilitating protein maturation and stability, before PB2 is imported into the nucleus and united with the PA-PB1 heterodimer to form the functional viral polymerase complex. This theory is supported by the observation that HSPA8 depletion leads to a depletion of PB2 and downregulation of viral polymerase activity, whilst viral polymerase activity is also decreased by overexpression of the HSPA8 co-factor BAG2 (figure 3.19 and 3.14). *Fislová et al.* obtained similar results regarding PB2 levels and viral growth after depletion of the chaperonin containing TCP-1 (CCT) protein, proposing that CCT might act as a chaperone for PB2 in the cytoplasm [188]. A similar role in maintaining the activity of influenza virus polymerase subunits before the formation of mature vRNP complexes was also described for the heat shock protein Hsp90 [64]. After successful formation of new vRNPs in the nucleus, the viral M1 protein is expressed and transported into the nucleus, where M1 plays a role in the nuclear export of vRNPs. At this point HSPA8, no longer essential in the cytoplasm since expressed PB2 is now already part of newly formed vRNPs in the nucleus, accumulates in the nucleus and regulates vRNP export through its interaction with M1. Since HSPA8 is also known to aid the import of cytoplasmic proteins into the nucleus [119], an additional role for HSPA8 in the nuclear import of newly translated PB2 and/or M1 is also possible.

As there were seemingly contradictory results, a clear cut role for HSPA8 in A/Thai/04 polymerase activity is less obvious. A feature of H5N1 viruses is their ability to replicate to high viral titers [189]. This was also observed in the present study; A/Thai/04 grew to higher viral titers, led to more profound CPE in infected cells and exhibited higher PB2 expression levels than seasonal A/Pan/99. Given that H5N1 viruses replicate to high viral loads in several mammalian species without adaptation [189], a lower dependency on host cell factors and a less balanced interplay with the host cell can be assumed. Hence, the sheer amount of PB2 generated in the host cell during infection may abolish their dependency on host cell chaperone proteins. Therefore even though HSPA8 may support correct protein folding when supplied by overexpression, the lack of HSPA8 may not necessarily result in lower viral polymerase activity. The likelihood of sufficient numbers of correctly folded PB2 protein to support high levels of viral polymerase activity being generated by chance is expected to be increased when high amounts of newly synthesized proteins are produced. Under these circumstances, the decrease in HSPA8 mediated proteasomal degradation of highly abundant PB2 may outdo the slightly inhibitory effects of HSPA8 depletion on protein folding, thus resulting in a small

increase of A/Thai/04 polymerase activity in HSPA8 depleted cells. Whether the inhibitory effect on protein folding becomes more important in an infectious/cellular stress context as suggested by *Bortz et al.* [127] cannot be elucidated with the results at hand. However, decreased viral titers in HSPA8 depleted cells at 16 hours p.i. may support this hypothesis.

HSPA8 is a constitutively expressed protein of the HSP70 heat shock protein family [119]. In addition to its various functions in normal cellular processes, HSPA8 has also been shown to play a role in several aspects of the replication cycle of different viruses, including HSV-1 [122], Japanese encephalitis [123] and turnip mosaic virus [124]. With regards to the potential role of HSPA8 in the influenza virus replication cycle, an influence on influenza virus polymerase activity due to the function of HSPA8 in cellular stress response [127], as well as a regulatory role in vRNP nuclear export through the interaction of HSPA8 with viral M1 protein, have previously been proposed [62,125,126]. In this study, HSPA8 was shown to co-precipitate with PB2 of the seasonal A/Pan/99 and the highly pathogenic A/Thai/04 influenza virus strains. In addition, it was demonstrated that HSPA8 is important for A/Pan/99 PB2 integrity and, as a result, for its polymerase activity. Thus, a role for the chaperone activity in facilitating PB2 maturation and increasing PB2 stability, in addition to the role of HSPA8 in vRNP export, is proposed.

The data presented in this thesis demonstrates that mass spectrometry is a powerful approach for identifying cellular interaction partners of viral proteins and, in combination with classical virological and molecular methods, a valuable tool for unravelling new cellular regulators of viral replication.

Bibliography

1 WHO. Influenza (seasonal) Fact sheet n°211. *http://www.who.int/mediacentre/factsheets/fs211/en/* (2016).

2 Nicholls, J. M. *et al.* Tropism of avian influenza A (H5N1) in the upper and lower respiratory tract. *Nat Med* **13**, 147-149, doi:http://www.nature.com/nm/journal/v13/n2/suppinfo/nm1529_S1.html (2007).

3 Carrat, F. *et al.* Time Lines of Infection and Disease in Human Influenza: A Review of Volunteer Challenge Studies. *American Journal of Epidemiology* **167**, 775-785, doi:10.1093/aje/kwm375 (2008).

4 Collin, E. A. *et al.* Cocirculation of two distinct genetic and antigenic lineages of proposed influenza D virus in cattle. *J Virol* **89**, 1036-1042, doi:10.1128/JVI.02718-14 (2015).

5 Hause, B. M. *et al.* Characterization of a Novel Influenza Virus in Cattle and Swine: Proposal for a New Genus in the Orthomyxoviridae Family. *mBio* **5**, doi:10.1128/mBio.00031-14 (2014).

6 Mänz, B., Schwemmle, M. & Brunotte, L. Adaptation of Avian Influenza A Virus Polymerase in Mammals To Overcome the Host Species Barrier. *Journal of Virology* **87**, 7200-7209, doi:10.1128/jvi.00980-13 (2013).

7 Osterhaus, A. D. M. E., Rimmelzwaan, G. F., Martina, B. E. E., Bestebroer, T. M. & Fouchier, R. A. M. Influenza B Virus in Seals. *Science* **288**, 1051-1053, doi:10.1126/science.288.5468.1051 (2000).

8 Ohwada, K. *et al.* Distribution of the antibody to influenza C virus in dogs and pigs in Yamagata Prefecture, Japan. *Microbiology and immunology* **31**, 1173-1180 (1987).

9 Tong, S. *et al.* New world bats harbor diverse influenza A viruses. *PLoS Pathog* **9**, e1003657, doi:10.1371/journal.ppat.1003657 (2013).

10 A revision of the system of nomenclature for influenza viruses: a WHO memorandum. *Bull World Health Organ* **58**, 585-591 (1980).

11 Bouvier, N. M. & Palese, P. The biology of influenza viruses. *Vaccine* **26 Suppl 4**, D49-53 (2008).

12 Badham, M. D. & Rossman, J. S. Filamentous Influenza Viruses. *Current clinical microbiology reports* **3**, 155-161, doi:10.1007/s40588-016-0041-7 (2016).

13 Compans, R. W., Content, J. & Duesberg, P. H. Structure of the ribonucleoprotein of influenza virus. *J Virol* **10**, 795-800 (1972).

14 Murti, K. G., Webster, R. G. & Jones, I. M. Localization of RNA polymerases on influenza viral ribonucleoproteins by immunogold labeling. *Virology* **164**, 562-566 (1988).

15 Arranz, R. *et al.* The Structure of Native Influenza Virion Ribonucleoproteins. *Science* **338**, 1634-1637, doi:10.1126/science.1228172 (2012).

16 Fodor, E., Seong, B. L. & Brownlee, G. G. Photochemical cross-linking of influenza A polymerase to its virion RNA promoter defines a polymerase binding site at residues 9 to 12 of the promoter. *J. Gen. Virol.* **74**, 1327-1333, doi:doi:10.1099/0022-1317-74-7-1327 (1993).

17 Hsu, M. T., Parvin, J. D., Gupta, S., Krystal, M. & Palese, P. Genomic RNAs of influenza viruses are held in a circular conformation in virions and in infected cells by a terminal panhandle. *Proc Natl Acad Sci U S A* **84**, 8140-8144 (1987).

18 Desselberger, U., Racaniello, V. R., Zazra, J. J. & Palese, P. The 3' and 5'-terminal sequences of influenza A, B and C virus RNA segments are highly conserved and show partial inverted complementarity. *Gene* **8**, 315-328 (1980).

19 Flick, R., Neumann, G., Hoffmann, E., Neumeier, E. & Hobom, G. Promoter elements in the influenza vRNA terminal structure. *RNA* **2**, 1046-1057 (1996).

20 Nagayama, K. & Danev, R. Phase contrast electron microscopy: development of thin-film phase plates and biological applications. *Philosophical Transactions of the Royal Society B: Biological Sciences* **363**, 2153-2162, doi:10.1098/rstb.2008.2268 (2008).

21 Horimoto, T. & Kawaoka, Y. Influenza: lessons from past pandemics, warnings from current incidents. *Nature reviews. Microbiology* **3**, 591-600, doi:10.1038/nrmicro1208 (2005).

22 Eisfeld, A. J., Neumann, G. & Kawaoka, Y. At the centre: influenza A virus ribonucleoproteins. *Nature reviews. Microbiology* **13**, 28-41, doi:10.1038/nrmicro3367 (2015).
23 te Velthuis, A. J. W. & Fodor, E. Influenza virus RNA polymerase: insights into the mechanisms of viral RNA synthesis. *Nat Rev Micro* **14**, 479-493, doi:10.1038/nrmicro.2016.87
http://www.nature.com/nrmicro/journal/v14/n8/abs/nrmicro.2016.87.html#supplementary-information (2016).
24 Holsinger, L. J., Nichani, D., Pinto, L. H. & Lamb, R. A. Influenza A virus M2 ion channel protein: a structure-function analysis. *J Virol* **68**, 1551-1563 (1994).
25 Robb, N. C., Smith, M., Vreede, F. T. & Fodor, E. NS2/NEP protein regulates transcription and replication of the influenza virus RNA genome. *J Gen Virol* **90**, 1398-1407, doi:10.1099/vir.0.009639-0 (2009).
26 Muramoto, Y., Noda, T., Kawakami, E., Akkina, R. & Kawaoka, Y. Identification of novel influenza A virus proteins translated from PA mRNA. *J Virol* **87**, 2455-2462, doi:10.1128/jvi.02656-12 (2013).
27 Wise, H. M. *et al.* A Complicated Message: Identification of a Novel PB1-Related Protein Translated from Influenza A Virus Segment 2 mRNA. *Journal of Virology* **83**, 8021-8031, doi:10.1128/jvi.00826-09 (2009).
28 Wise, H. M. *et al.* Identification of a novel splice variant form of the influenza A virus M2 ion channel with an antigenically distinct ectodomain. *PLoS Pathog* **8**, e1002998, doi:10.1371/journal.ppat.1002998 (2012).
29 Yamayoshi, S., Watanabe, M., Goto, H. & Kawaoka, Y. Identification of A Novel Viral Protein Expressed from the PB2 Segment of Influenza A Virus. *Journal of Virology*, doi:10.1128/jvi.02175-15 (2015).
30 Zamarin, D., Ortigoza, M. B. & Palese, P. Influenza A Virus PB1-F2 Protein Contributes to Viral Pathogenesis in Mice. *Journal of Virology* **80**, 7976-7983, doi:10.1128/jvi.00415-06 (2006).
31 Vasin, A. V. *et al.* Molecular mechanisms enhancing the proteome of influenza A viruses: an overview of recently discovered proteins. *Virus Res* **185**, 53-63, doi:10.1016/j.virusres.2014.03.015 (2014).
32 Noton, S. L. *et al.* Identification of the domains of the influenza A virus M1 matrix protein required for NP binding, oligomerization and incorporation into virions. *J Gen Virol* **88**, 2280-2290, doi:10.1099/vir.0.82809-0 (2007).
33 Schnell, J. R. & Chou, J. J. Structure and mechanism of the M2 proton channel of influenza A virus. *Nature* **451**, 591-595, doi:10.1038/nature06531 (2008).
34 Steinhauer, D. A. Role of hemagglutinin cleavage for the pathogenicity of influenza virus. *Virology* **258**, 1-20, doi:10.1006/viro.1999.9716 (1999).
35 Klenk, H. D., Rott, R., Orlich, M. & Blodorn, J. Activation of influenza A viruses by trypsin treatment. *Virology* **68**, 426-439 (1975).
36 Wagner, R., Matrosovich, M. & Klenk, H.-D. Functional balance between haemagglutinin and neuraminidase in influenza virus infections. *Reviews in Medical Virology* **12**, 159-166, doi:10.1002/rmv.352 (2002).
37 O'Neill, R. E., Talon, J. & Palese, P. The influenza virus NEP (NS2 protein) mediates the nuclear export of viral ribonucleoproteins. *The EMBO Journal* **17**, 288-296, doi:10.1093/emboj/17.1.288 (1998).
38 Yasuda, J., Nakada, S., Kato, A., Toyoda, T. & Ishihama, A. Molecular assembly of influenza virus: association of the NS2 protein with virion matrix. *Virology* **196**, 249-255, doi:10.1006/viro.1993.1473 (1993).
39 Hale, B. G., Randall, R. E., Ortin, J. & Jackson, D. The multifunctional NS1 protein of influenza A viruses. *J Gen Virol* **89**, 2359-2376, doi:10.1099/vir.0.2008/004606-0 (2008).
40 Gibbs, J. S., Malide, D., Hornung, F., Bennink, J. R. & Yewdell, J. W. The Influenza A Virus PB1-F2 Protein Targets the Inner Mitochondrial Membrane via a Predicted Basic Amphipathic Helix That Disrupts Mitochondrial Function. *Journal of Virology* **77**, 7214-7224, doi:10.1128/jvi.77.13.7214-7224.2003 (2003).
41 Rogers, G. N. *et al.* Single amino acid substitutions in influenza haemagglutinin change receptor binding specificity. *Nature* **304**, 76-78 (1983).
42 Lakadamyali, M., Rust, M. J. & Zhuang, X. Endocytosis of influenza viruses. *Microbes and Infection* **6**, 929-936, doi:https://doi.org/10.1016/j.micinf.2004.05.002 (2004).

43 Hamilton, B. S., Whittaker, G. R. & Daniel, S. Influenza virus-mediated membrane fusion: determinants of hemagglutinin fusogenic activity and experimental approaches for assessing virus fusion. *Viruses* **4**, 1144-1168, doi:10.3390/v4071144 (2012).

44 Li, S. *et al.* pH-Controlled two-step uncoating of influenza virus. *Biophysical journal* **106**, 1447-1456, doi:10.1016/j.bpj.2014.02.018 (2014).

45 Das, K., Aramini, J. M., Ma, L. C., Krug, R. M. & Arnold, E. Structures of influenza A proteins and insights into antiviral drug targets. *Nat Struct Mol Biol* **17**, 530-538, doi:10.1038/nsmb.1779 (2010).

46 Pielak, R. M. & Chou, J. J. Influenza M2 proton channels. *Biochimica et Biophysica Acta (BBA) - Biomembranes* **1808**, 522-529, doi:https://doi.org/10.1016/j.bbamem.2010.04.015 (2011).

47 Boulo, S., Akarsu, H., Ruigrok, R. W. H. & Baudin, F. Nuclear traffic of influenza virus proteins and ribonucleoprotein complexes. *Virus Research* **124**, 12-21, doi:https://doi.org/10.1016/j.virusres.2006.09.013 (2007).

48 Shimizu, T., Takizawa, N., Watanabe, K., Nagata, K. & Kobayashi, N. Crucial role of the influenza virus NS2 (NEP) C-terminal domain in M1 binding and nuclear export of vRNP. *FEBS letters* **585**, 41-46, doi:10.1016/j.febslet.2010.11.017 (2011).

49 Smith, G. L., Levin, J. Z., Palese, P. & Moss, B. Synthesis and cellular location of the ten influenza polypeptides individually expressed by recombinant vaccinia viruses. *Virology* **160**, 336-345 (1987).

50 Leser, G. P. & Lamb, R. A. Influenza virus assembly and budding in raft-derived microdomains: a quantitative analysis of the surface distribution of HA, NA and M2 proteins. *Virology* **342**, 215-227, doi:10.1016/j.virol.2005.09.049 (2005).

51 Rossman, J. S. & Lamb, R. A. Influenza virus assembly and budding. *Virology* **411**, 229-236, doi:https://doi.org/10.1016/j.virol.2010.12.003 (2011).

52 Manzoor, R., Igarashi, M. & Takada, A. Influenza A Virus M2 Protein: Roles from Ingress to Egress. *International Journal of Molecular Sciences* **18**, 2649, doi:10.3390/ijms18122649 (2017).

53 Severin, C. *et al.* The cap-binding site of influenza virus protein PB2 as a drug target. *Acta crystallographica. Section D, Structural biology* **72**, 245-253, doi:10.1107/s2059798316000085 (2016).

54 Perez, D. R. & Donis, R. O. Functional Analysis of PA Binding by Influenza A Virus PB1: Effects on Polymerase Activity and Viral Infectivity. *Journal of Virology* **75**, 8127-8136, doi:10.1128/JVI.75.17.8127-8136.2001 (2001).

55 Te Velthuis, A. J., Robb, N. C., Kapanidis, A. N. & Fodor, E. The role of the priming loop in Influenza A virus RNA synthesis. *Nature microbiology* **1**, doi:10.1038/nmicrobiol.2016.29 (2016).

56 Mark, G. E., Taylor, J. M., Broni, B. & Krug, R. M. Nuclear accumulation of influenza viral RNA transcripts and the effects of cycloheximide, actinomycin D, and alpha-amanitin. *J Virol* **29**, 744-752 (1979).

57 Reich, S. *et al.* Structural insight into cap-snatching and RNA synthesis by influenza polymerase. *Nature* **516**, 361-366, doi:10.1038/nature14009 (2014).

58 Kobayashi, M., Toyoda, T. & Ishihama, A. Influenza virus PB1 protein is the minimal and essential subunit of RNA polymerase. *Archives of virology* **141**, 525-539 (1996).

59 Bier, K., York, A. & Fodor, E. Cellular cap-binding proteins associate with influenza virus mRNAs. *J Gen Virol* **92**, 1627-1634, doi:10.1099/vir.0.029231-0 (2011).

60 Burgui, I., Yanguez, E., Sonenberg, N. & Nieto, A. Influenza virus mRNA translation revisited: is the eIF4E cap-binding factor required for viral mRNA translation? *J Virol* **81**, 12427-12438, doi:10.1128/jvi.01105-07 (2007).

61 Rodriguez, P., Perez-Morgado, M. I., Gonzalez, V. M., Martin, M. E. & Nieto, A. Inhibition of Influenza Virus Replication by DNA Aptamers Targeting a Cellular Component of Translation Initiation. *Molecular therapy. Nucleic acids* **5**, e308, doi:10.1038/mtna.2016.20 (2016).

62 Watanabe, K. *et al.* Hsc70 regulates the nuclear export but not the import of influenza viral RNP: A possible target for the development of anti-influenza virus drugs. *Drug Discov Ther* **2**, 77-84 (2008).

63 Fodor, E. The RNA polymerase of influenza a virus: mechanisms of viral transcription and replication. *Acta virologica* **57**, 113-122 (2013).

64 Naito, T., Momose, F., Kawaguchi, A. & Nagata, K. Involvement of Hsp90 in Assembly and Nuclear Import of Influenza Virus RNA Polymerase Subunits. *Journal of Virology* **81**, 1339-1349, doi:10.1128/jvi.01917-06 (2007).

65 Vreede, F. T., Jung, T. E. & Brownlee, G. G. Model suggesting that replication of influenza virus is regulated by stabilization of replicative intermediates. *J Virol* **78**, 9568-9572, doi:10.1128/jvi.78.17.9568-9572.2004 (2004).
66 Bentley, D. L. Coupling mRNA processing with transcription in time and space. *Nature reviews. Genetics* **15**, 163-175, doi:10.1038/nrg3662 (2014).
67 Kawaguchi, A. & Nagata, K. De novo replication of the influenza virus RNA genome is regulated by DNA replicative helicase, MCM. *Embo j* **26**, 4566-4575, doi:10.1038/sj.emboj.7601881 (2007).
68 Long, J. S. *et al.* Species difference in ANP32A underlies influenza A virus polymerase host restriction. *Nature* **529**, 101-104, doi:10.1038/nature16474 (2016).
69 Resa-Infante, P. *et al.* The host-dependent interaction of alpha-importins with influenza PB2 polymerase subunit is required for virus RNA replication. *PloS one* **3**, e3904, doi:10.1371/journal.pone.0003904 (2008).
70 Hatakeyama, D. *et al.* A novel functional site in the PB2 subunit of influenza A virus essential for acetyl-CoA interaction, RNA polymerase activity, and viral replication. *The Journal of biological chemistry* **289**, 24980-24994, doi:10.1074/jbc.M114.559708 (2014).
71 Min, J.-Y. *et al.* Mammalian Adaptation in the PB2 Gene of Avian H5N1 Influenza Virus. *Journal of Virology* **87**, 10884-10888, doi:10.1128/JVI.01016-13 (2013).
72 Graef, K. M. *et al.* The PB2 subunit of the influenza virus RNA polymerase affects virulence by interacting with the mitochondrial antiviral signaling protein and inhibiting expression of beta interferon. *J Virol* **84**, 8433-8445, doi:10.1128/jvi.00879-10 (2010).
73 Pflug, A., Guilligay, D., Reich, S. & Cusack, S. Structure of influenza A polymerase bound to the viral RNA promoter. *Nature* **516**, 355, doi:10.1038/nature14008 https://www.nature.com/articles/nature14008#supplementary-information (2014).
74 (OIE), W. o. f. a. h. Avian Influenza (Infection with Avian Influenza viruses). *https://www.oie.int/fileadmin/Home/eng/Health_standards/tahm/2.03.04_AI.pdf* (2015).
75 Alexander, D. J. A review of avian influenza in different bird species. *Veterinary Microbiology* **74**, 3-13, doi:https://doi.org/10.1016/S0378-1135(00)00160-7 (2000).
76 WHO. Avian and other zoonotic Influenza Fact sheet *http://www.who.int/mediacentre/factsheets/avian_influenza/en/* (2016).
77 Association, A. P. H. Control of Communicable Disease Manual 20th Edition. *APHA Press, Washington DC* (2015).
78 Li , Q. *et al.* Epidemiology of Human Infections with Avian Influenza A(H7N9) Virus in China. *New England Journal of Medicine* **370**, 520-532, doi:10.1056/NEJMoa1304617 (2014).
79 A/H5, T. W. C. o. t. W. H. O. C. o. H. I. Avian Influenza A (H5N1) Infection in Humans. *New England Journal of Medicine* **353**, 1374-1385, doi:10.1056/NEJMra052211 (2005).
80 WHO. Cumulative number of confirmed human cases for avian influenza A(H5N1) reported to WHO, 2003-2017. *http://www.who.int/influenza/human_animal_interface/2017_05_16_tableH5N1.pdf?ua=1* (2017).
81 WHO. H5N1 highly pathogenic avian influenza: Timeline of major events. *http://www.who.int/influenza/human_animal_interface/H5N1_avian_influenza_update20141204.pdf?ua=1* (2014).
82 WHO. Influenza at the human-animal interface. *http://www.who.int/influenza/human_animal_interface/Influenza_Summary_IRA_HA_interface_05_16_2017.pdf?ua=1* (2017).
83 Taubenberger, J. K. & Morens, D. M. 1918 Influenza: the mother of all pandemics. *Emerging infectious diseases* **12**, 15-22, doi:10.3201/eid1201.050979 (2006).
84 WHO. Influenza at the human-animal interface. Summary and assessment. *http://www.who.int/influenza/human_animal_interface/Influenza_Summary_IRA_HA_interface_05_16_2017.pdf?ua=1* (2017).
85 Ungchusak , K. *et al.* Probable Person-to-Person Transmission of Avian Influenza A (H5N1). *New England Journal of Medicine* **352**, 333-340, doi:10.1056/NEJMoa044021 (2005).
86 WHO. Frequently asked questions on human infection caused by the avian influenza A(H7N9) virus. *http://www.who.int/influenza/human_animal_interface/faq_H7N9/en/* (2014).

87 Herfst, S. *et al.* Airborne transmission of influenza A/H5N1 virus between ferrets. *Science* **336**, 1534-1541, doi:10.1126/science.1213362 (2012).
88 Varki, A. Sialic acids in human health and disease. *Trends in Molecular Medicine* **14**, 351-360, doi:10.1016/j.molmed.2008.06.002.
89 Ramos, I. *et al.* Effects of Receptor Binding Specificity of Avian Influenza Virus on the Human Innate Immune Response. *Journal of Virology* **85**, 4421-4431, doi:10.1128/JVI.02356-10 (2011).
90 Shinya, K. *et al.* Avian flu: influenza virus receptors in the human airway. *Nature* **440**, 435-436, doi:10.1038/440435a (2006).
91 Pillai, S. P. & Lee, C. W. Species and age related differences in the type and distribution of influenza virus receptors in different tissues of chickens, ducks and turkeys. *Virology journal* **7**, 5, doi:10.1186/1743-422x-7-5 (2010).
92 van Riel, D. *et al.* H5N1 Virus Attachment to Lower Respiratory Tract. *Science* **312**, 399, doi:10.1126/science.1125548 (2006).
93 Stevens, J., Blixt, O., Paulson, J. C. & Wilson, I. A. Glycan microarray technologies: tools to survey host specificity of influenza viruses. *Nat Rev Micro* **4**, 857-864 (2006).
94 Schrauwen, E. J. *et al.* Determinants of virulence of influenza A virus. *European journal of clinical microbiology & infectious diseases : official publication of the European Society of Clinical Microbiology* **33**, 479-490, doi:10.1007/s10096-013-1984-8 (2014).
95 Weinheimer, V. K. *et al.* Influenza A viruses target type II pneumocytes in the human lung. *The Journal of infectious diseases* **206**, 1685-1694, doi:10.1093/infdis/jis455 (2012).
96 de Jong, M. D. *et al.* Fatal avian influenza A (H5N1) in a child presenting with diarrhea followed by coma. *N Engl J Med* **352**, 686-691, doi:10.1056/NEJMoa044307 (2005).
97 de Jong, M. D. *et al.* Fatal outcome of human influenza A (H5N1) is associated with high viral load and hypercytokinemia. *Nat Med* **12**, 1203-1207, doi:10.1038/nm1477 (2006).
98 Horimoto, T. & Kawaoka, Y. Reverse genetics provides direct evidence for a correlation of hemagglutinin cleavability and virulence of an avian influenza A virus. *Journal of Virology* **68**, 3120-3128 (1994).
99 Chen, J. *et al.* Structure of the Hemagglutinin Precursor Cleavage Site, a Determinant of Influenza Pathogenicity and the Origin of the Labile Conformation. *Cell* **95**, 409-417, doi:10.1016/S0092-8674(00)81771-7.
100 Klenk, H.-D. & Garten, W. Host cell proteases controlling virus pathogenicity. *Trends in Microbiology* **2**, 39-43, doi:http://dx.doi.org/10.1016/0966-842X(94)90123-6 (1994).
101 Bertram, S., Glowacka, I., Steffen, I., Kühl, A. & Pöhlmann, S. Novel insights into proteolytic cleavage of influenza virus hemagglutinin. *Reviews in Medical Virology* **20**, 298-310, doi:10.1002/rmv.657 (2010).
102 Stieneke-Grober, A. *et al.* Influenza virus hemagglutinin with multibasic cleavage site is activated by furin, a subtilisin-like endoprotease. *Embo j* **11**, 2407-2414 (1992).
103 Schrauwen, E. J. A. *et al.* Insertion of a multibasic cleavage site in the haemagglutinin of human influenza H3N2 virus does not increase pathogenicity in ferrets. *The Journal of General Virology* **92**, 1410-1415, doi:10.1099/vir.0.030379-0 (2011).
104 Schrauwen, E. J. A. *et al.* The Multibasic Cleavage Site in H5N1 Virus Is Critical for Systemic Spread along the Olfactory and Hematogenous Routes in Ferrets. *Journal of Virology* **86**, 3975-3984, doi:10.1128/jvi.06828-11 (2012).
105 Korteweg, C. & Gu, J. Pathology, molecular biology, and pathogenesis of avian influenza A (H5N1) infection in humans. *The American journal of pathology* **172**, 1155-1170, doi:10.2353/ajpath.2008.070791 (2008).
106 Xu, C. *et al.* Amino acids 473V and 598P of PB1 from an avian-origin influenza A virus contribute to polymerase activity, especially in mammalian cells. *Journal of General Virology* **93**, 531-540, doi:doi:10.1099/vir.0.036434-0 (2012).
107 Gabriel, G., Czudai-Matwich, V. & Klenk, H. D. Adaptive mutations in the H5N1 polymerase complex. *Virus Res* **178**, 53-62, doi:10.1016/j.virusres.2013.05.010 (2013).
108 Gabriel, G. *et al.* The viral polymerase mediates adaptation of an avian influenza virus to a mammalian host. *Proc Natl Acad Sci U S A* **102**, 18590-18595, doi:10.1073/pnas.0507415102 (2005).
109 Hatta, M. *et al.* Growth of H5N1 influenza A viruses in the upper respiratory tracts of mice. *PLoS Pathog* **3**, 1374-1379, doi:10.1371/journal.ppat.0030133 (2007).

110 Hatta, M., Gao, P., Halfmann, P. & Kawaoka, Y. Molecular Basis for High Virulence of Hong Kong H5N1 Influenza A Viruses. *Science* **293**, 1840-1842, doi:10.1126/science.1062882 (2001).

111 Chokephaibulkit, K. *et al.* A child with avian influenza A (H5N1) infection. *The Pediatric infectious disease journal* **24**, 162-166 (2005).

112 Manz, B., Brunotte, L., Reuther, P. & Schwemmle, M. Adaptive mutations in NEP compensate for defective H5N1 RNA replication in cultured human cells. *Nature communications* **3**, 802, doi:10.1038/ncomms1804 (2012).

113 Lindquist, S. & Craig, E. A. The heat-shock proteins. *Annual review of genetics* **22**, 631-677, doi:10.1146/annurev.ge.22.120188.003215 (1988).

114 Whitley, D., Goldberg, S. P. & Jordan, W. D. Heat shock proteins: A review of the molecular chaperones. *Journal of Vascular Surgery* **29**, 748-751, doi:https://doi.org/10.1016/S0741-5214(99)70329-0 (1999).

115 Park, C.-J. & Seo, Y.-S. Heat Shock Proteins: A Review of the Molecular Chaperones for Plant Immunity. *The Plant Pathology Journal* **31**, 323-333, doi:10.5423/PPJ.RW.08.2015.0150 (2015).

116 Bakthisaran, R., Tangirala, R. & Rao, C. M. Small heat shock proteins: Role in cellular functions and pathology. *Biochimica et Biophysica Acta (BBA) - Proteins and Proteomics* **1854**, 291-319, doi:https://doi.org/10.1016/j.bbapap.2014.12.019 (2015).

117 Saibil, H. Chaperone machines for protein folding, unfolding and disaggregation. *Nature reviews. Molecular cell biology* **14**, 630-642, doi:10.1038/nrm3658 (2013).

118 Liu, T., Daniels, C. K. & Cao, S. Comprehensive review on the HSC70 functions, interactions with related molecules and involvement in clinical diseases and therapeutic potential. *Pharmacol Ther* **136**, 354-374, doi:10.1016/j.pharmthera.2012.08.014 (2012).

119 Stricher, F., Macri, C., Ruff, M. & Muller, S. HSPA8/HSC70 chaperone protein: structure, function, and chemical targeting. *Autophagy* **9**, 1937-1954, doi:10.4161/auto.26448 (2013).

120 Tzankov, S., Wong, M. J., Shi, K., Nassif, C. & Young, J. C. Functional divergence between co-chaperones of Hsc70. *The Journal of biological chemistry* **283**, 27100-27109, doi:10.1074/jbc.M803923200 (2008).

121 Chappell, T. G. *et al.* Uncoating ATPase is a member of the 70 kilodalton family of stress proteins. *Cell* **45**, 3-13 (1986).

122 Livingston, C. M., DeLuca, N. A., Wilkinson, D. E. & Weller, S. K. Oligomerization of ICP4 and rearrangement of heat shock proteins may be important for herpes simplex virus type 1 prereplicative site formation. *J Virol* **82**, 6324-6336, doi:10.1128/JVI.00455-08 (2008).

123 Ren, J., Ding, T., Zhang, W., Song, J. & Ma, W. Does Japanese encephalitis virus share the same cellular receptor with other mosquito-borne flaviviruses on the C6/36 mosquito cells? *Virology journal* **4**, 83, doi:10.1186/1743-422x-4-83 (2007).

124 Dufresne, P. J. *et al.* Heat shock 70 protein interaction with Turnip mosaic virus RNA-dependent RNA polymerase within virus-induced membrane vesicles. *Virology* **374**, 217-227, doi:https://doi.org/10.1016/j.virol.2007.12.014 (2008).

125 Watanabe, K. *et al.* Identification of Hsc70 as an influenza virus matrix protein (M1) binding factor involved in the virus life cycle. *FEBS letters* **580**, 5785-5790, doi:10.1016/j.febslet.2006.09.040 (2006).

126 Watanabe, K. *et al.* Nuclear export of the influenza virus ribonucleoprotein complex: Interaction of Hsc70 with viral proteins M1 and NS2. *FEBS Open Bio* **4**, 683-688, doi:10.1016/j.fob.2014.07.004 (2014).

127 Bortz, E. *et al.* Host- and Strain-Specific Regulation of Influenza Virus Polymerase Activity by Interacting Cellular Proteins. *mBio* **2**, e00151-00111, doi:10.1128/mBio.00151-11 (2011).

128 Wilkins, M. R. *et al.* From proteins to proteomes: large scale protein identification by two-dimensional electrophoresis and amino acid analysis. *Bio/technology (Nature Publishing Company)* **14**, 61-65 (1996).

129 Han, X., Aslanian, A. & Yates, J. R. Mass Spectrometry for Proteomics. *Current opinion in chemical biology* **12**, 483-490, doi:10.1016/j.cbpa.2008.07.024 (2008).

130 Domon, B. & Aebersold, R. Mass spectrometry and protein analysis. *Science* **312**, 212-217, doi:10.1126/science.1124619 (2006).

131 Hu, Q. *et al.* The Orbitrap: a new mass spectrometer. *Journal of mass spectrometry : JMS* **40**, 430-443, doi:10.1002/jms.856 (2005).

132 Cox, J. MaxQuant. *http://www.biochem.mpg.de/5111795/maxquant*.

133 Elias, J. E. & Gygi, S. P. Target-decoy search strategy for increased confidence in large-scale protein identifications by mass spectrometry. *Nature methods* **4**, 207-214, doi:10.1038/nmeth1019 (2007).
134 Ong, S. E. *et al.* Stable isotope labeling by amino acids in cell culture, SILAC, as a simple and accurate approach to expression proteomics. *Mol Cell Proteomics* **1**, 376-386 (2002).
135 Zhu, H., Pan, S., Gu, S., Bradbury, E. M. & Chen, X. Amino acid residue specific stable isotope labeling for quantitative proteomics. *Rapid communications in mass spectrometry : RCM* **16**, 2115-2123, doi:10.1002/rcm.831 (2002).
136 Mann, M. Functional and quantitative proteomics using SILAC. *Nat Rev Mol Cell Biol* **7**, 952-958, doi:10.1038/nrm2067 (2006).
137 Nilsson, B. E., te Velthuis, A. J. W. & Fodor, E. Role of the PB2 627 Domain in Influenza A Virus Polymerase Function. *Journal of Virology* **91**, e02467-02416, doi:10.1128/JVI.02467-16 (2017).
138 Bradel-Tretheway, B. G. *et al.* Comprehensive proteomic analysis of influenza virus polymerase complex reveals a novel association with mitochondrial proteins and RNA polymerase accessory factors. *J Virol* **85**, 8569-8581, doi:10.1128/jvi.00496-11 (2011).
139 Heaton, Nicholas S. *et al.* Targeting Viral Proteostasis Limits Influenza Virus, HIV, and Dengue Virus Infection. *Immunity* **44**, 46-58, doi:http://dx.doi.org/10.1016/j.immuni.2015.12.017 (2016).
140 Wang, L. *et al.* Comparative influenza protein interactomes identify the role of plakophilin 2 in virus restriction. *Nature communications* **8**, 13876, doi:10.1038/ncomms13876 (2017).
141 Watanabe, T. *et al.* Influenza virus-host interactome screen as a platform for antiviral drug development. *Cell host & microbe* **16**, 795-805, doi:10.1016/j.chom.2014.11.002 (2014).
142 York, A., Hutchinson, E. C. & Fodor, E. Interactome analysis of the influenza A virus transcription/replication machinery identifies protein phosphatase 6 as a cellular factor required for efficient virus replication. *J Virol* **88**, 13284-13299, doi:10.1128/jvi.01813-14 (2014).
143 Fislova, T., Thomas, B., Graef, K. M. & Fodor, E. Association of the influenza virus RNA polymerase subunit PB2 with the host chaperonin CCT. *J Virol* **84**, 8691-8699, doi:10.1128/jvi.00813-10 (2010).
144 Jorba, N. *et al.* Analysis of the interaction of influenza virus polymerase complex with human cell factors. *Proteomics* **8**, 2077-2088, doi:10.1002/pmic.200700508 (2008).
145 Hoffmann, E., Neumann, G., Kawaoka, Y., Hobom, G. & Webster, R. G. A DNA transfection system for generation of influenza A virus from eight plasmids. *Proceedings of the National Academy of Sciences of the United States of America* **97**, 6108-6113 (2000).
146 Killian, M. L. Hemagglutination assay for the avian influenza virus. *Methods in molecular biology (Clifton, N.J.)* **436**, 47-52, doi:10.1007/978-1-59745-279-3_7 (2008).
147 Rameix-Welti, M.-A., Tomoiu, A., Dos Santos Afonso, E., van der Werf, S. & Naffakh, N. Avian Influenza A Virus Polymerase Association with Nucleoprotein, but Not Polymerase Assembly, Is Impaired in Human Cells during the Course of Infection. *Journal of Virology* **83**, 1320-1331, doi:10.1128/jvi.00977-08 (2009).
148 Ong, S. E. & Mann, M. A practical recipe for stable isotope labeling by amino acids in cell culture (SILAC). *Nature protocols* **1**, 2650-2660, doi:10.1038/nprot.2006.427 (2006).
149 Meyer, K. & Selbach, M. Quantitative affinity purification mass spectrometry: a versatile technology to study protein-protein interactions. *Frontiers in genetics* **6**, 237, doi:10.3389/fgene.2015.00237 (2015).
150 Cox, J. & Mann, M. MaxQuant enables high peptide identification rates, individualized p.p.b.-range mass accuracies and proteome-wide protein quantification. *Nat Biotech* **26**, 1367-1372, doi:http://www.nature.com/nbt/journal/v26/n12/suppinfo/nbt.1511_S1.html (2008).
151 Dufresne, P. J. *et al.* Heat shock 70 protein interaction with Turnip mosaic virus RNA-dependent RNA polymerase within virus-induced membrane vesicles. *Virology* **374**, 217-227, doi:10.1016/j.virol.2007.12.014 (2008).
152 Kodiha, M., Chu, A., Lazrak, O. & Stochaj, U. Stress inhibits nucleocytoplasmic shuttling of heat shock protein hsc70. *American journal of physiology. Cell physiology* **289**, C1034-1041, doi:10.1152/ajpcell.00590.2004 (2005).

153 Radigan, K. A., Misharin, A. V., Chi, M. & Budinger, G. R. S. Modeling human influenza infection in the laboratory. *Infection and Drug Resistance* **8**, 311-320 (2015).
154 Databse, I. R. Influenza Strain Details for A/Panama/2007/1999(H3N2). *https://www.fludb.org/brc/fluStrainDetails.spg?strainName=A/Panama/2007/1999(H3N2)&decorator=influenza* (2017).
155 Manz, B., Schwemmle, M. & Brunotte, L. Adaptation of avian influenza A virus polymerase in mammals to overcome the host species barrier. *J Virol* **87**, 7200-7209, doi:10.1128/JVI.00980-13 (2013).
156 Gabriel, G. *et al.* Differential use of importin-α isoforms governs cell tropism and host adaptation of influenza virus. **2**, 156, doi:10.1038/ncomms1158 https://www.nature.com/articles/ncomms1158#supplementary-information (2011).
157 Matthaei, M., Budt, M. & Wolff, T. Highly Pathogenic H5N1 Influenza A Virus Strains Provoke Heterogeneous IFN-α/β Responses That Distinctively Affect Viral Propagation in Human Cells. *PloS one* **8**, e56659, doi:10.1371/journal.pone.0056659 (2013).
158 McCown, M. F. & Pekosz, A. The influenza A virus M2 cytoplasmic tail is required for infectious virus production and efficient genome packaging. *J Virol* **79**, 3595-3605, doi:10.1128/jvi.79.6.3595-3605.2005 (2005).
159 Zhang, J., Leser, G. P., Pekosz, A. & Lamb, R. A. The cytoplasmic tails of the influenza virus spike glycoproteins are required for normal genome packaging. *Virology* **269**, 325-334, doi:10.1006/viro.2000.0228 (2000).
160 Akarsu, H. *et al.* Crystal structure of the M1 protein-binding domain of the influenza A virus nuclear export protein (NEP/NS2). *The EMBO Journal* **22**, 4646-4655, doi:10.1093/emboj/cdg449 (2003).
161 Robb, N. C. *et al.* The Influenza A Virus NS1 Protein Interacts with the Nucleoprotein of Viral Ribonucleoprotein Complexes. *Journal of Virology* **85**, 5228-5231, doi:10.1128/JVI.02562-10 (2011).
162 Konig, R. & Stertz, S. Recent strategies and progress in identifying host factors involved in virus replication. *Current opinion in microbiology* **26**, 79-88, doi:10.1016/j.mib.2015.06.001 (2015).
163 Tripathi, S. *et al.* Meta- and Orthogonal Integration of Influenza "OMICs" Data Defines a Role for UBR4 in Virus Budding. *Cell host & microbe* **18**, 723-735, doi:10.1016/j.chom.2015.11.002 (2015).
164 Zamarin, D., García-Sastre, A., Xiao, X., Wang, R. & Palese, P. Influenza Virus PB1-F2 Protein Induces Cell Death through Mitochondrial ANT3 and VDAC1. *PLOS Pathogens* **1**, e4, doi:10.1371/journal.ppat.0010004 (2005).
165 Qin, L., Guo, J., Zheng, Q. & Zhang, H. BAG2 structure, function and involvement in disease. *Cellular & molecular biology letters* **21**, 18, doi:10.1186/s11658-016-0020-2 (2016).
166 König, J. *et al.* iCLIP reveals the function of hnRNP particles in splicing at individual nucleotide resolution. *Nature structural & molecular biology* **17**, 909-915, doi:10.1038/nsmb.1838 (2010).
167 Fournier, G. *et al.* Recruitment of RED-SMU1 complex by Influenza A Virus RNA polymerase to control Viral mRNA splicing. *PLoS Pathog* **10**, e1004164, doi:10.1371/journal.ppat.1004164 (2014).
168 Dechtawewat, T. *et al.* Role of human heterogeneous nuclear ribonucleoprotein C1/C2 in dengue virus replication. *Virology journal* **12**, 14, doi:10.1186/s12985-014-0219-7 (2015).
169 Hou, J., Lam, F., Proud, C. & Wang, S. *Targeting Mnks for Cancer Therapy*. Vol. 3 (2012).
170 Wells, S. E., Hillner, P. E., Vale, R. D. & Sachs, A. B. Circularization of mRNA by eukaryotic translation initiation factors. *Molecular cell* **2**, 135-140 (1998).
171 Archer, S. K., Shirokikh, N. E., Hallwirth, C. V., Beilharz, T. H. & Preiss, T. Probing the closed-loop model of mRNA translation in living cells. *RNA biology* **12**, 248-254, doi:10.1080/15476286.2015.1017242 (2015).
172 Burgui, I., Aragon, T., Ortin, J. & Nieto, A. PABP1 and eIF4GI associate with influenza virus NS1 protein in viral mRNA translation initiation complexes. *J Gen Virol* **84**, 3263-3274, doi:10.1099/vir.0.19487-0 (2003).
173 Salvatore, M. *et al.* Effects of influenza A virus NS1 protein on protein expression: the NS1 protein enhances translation and is not required for shutoff of host protein synthesis. *J Virol* **76**, 1206-1212 (2002).

174 Yángüez, E., Rodriguez, P., Goodfellow, I. & Nieto, A. Influenza virus polymerase confers independence of the cellular cap-binding factor eIF4E for viral mRNA translation. *Virology* **422**, 297-307, doi:10.1016/j.virol.2011.10.028 (2012).
175 Feigenblum, D. & Schneider, R. J. Modification of eukaryotic initiation factor 4F during infection by influenza virus. *Journal of Virology* **67**, 3027-3035 (1993).
176 Hosoda, N., Lejeune, F. & Maquat, L. E. Evidence that Poly(A) Binding Protein C1 Binds Nuclear Pre-mRNA Poly(A) Tails. *Molecular and Cellular Biology* **26**, 3085-3097, doi:10.1128/mcb.26.8.3085-3097.2006 (2006).
177 Lemay, J. F., Lemieux, C., St-Andre, O. & Bachand, F. Crossing the borders: poly(A)-binding proteins working on both sides of the fence. *RNA biology* **7**, 291-295 (2010).
178 Momose, F. *et al.* Cellular Splicing Factor RAF-2p48/NPI-5/BAT1/UAP56 Interacts with the Influenza Virus Nucleoprotein and Enhances Viral RNA Synthesis. *Journal of Virology* **75**, 1899-1908, doi:10.1128/JVI.75.4.1899-1908.2001 (2001).
179 Haas, M. The Na-K-Cl cotransporters. *The American journal of physiology* **267**, C869-885, doi:10.1152/ajpcell.1994.267.4.C869 (1994).
180 Hoffmann, H. H., Palese, P. & Shaw, M. L. Modulation of influenza virus replication by alteration of sodium ion transport and protein kinase C activity. *Antiviral research* **80**, 124-134, doi:10.1016/j.antiviral.2008.05.008 (2008).
181 Li, G., Zhang, J., Tong, X., Liu, W. & Ye, X. Heat Shock Protein 70 Inhibits the Activity of Influenza A Virus Ribonucleoprotein and Blocks the Replication of Virus In Vitro and In Vivo. *PloS one* **6**, e16546, doi:10.1371/journal.pone.0016546 (2011).
182 Beckmann, R. P., Mizzen, L. E. & Welch, W. J. Interaction of Hsp 70 with newly synthesized proteins: implications for protein folding and assembly. *Science* **248**, 850-854 (1990).
183 Bercovich, B. *et al.* Ubiquitin-dependent degradation of certain protein substrates in vitro requires the molecular chaperone Hsc70. *The Journal of biological chemistry* **272**, 9002-9010 (1997).
184 Kose, S., Furuta, M., Koike, M., Yoneda, Y. & Imamoto, N. The 70-kD heat shock cognate protein (hsc70) facilitates the nuclear export of the import receptors. *The Journal of cell biology* **171**, 19-25, doi:10.1083/jcb.200506074 (2005).
185 Kabbage, M. & Dickman, M. B. The BAG proteins: a ubiquitous family of chaperone regulators. *Cellular and molecular life sciences : CMLS* **65**, 1390-1402, doi:10.1007/s00018-008-7535-2 (2008).
186 Takayama, S., Xie, Z. & Reed, J. C. An evolutionarily conserved family of Hsp70/Hsc70 molecular chaperone regulators. *The Journal of biological chemistry* **274**, 781-786 (1999).
187 Wang, H. & Jiang, C. Influenza A virus H5N1 entry into host cells is through clathrin-dependent endocytosis. *Science in China. Series C, Life sciences* **52**, 464-469, doi:10.1007/s11427-009-0061-0 (2009).
188 Fislová, T., Thomas, B., Graef, K. M. & Fodor, E. Association of the Influenza Virus RNA Polymerase Subunit PB2 with the Host Chaperonin CCT. *Journal of Virology* **84**, 8691-8699, doi:10.1128/jvi.00813-10 (2010).
189 Hatta, Y. *et al.* Viral Replication Rate Regulates Clinical Outcome and CD8 T Cell Responses during Highly Pathogenic H5N1 Influenza Virus Infection in Mice. *PLoS Pathogens* **6**, e1001139, doi:10.1371/journal.ppat.1001139 (2010).

Supplementary information

Table S.1. Cellular protein groups identified in the MS screen with a p-value of < 0.05 and a t-test difference of > 0. They represent protein groups that are significantly changed and are more abundant in A/Pan/99-PB2-Strep and/or A/Thai/04-PB2-Strep samples compared to the A/Pan/99-WT control.

№	Gene	Statistically significant and t-test difference of > 0 in
1	ABCC1	A/Pan/99-PB2-Strep and A/Thai/04-PB2-Strep
2	ABCC3	A/Thai/04-PB2-Strep
3	ACAA1	A/Pan/99-PB2-Strep and A/Thai/04-PB2-Strep
4	ACAA2	A/Thai/04-PB2-Strep
5	ACACA	A/Pan/99-PB2-Strep and A/Thai/04-PB2-Strep
6	ACADM	A/Pan/99-PB2-Strep and A/Thai/04-PB2-Strep
7	ACAT1	A/Thai/04-PB2-Strep
8	ACO1	A/Pan/99-PB2-Strep and A/Thai/04-PB2-Strep
9	ACO2	A/Pan/99-PB2-Strep and A/Thai/04-PB2-Strep
10	ACOT1;ACOT2	A/Thai/04-PB2-Strep
11	ACOT9	A/Thai/04-PB2-Strep
12	ACOX1	A/Pan/99-PB2-Strep and A/Thai/04-PB2-Strep
13	AGFG1	A/Pan/99-PB2-Strep
14	AGL	A/Pan/99-PB2-Strep
15	AGR2	A/Pan/99-PB2-Strep and A/Thai/04-PB2-Strep
16	AIFM1	A/Thai/04-PB2-Strep
17	AK2	A/Thai/04-PB2-Strep
18	AKR1A1	A/Pan/99-PB2-Strep
19	AKR1B1	A/Pan/99-PB2-Strep
20	AKR1B10	A/Pan/99-PB2-Strep and A/Thai/04-PB2-Strep
21	AKR1C2	A/Pan/99-PB2-Strep
22	AKR1D1	A/Pan/99-PB2-Strep and A/Thai/04-PB2-Strep
23	ALDH18A1	A/Thai/04-PB2-Strep
24	ALDH1A1	A/Pan/99-PB2-Strep
25	ALDH1B1	A/Pan/99-PB2-Strep and A/Thai/04-PB2-Strep
26	ALDH2	A/Thai/04-PB2-Strep
27	ALDH3A1	A/Pan/99-PB2-Strep and A/Thai/04-PB2-Strep
28	ALDH3A2	A/Thai/04-PB2-Strep
29	ANP32A	A/Thai/04-PB2-Strep
30	ANP32B	A/Pan/99-PB2-Strep and A/Thai/04-PB2-Strep
31	ANXA1	A/Pan/99-PB2-Strep
32	ANXA4	A/Pan/99-PB2-Strep and A/Thai/04-PB2-Strep
33	ANXA5	A/Pan/99-PB2-Strep
34	ANXA6	A/Pan/99-PB2-Strep
35	APEH	A/Pan/99-PB2-Strep
36	APOBEC3C	A/Pan/99-PB2-Strep
37	AQR	A/Thai/04-PB2-Strep

№	Gene	Statistically significant and t-test difference of > 0 in
38	ARF1;ARF3	A/Pan/99-PB2-Strep
39	ARF4	A/Pan/99-PB2-Strep
40	ARL1	A/Thai/04-PB2-Strep
41	ARPC5	A/Pan/99-PB2-Strep
42	ASPH	A/Thai/04-PB2-Strep
43	ATP2A2	A/Thai/04-PB2-Strep
44	ATP2B1	A/Pan/99-PB2-Strep and A/Thai/04-PB2-Strep
45	ATP5A1	A/Thai/04-PB2-Strep
46	ATP5B	A/Thai/04-PB2-Strep
47	ATP5C1	A/Thai/04-PB2-Strep
48	ATP5D	A/Thai/04-PB2-Strep
49	ATP5F1	A/Thai/04-PB2-Strep
50	ATP5O	A/Thai/04-PB2-Strep
51	BAG2	A/Pan/99-PB2-Strep and A/Thai/04-PB2-Strep
52	BCAP31	A/Thai/04-PB2-Strep
53	BLVRB	A/Pan/99-PB2-Strep
54	BPHL	A/Thai/04-PB2-Strep
55	C19orf10	A/Thai/04-PB2-Strep
56	C1QBP	A/Thai/04-PB2-Strep
57	C21orf33	A/Thai/04-PB2-Strep
58	CALM1;CALM2	A/Pan/99-PB2-Strep
59	CALR	A/Thai/04-PB2-Strep
60	CALU	A/Thai/04-PB2-Strep
61	CAND1	A/Pan/99-PB2-Strep
62	CANX	A/Thai/04-PB2-Strep
63	CAPG	A/Pan/99-PB2-Strep and A/Thai/04-PB2-Strep
64	CARS	A/Pan/99-PB2-Strep
65	CAST	A/Pan/99-PB2-Strep and A/Thai/04-PB2-Strep
66	CBR1	A/Pan/99-PB2-Strep
67	CBR3	A/Pan/99-PB2-Strep
68	CBR4	A/Thai/04-PB2-Strep
69	CBX3	A/Thai/04-PB2-Strep
70	CCDC58	A/Thai/04-PB2-Strep
71	CECR5	A/Thai/04-PB2-Strep
72	CKMT1A; CKMT1B	A/Pan/99-PB2-Strep and A/Thai/04-PB2-Strep
73	CLTC	A/Pan/99-PB2-Strep
74	CMAS	A/Thai/04-PB2-Strep
75	CMBL	A/Pan/99-PB2-Strep
76	CMPK1	A/Pan/99-PB2-Strep
77	COPA	A/Pan/99-PB2-Strep
78	COPS4	A/Thai/04-PB2-Strep
79	COX4I1	A/Thai/04-PB2-Strep
80	CPD	A/Thai/04-PB2-Strep
81	CPS1	A/Pan/99-PB2-Strep and A/Thai/04-PB2-Strep
82	CRAT	A/Pan/99-PB2-Strep and A/Thai/04-PB2-Strep

№	Gene	Statistically significant and t-test difference of > 0 in
83	CRIP2	A/Pan/99-PB2-Strep and A/Thai/04-PB2-Strep
84	CROCC	A/Pan/99-PB2-Strep
85	CRYZ	A/Pan/99-PB2-Strep and A/Thai/04-PB2-Strep
86	CS	A/Thai/04-PB2-Strep
87	CST3	A/Thai/04-PB2-Strep
88	CTSA	A/Pan/99-PB2-Strep and A/Thai/04-PB2-Strep
89	CTSB	A/Thai/04-PB2-Strep
90	CTSC	A/Thai/04-PB2-Strep
91	CTSC	A/Pan/99-PB2-Strep and A/Thai/04-PB2-Strep
92	CTSZ	A/Thai/04-PB2-Strep
93	CYB5B	A/Thai/04-PB2-Strep
94	CYC1	A/Thai/04-PB2-Strep
95	CYCS	A/Thai/04-PB2-Strep
96	CYFIP2	A/Pan/99-PB2-Strep
97	DAP3	A/Thai/04-PB2-Strep
98	DBT	A/Thai/04-PB2-Strep
99	DDB1	A/Thai/04-PB2-Strep
100	DDOST	A/Thai/04-PB2-Strep
101	DDX17	A/Thai/04-PB2-Strep
102	DDX23	A/Thai/04-PB2-Strep
103	DDX5	A/Thai/04-PB2-Strep
104	DECR1	A/Thai/04-PB2-Strep
105	DECR2	A/Thai/04-PB2-Strep
106	DEK	A/Thai/04-PB2-Strep
107	DHCR7	A/Pan/99-PB2-Strep and A/Thai/04-PB2-Strep
108	DHTKD1	A/Thai/04-PB2-Strep
109	DHX15	A/Pan/99-PB2-Strep and A/Thai/04-PB2-Strep
110	DHX9	A/Thai/04-PB2-Strep
111	DIABLO	A/Thai/04-PB2-Strep
112	DIAPH1	A/Pan/99-PB2-Strep
113	DLD	A/Thai/04-PB2-Strep
114	DLST	A/Thai/04-PB2-Strep
115	DNAJB11	A/Thai/04-PB2-Strep
116	DTD2	A/Pan/99-PB2-Strep
117	DYNC1H1	A/Pan/99-PB2-Strep
118	ECH1	A/Pan/99-PB2-Strep and A/Thai/04-PB2-Strep
119	ECHS1	A/Thai/04-PB2-Strep
120	ECI1;DCI	A/Thai/04-PB2-Strep
121	EFTUD2	A/Thai/04-PB2-Strep
122	EML4	A/Pan/99-PB2-Strep
123	EPDR1	A/Pan/99-PB2-Strep and A/Thai/04-PB2-Strep
124	EPHX1	A/Pan/99-PB2-Strep and A/Thai/04-PB2-Strep
125	ERP29	A/Thai/04-PB2-Strep
126	ERP44	A/Thai/04-PB2-Strep
127	ESYT2	A/Pan/99-PB2-Strep

№	Gene	Statistically significant and t-test difference of > 0 in
128	ETFA	A/Thai/04-PB2-Strep
129	ETFB	A/Thai/04-PB2-Strep
130	ETHE1	A/Thai/04-PB2-Strep
131	EZR	A/Pan/99-PB2-Strep
132	FAH	A/Pan/99-PB2-Strep
133	FAM21C;FAM21A	A/Pan/99-PB2-Strep
134	FARSB	A/Pan/99-PB2-Strep
135	FASN	A/Pan/99-PB2-Strep
136	FBL	A/Thai/04-PB2-Strep
137	FH	A/Thai/04-PB2-Strep
138	FIS1	A/Thai/04-PB2-Strep
139	FKBP3	A/Pan/99-PB2-Strep
140	FN1	A/Pan/99-PB2-Strep and A/Thai/04-PB2-Strep
141	FTH1	A/Thai/04-PB2-Strep
142	FTL	A/Thai/04-PB2-Strep
143	G6PD	A/Pan/99-PB2-Strep
144	GAA	A/Pan/99-PB2-Strep and A/Thai/04-PB2-Strep
145	GALM	A/Pan/99-PB2-Strep
146	GCLM	A/Pan/99-PB2-Strep
147	GGH	A/Pan/99-PB2-Strep and A/Thai/04-PB2-Strep
148	GLA	A/Thai/04-PB2-Strep
149	GLB1	A/Pan/99-PB2-Strep and A/Thai/04-PB2-Strep
150	GLUD1;GLUD2	A/Thai/04-PB2-Strep
151	GOLGA3	A/Pan/99-PB2-Strep
152	GOT2	A/Thai/04-PB2-Strep
153	GPC1	A/Thai/04-PB2-Strep
154	GRHPR	A/Pan/99-PB2-Strep and A/Thai/04-PB2-Strep
155	GSS	A/Pan/99-PB2-Strep
156	GSTK1	A/Pan/99-PB2-Strep
157	GTF2I	A/Thai/04-PB2-Strep
158	GTF3C1	A/Thai/04-PB2-Strep
159	H3F3B	A/Pan/99-PB2-Strep and A/Thai/04-PB2-Strep
160	HADH	A/Thai/04-PB2-Strep
161	HADHA	A/Pan/99-PB2-Strep and A/Thai/04-PB2-Strep
162	HADHB	A/Pan/99-PB2-Strep and A/Thai/04-PB2-Strep
163	HEXA	A/Thai/04-PB2-Strep
164	HEXB	A/Thai/04-PB2-Strep
165	HIBADH	A/Thai/04-PB2-Strep
166	HIBCH	A/Pan/99-PB2-Strep and A/Thai/04-PB2-Strep
167	HINT2	A/Thai/04-PB2-Strep
168	HIST1H2AJ	A/Thai/04-PB2-Strep
169	HIST1H2BL	A/Pan/99-PB2-Strep and A/Thai/04-PB2-Strep
170	HIST1H4A	A/Pan/99-PB2-Strep and A/Thai/04-PB2-Strep
171	HK1	A/Pan/99-PB2-Strep and A/Thai/04-PB2-Strep
172	HMGN1	A/Thai/04-PB2-Strep

№	Gene	Statistically significant and t-test difference of > 0 in
173	HMGN2	A/Thai/04-PB2-Strep
174	HNRNPA1;L2	A/Thai/04-PB2-Strep
175	HNRNPC	A/Thai/04-PB2-Strep
176	HNRNPM	A/Thai/04-PB2-Strep
177	HNRNPU	A/Thai/04-PB2-Strep
178	HNRNPUL1	A/Thai/04-PB2-Strep
179	HNRNPUL2	A/Thai/04-PB2-Strep
180	HSD17B10	A/Thai/04-PB2-Strep
181	HSD17B4	A/Thai/04-PB2-Strep
182	HSD17B8	A/Pan/99-PB2-Strep and A/Thai/04-PB2-Strep
183	HSP90B1	A/Thai/04-PB2-Strep
184	HSPA1A; HSPA1B	A/Thai/04-PB2-Strep
185	HSPA2	A/Pan/99-PB2-Strep and A/Thai/04-PB2-Strep
186	HSPA4	A/Thai/04-PB2-Strep
187	HSPA5	A/Pan/99-PB2-Strep and A/Thai/04-PB2-Strep
188	HSPA6	A/Thai/04-PB2-Strep
189	HSPA8	A/Thai/04-PB2-Strep
190	HSPA9	A/Thai/04-PB2-Strep
191	HSPD1	A/Thai/04-PB2-Strep
192	HTATIP2	A/Pan/99-PB2-Strep and A/Thai/04-PB2-Strep
193	HTATSF1	A/Thai/04-PB2-Strep
194	HYOU1	A/Thai/04-PB2-Strep
195	IARS	A/Pan/99-PB2-Strep
196	IARS2	A/Thai/04-PB2-Strep
197	ICT1	A/Thai/04-PB2-Strep
198	IDH1	A/Pan/99-PB2-Strep and A/Thai/04-PB2-Strep
199	IDH2	A/Thai/04-PB2-Strep
200	IDH3A	A/Thai/04-PB2-Strep
201	IDH3B	A/Thai/04-PB2-Strep
202	IL18	A/Pan/99-PB2-Strep
203	ILF3	A/Thai/04-PB2-Strep
204	ILKAP;ILKAP3	A/Pan/99-PB2-Strep
205	IQGAP1	A/Pan/99-PB2-Strep
206	ISOC2	A/Thai/04-PB2-Strep
207	ITGA6	A/Thai/04-PB2-Strep
208	ITGAV	A/Thai/04-PB2-Strep
209	ITGB5	A/Pan/99-PB2-Strep and A/Thai/04-PB2-Strep
210	KCNJ8	A/Pan/99-PB2-Strep and A/Thai/04-PB2-Strep
211	KDELR1	A/Pan/99-PB2-Strep and A/Thai/04-PB2-Strep
212	KIAA1598	A/Pan/99-PB2-Strep
213	KIF5B	A/Pan/99-PB2-Strep
214	KRT18	A/Pan/99-PB2-Strep and A/Thai/04-PB2-Strep
215	KTN1	A/Thai/04-PB2-Strep
216	KYNU	A/Pan/99-PB2-Strep
217	LACTB2	A/Pan/99-PB2-Strep and A/Thai/04-PB2-Strep

№	Gene	Statistically significant and t-test difference of > 0 in
218	LAMB1	A/Thai/04-PB2-Strep
219	LAMC1	A/Thai/04-PB2-Strep
220	LAMP1	A/Thai/04-PB2-Strep
221	LDHB	A/Pan/99-PB2-Strep
222	LGALS3	A/Pan/99-PB2-Strep and A/Thai/04-PB2-Strep
223	LGALS3BP	A/Thai/04-PB2-Strep
224	LMAN1	A/Thai/04-PB2-Strep
225	LRPPRC	A/Thai/04-PB2-Strep
226	LRRFIP1	A/Pan/99-PB2-Strep
227	LTA4H	A/Pan/99-PB2-Strep
228	LXN	A/Pan/99-PB2-Strep and A/Thai/04-PB2-Strep
229	LYPLAL1	A/Pan/99-PB2-Strep
230	MANF	A/Thai/04-PB2-Strep
231	MATR3	A/Thai/04-PB2-Strep
232	MB	A/Pan/99-PB2-Strep and A/Thai/04-PB2-Strep
233	MCCC2	A/Thai/04-PB2-Strep
234	MCM2	A/Thai/04-PB2-Strep
235	MCM3	A/Thai/04-PB2-Strep
236	MCM4	A/Thai/04-PB2-Strep
237	MCM6	A/Thai/04-PB2-Strep
238	MCM7	A/Thai/04-PB2-Strep
239	MCU	A/Pan/99-PB2-Strep and A/Thai/04-PB2-Strep
240	MDH1	A/Pan/99-PB2-Strep
241	MDH2	A/Thai/04-PB2-Strep
242	ME1	A/Pan/99-PB2-Strep
243	MESDC2	A/Thai/04-PB2-Strep
244	MGST1	A/Thai/04-PB2-Strep
245	MLEC	A/Thai/04-PB2-Strep
246	MPST	A/Pan/99-PB2-Strep and A/Thai/04-PB2-Strep
247	MRE11A	A/Thai/04-PB2-Strep
248	MRPL17	A/Thai/04-PB2-Strep
249	MRPL18	A/Thai/04-PB2-Strep
250	MRPL19	A/Thai/04-PB2-Strep
251	MRPL20	A/Thai/04-PB2-Strep
252	MRPL21	A/Thai/04-PB2-Strep
253	MRPL30	A/Thai/04-PB2-Strep
254	MRPL43	A/Thai/04-PB2-Strep
255	MRPL46	A/Thai/04-PB2-Strep
256	MRPS24	A/Thai/04-PB2-Strep
257	MRPS28	A/Thai/04-PB2-Strep
258	MRPS34	A/Thai/04-PB2-Strep
259	MRRF	A/Thai/04-PB2-Strep
260	MT-CO2	A/Thai/04-PB2-Strep
261	MVP	A/Pan/99-PB2-Strep
262	MYH10	A/Pan/99-PB2-Strep and A/Thai/04-PB2-Strep

№	Gene	Statistically significant and t-test difference of > 0 in
263	MYO1B	A/Pan/99-PB2-Strep
264	NANS	A/Pan/99-PB2-Strep and A/Thai/04-PB2-Strep
265	NCBP1	A/Thai/04-PB2-Strep
266	NCBP2	A/Thai/04-PB2-Strep
267	NCL	A/Thai/04-PB2-Strep
268	NCSTN	A/Thai/04-PB2-Strep
269	NDUFA12	A/Thai/04-PB2-Strep
270	NDUFA6	A/Thai/04-PB2-Strep
271	NDUFS1	A/Thai/04-PB2-Strep
272	NDUFS3	A/Thai/04-PB2-Strep
273	NHP2L1	A/Thai/04-PB2-Strep
274	NIPSNAP1	A/Thai/04-PB2-Strep
275	NIPSNAP3A	A/Pan/99-PB2-Strep and A/Thai/04-PB2-Strep
276	NME2;NME1	A/Pan/99-PB2-Strep
277	NME3	A/Pan/99-PB2-Strep and A/Thai/04-PB2-Strep
278	NME4	A/Thai/04-PB2-Strep
279	NOMO1;2;3	A/Thai/04-PB2-Strep
280	NONO	A/Thai/04-PB2-Strep
281	NPEPL1	A/Pan/99-PB2-Strep and A/Thai/04-PB2-Strep
282	NPLOC4	A/Pan/99-PB2-Strep
283	NPM1	A/Thai/04-PB2-Strep
284	NQO2	A/Pan/99-PB2-Strep and A/Thai/04-PB2-Strep
285	NUDT21	A/Thai/04-PB2-Strep
286	NUP155	A/Thai/04-PB2-Strep
287	NUP210	A/Thai/04-PB2-Strep
288	OGDH	A/Thai/04-PB2-Strep
289	P4HB	A/Thai/04-PB2-Strep
290	PABPC1;PABPC3	A/Thai/04-PB2-Strep
291	PAFAH1B2	A/Pan/99-PB2-Strep
292	PARK7	A/Pan/99-PB2-Strep
293	PC	A/Thai/04-PB2-Strep
294	PCCA	A/Thai/04-PB2-Strep
295	PCCB	A/Thai/04-PB2-Strep
296	PCK2	A/Thai/04-PB2-Strep
297	PDHA1	A/Pan/99-PB2-Strep and A/Thai/04-PB2-Strep
298	PDHB	A/Thai/04-PB2-Strep
299	PDIA3	A/Pan/99-PB2-Strep and A/Thai/04-PB2-Strep
300	PDIA4	A/Thai/04-PB2-Strep
301	PDIA6	A/Thai/04-PB2-Strep
302	PGD	A/Pan/99-PB2-Strep
303	PHB	A/Thai/04-PB2-Strep
304	PHB2	A/Thai/04-PB2-Strep
305	PIR	A/Pan/99-PB2-Strep
306	PLD3	A/Thai/04-PB2-Strep
307	PLOD3	A/Thai/04-PB2-Strep

№	Gene	Statistically significant and t-test difference of > 0 in
308	PLXNB2	A/Thai/04-PB2-Strep
309	POFUT1	A/Thai/04-PB2-Strep
310	POLR1A	A/Thai/04-PB2-Strep
311	PON2	A/Thai/04-PB2-Strep
312	POR	A/Thai/04-PB2-Strep
313	PPA2	A/Thai/04-PB2-Strep
314	PPIB	A/Thai/04-PB2-Strep
315	PPP2R4	A/Pan/99-PB2-Strep
316	PRDX1	A/Pan/99-PB2-Strep
317	PRDX3	A/Thai/04-PB2-Strep
318	PRDX4	A/Thai/04-PB2-Strep
319	PRDX5	A/Thai/04-PB2-Strep
320	PRKDC	A/Thai/04-PB2-Strep
321	PRPF19	A/Thai/04-PB2-Strep
322	PRPF8	A/Thai/04-PB2-Strep
323	PSMA3	A/Pan/99-PB2-Strep
324	PSMB1	A/Thai/04-PB2-Strep
325	PSMB5	A/Thai/04-PB2-Strep
326	PSMD5	A/Pan/99-PB2-Strep
327	PSME2	A/Pan/99-PB2-Strep
328	PTCD3	A/Thai/04-PB2-Strep
329	PYCARD	A/Pan/99-PB2-Strep
330	RAB10	A/Pan/99-PB2-Strep and A/Thai/04-PB2-Strep
331	RAB11A;B	A/Pan/99-PB2-Strep and A/Thai/04-PB2-Strep
332	RAB1A	A/Thai/04-PB2-Strep
333	RAB27B	A/Thai/04-PB2-Strep
334	RAB2A;B	A/Thai/04-PB2-Strep
335	RAD50	A/Thai/04-PB2-Strep
336	RAP1B;A	A/Thai/04-PB2-Strep
337	RBM12	A/Thai/04-PB2-Strep
338	RBM12B	A/Thai/04-PB2-Strep
339	RBMX;L1	A/Thai/04-PB2-Strep
340	RCN1	A/Thai/04-PB2-Strep
341	RCN2	A/Thai/04-PB2-Strep
342	RDH11	A/Thai/04-PB2-Strep
343	RDX	A/Pan/99-PB2-Strep
344	RECQL	A/Pan/99-PB2-Strep
345	REEP5	A/Thai/04-PB2-Strep
346	RNPEP	A/Pan/99-PB2-Strep
347	RPL12	A/Pan/99-PB2-Strep and A/Thai/04-PB2-Strep
348	RPL13a	A/Pan/99-PB2-Strep
349	RPL17	A/Pan/99-PB2-Strep
350	RPL24	A/Pan/99-PB2-Strep
351	RPL28	A/Pan/99-PB2-Strep
352	RPL30	A/Thai/04-PB2-Strep

№	Gene	Statistically significant and t-test difference of > 0 in
353	RPL35	A/Thai/04-PB2-Strep
354	RPL9	A/Thai/04-PB2-Strep
355	RPN2	A/Thai/04-PB2-Strep
356	RPP25	A/Thai/04-PB2-Strep
357	RPP30	A/Thai/04-PB2-Strep
358	RPS11	A/Pan/99-PB2-Strep
359	RPS12	A/Pan/99-PB2-Strep
360	RPS15A	A/Pan/99-PB2-Strep
361	RPS18	A/Pan/99-PB2-Strep
362	RPS24	A/Pan/99-PB2-Strep
363	RPS27A;UBB;P4C;UBA52	A/Thai/04-PB2-Strep
364	RPS6	A/Pan/99-PB2-Strep
365	RPS6KA3	A/Pan/99-PB2-Strep
366	RRAGB;RRAGA	A/Pan/99-PB2-Strep
367	RRBP1	A/Thai/04-PB2-Strep
368	RTN3	A/Thai/04-PB2-Strep
369	SAE1	A/Pan/99-PB2-Strep and A/Thai/04-PB2-Strep
370	SARS2	A/Thai/04-PB2-Strep
371	SART3	A/Pan/99-PB2-Strep and A/Thai/04-PB2-Strep
372	SCARB2	A/Thai/04-PB2-Strep
373	SCO1	A/Thai/04-PB2-Strep
374	SCP2	A/Pan/99-PB2-Strep and A/Thai/04-PB2-Strep
375	SDF2	A/Thai/04-PB2-Strep
376	SDF2L1	A/Thai/04-PB2-Strep
377	SDHB	A/Thai/04-PB2-Strep
378	SEC11A	A/Thai/04-PB2-Strep
379	SEC22B	A/Thai/04-PB2-Strep
380	SEC23A	A/Pan/99-PB2-Strep
381	SEC31A	A/Pan/99-PB2-Strep
382	SEL1L	A/Thai/04-PB2-Strep
383	SERPINB1	A/Pan/99-PB2-Strep and A/Thai/04-PB2-Strep
384	SERPINH1	A/Thai/04-PB2-Strep
385	SET	A/Thai/04-PB2-Strep
386	SF3A1	A/Thai/04-PB2-Strep
387	SF3A3	A/Thai/04-PB2-Strep
388	SF3B1	A/Thai/04-PB2-Strep
389	SF3B2	A/Thai/04-PB2-Strep
390	SF3B3	A/Thai/04-PB2-Strep
391	SFPQ	A/Thai/04-PB2-Strep
392	SFXN1	A/Thai/04-PB2-Strep
393	SGTA	A/Thai/04-PB2-Strep
394	SIN3A	A/Thai/04-PB2-Strep
395	SLC12A2	A/Pan/99-PB2-Strep and A/Thai/04-PB2-Strep
396	SLC25A1	A/Thai/04-PB2-Strep
397	SLC25A5	A/Thai/04-PB2-Strep

№	Gene	Statistically significant and t-test difference of > 0 in
398	SLC25A6	A/Thai/04-PB2-Strep
399	SLC4A1AP	A/Thai/04-PB2-Strep
400	SMARCC2	A/Thai/04-PB2-Strep
401	SMC1A	A/Thai/04-PB2-Strep
402	SMEK1	A/Thai/04-PB2-Strep
403	SNRNP200	A/Thai/04-PB2-Strep
404	SNRNP70	A/Thai/04-PB2-Strep
405	SNRPA1	A/Thai/04-PB2-Strep
406	SNRPB;SNRPN	A/Thai/04-PB2-Strep
407	SNRPB2	A/Thai/04-PB2-Strep
408	SNRPD1	A/Thai/04-PB2-Strep
409	SNRPD2	A/Thai/04-PB2-Strep
410	SNRPD3	A/Thai/04-PB2-Strep
411	SOD1	A/Pan/99-PB2-Strep and A/Thai/04-PB2-Strep
412	SPCS2	A/Thai/04-PB2-Strep
413	SPCS3	A/Thai/04-PB2-Strep
414	SPR	A/Pan/99-PB2-Strep
415	SRC	A/Thai/04-PB2-Strep
416	SRP14	A/Thai/04-PB2-Strep
417	SRRT	A/Thai/04-PB2-Strep
418	SRSF1	A/Thai/04-PB2-Strep
419	SRSF2	A/Thai/04-PB2-Strep
420	SRSF3	A/Thai/04-PB2-Strep
421	SRSF6	A/Thai/04-PB2-Strep
422	SSB	A/Thai/04-PB2-Strep
423	SSBP1	A/Thai/04-PB2-Strep
424	SSR4	A/Thai/04-PB2-Strep
425	SSRP1	A/Thai/04-PB2-Strep
426	STAG2	A/Thai/04-PB2-Strep
427	SUB1	A/Thai/04-PB2-Strep
428	SUCLA2	A/Pan/99-PB2-Strep and A/Thai/04-PB2-Strep
429	SUCLG1	A/Thai/04-PB2-Strep
430	SUCLG2	A/Thai/04-PB2-Strep
431	SUMO1	A/Thai/04-PB2-Strep
432	SUMO2	A/Thai/04-PB2-Strep
433	SUPT16H	A/Thai/04-PB2-Strep
434	SUPT5H	A/Thai/04-PB2-Strep
435	SUPT6H	A/Thai/04-PB2-Strep
436	SWAP70	A/Pan/99-PB2-Strep
437	SYNGR2	A/Thai/04-PB2-Strep
438	TALDO1	A/Pan/99-PB2-Strep and A/Thai/04-PB2-Strep
439	TBCB	A/Pan/99-PB2-Strep
440	TCERG1	A/Thai/04-PB2-Strep
441	TCOF1	A/Thai/04-PB2-Strep
442	THOC1	A/Thai/04-PB2-Strep

№	Gene	Statistically significant and t-test difference of > 0 in
443	THOP1	A/Pan/99-PB2-Strep
444	TIGAR	A/Pan/99-PB2-Strep
445	TKT	A/Pan/99-PB2-Strep and A/Thai/04-PB2-Strep
446	TLN1	A/Pan/99-PB2-Strep
447	TMED10	A/Thai/04-PB2-Strep
448	TMED2	A/Thai/04-PB2-Strep
449	TMED3	A/Thai/04-PB2-Strep
450	TMED9	A/Thai/04-PB2-Strep
451	TMEM106B	A/Pan/99-PB2-Strep
452	TMEM70	A/Thai/04-PB2-Strep
453	TOMM20	A/Thai/04-PB2-Strep
454	TOP2A	A/Thai/04-PB2-Strep
455	TOP2B	A/Thai/04-PB2-Strep
456	TPM1	A/Pan/99-PB2-Strep
457	TPP2	A/Pan/99-PB2-Strep
458	TPR	A/Thai/04-PB2-Strep
459	TPT1	A/Pan/99-PB2-Strep
460	TRAP1	A/Thai/04-PB2-Strep
461	TRAPPC3	A/Pan/99-PB2-Strep and A/Thai/04-PB2-Strep
462	TRMT61A	A/Thai/04-PB2-Strep
463	TST	A/Pan/99-PB2-Strep and A/Thai/04-PB2-Strep
464	TTBK2	A/Pan/99-PB2-Strep and A/Thai/04-PB2-Strep
465	TUFM	A/Thai/04-PB2-Strep
466	TXNDC12	A/Thai/04-PB2-Strep
467	TXNDC5	A/Thai/04-PB2-Strep
468	UBA1	A/Pan/99-PB2-Strep
469	UBA2	A/Pan/99-PB2-Strep and A/Thai/04-PB2-Strep
470	UGDH	A/Pan/99-PB2-Strep
471	UGGT1	A/Pan/99-PB2-Strep and A/Thai/04-PB2-Strep
472	UGP2	A/Pan/99-PB2-Strep
473	UQCRC1	A/Thai/04-PB2-Strep
474	UQCRC2	A/Thai/04-PB2-Strep
475	UQCRFS1;P1	A/Thai/04-PB2-Strep
476	USO1	A/Pan/99-PB2-Strep
477	USP7	A/Thai/04-PB2-Strep
478	UTRN	A/Pan/99-PB2-Strep and A/Thai/04-PB2-Strep
479	VAPA	A/Thai/04-PB2-Strep
480	VCP	A/Pan/99-PB2-Strep
481	VPS29	A/Pan/99-PB2-Strep
482	WDR5	A/Thai/04-PB2-Strep
483	XRCC5	A/Thai/04-PB2-Strep
484	YWHAB	A/Pan/99-PB2-Strep
485	YWHAG	A/Pan/99-PB2-Strep
486	YWHAZ	A/Pan/99-PB2-Strep
487	ZC3HAV1	A/Thai/04-PB2-Strep

Table S.2. t-test difference and p-values of A/Pan/99 viral proteins identified in MS screen. Data was calculated using Perseus 1.5.0.31.

Protein	t-test difference	p value
PB2	358.29	0.000041
PB1	24.10	0.000656
PA	214.38	0.000062
HA	5.27	0.005236
NA	3.15	0.041400
NP	76.11	0.000394
M1	9.02	0.080168
M2	6.35	1.000000
NS1	5.02	0.013032

Table S.3. t-test difference and p-values of A/Thai/04 viral proteins identified in MS screen. Data was calculated using Perseus 1.5.0.31.

Protein	t-test difference	p value
PB2	992.55	0.000033
PB1	318.03	0.001205
PA	601.74	0.001371
HA	118.44	0.002851
NA	5.94	0.043551
NP	125.80	0.000916
M1	206.36	0.002938
M2	97.68	0.002360
NS1	217.22	0.000220

Appendix

Acknowledgments

I want to thank…

… PD Dr. Thorsten Wolff, for giving me the chance to work on this project and for his supervision, help and shared knowledge over the last 5 years.

… Prof. Dr. Andreas Herrmann for his supervision and Dr. Benedikt Beckmann for the evaluation of this thesis.

… Dr. Kathryn Edenborough and Dr. Rebecca Surtees for proofreading this thesis. Even though it is written in American English.

… Gudrun Heins, for being the heart and soul of the lab. Thank you for being there, no matter what the situation was about.

…Katharina, Anne and Sandra, for their friendship and the hours of discussion about mass spectrometry and for keeping me sane through all the work.

… Rocío and Daniel, for the best and funniest coffee breaks and all the crocodiles and sharks.

… all the members of FG17 I had the chance to work with during this project. Matthias, Tina, Jessi, Jessi K., Christin and Marlena. For the fun, shared experiences and help.

… Prof. Dr. Andreas Nitsche, for having my back.

… Eva and Becky, for being the best travel buddies.

… Andreas Kurth, for inspiring me more than he will ever know.

… Sandra B., for being superwoman. Nicole, for being the kindest person I know. Luam, for always knowing how it feels. Thanks to all of you for your patience, unconditional love and support.

… Ulrike D., for helping me through the craziness of Oslo 15.

… Matt, for broadening my world.

… Saskia, for aaaaaaalways being there. More than half of our lives.

… Irene, for everything. We were there for each other in the dark. Now it`s time for us to enjoy the sun.

… my parents, for never ever leting me think that for me, as a girl, there is anything I cannot do or achieve. This is the foundation of all the things I accomplished.

Selbstständigkeitserklärung

Hiermit erkläre ich, die Dissertation selbstständig und nur unter Verwendung der angegebenen Hilfen und Hilfsmittel angefertigt zu haben. Ich habe mich anderwärts nicht um einen Doktorgrad beworben und besitze keinen entsprechenden Doktorgrad. Ich erkläre, dass ich die Dissertation oder Teile davon nicht bereits bei einer anderen wissenschaftlichen Einrichtung eingereicht habe und dass sie dort weder angenommen noch abgelehnt wurde. Ich erkläre die Kenntnisnahme der dem Verfahren zugrunde liegenden Promotionsordnung der Mathematisch-Naturwissenschaftlichen Fakultät I der Humboldt-Universität zu Berlin vom 27. Juni 2012.

Berlin, den 05.04.2018

Ulrike Arnold